The fate of Marine Magnetic Anomalies in Subduction Zone

Hanjin Choe

UNIVERSITÉ DE PARIS

Thèse préparée
à l'UNIVERSITÉ PARIS DIDEROT
École doctorale STEP'UP - ED N°560
IPGP - Équipe de Géosciences marines

The Fate of Marine Magnetic Anomalies in Subduction Zone

par
Hanjin Choe

présentée et soutenue publiquement le
18 Decembre 2019

Thèse de doctorat de Sciences de la Terre et de l'environnement
dirigée par : Jérôme Dyment

devant un jury composé de :

SEAMA Nobukazu Professeur (Kobe University)	Rapporteur
HUCHON Philippe Professeur (UPMC, Sorbonne Université)	Rapporteur
MAIA Marcia Directrice de recherche - CNRS (Bretagne Occidentale)	Membre
SINGH Satish Physicien (IPGP, Paris)	Membre
DYMENT Jérôme Directeur de recherche - CNRS (IPGP, Paris)	Directeur de thèse

Résumé

L'objet de cette étude est de comprendre les causes de la diminution des anomalies magnétiques océaniques dans la croûte océanique en subduction. Nous étudions l'aimantation de la croûte océanique avant et après l'entrée en subduction et étendons notre zone d'étude initiale des fosses du Japon et des Kouriles à d'autres zones de subduction afin de généraliser nos observations. Avant subduction, une perte de 20% de l'aimantation se produit entre la ride externe et la fosse pour un plancher océanique ancien, causée par le renouvellement de la circulation hydrothermale et l'altération des minéraux magnétiques. Une telle perte n'est pas observée pour un plancher océanique jeune car la flexure y est très faible. Après subduction, dans tous les cas sont observées une décroissance rapide de l'aimantation liée à la désaimantation thermique de la titanomagnétite (Tc 150-350°C) des basaltes extrusifs, suivie d'une décroissance plus lente liée à la désaimantation thermique de la magnétite (Tc 580°C) dans la croûte profonde. La première phase est plus rapidement achevée dans le plancher océanique jeune de par des différences de structure thermique. De manière générale, la disparition des anomalies magnétiques en subduction résulte de la flexure, de la fracturation et de la circulation hydrothermale avant subduction, et de la désaimantation thermique des différents minéraux magnétiques après subduction. L'eau de mer injectée dans la croûte avant subduction est piégée par la couverture sédimentaire après être entrée en subduction et pourrait significativement réchauffer le panneau plongeant par couverture thermique, s'ajoutant au gradient thermique initial et possiblement à la chaleur dégagée par la serpentinisation du coin mantellique. La vitesse de désaimantation thermique est modulée par l'épaisseur lithosphérique, le taux d'hydratation, et donc l'âge du plancher océanique.

Abstract

Subduction is a major geodynamic process that leads to the disappearance of oceanic lithosphere, the formation of volcanic arcs, and the generation of natural disasters such as earthquakes and tsunamis resulting in major damages and casualties. Many geophysical studies have been conducted over the subduction zones to understand their structure and how they work. However, very few studies used marine magnetics to study subduction zones. Most magnetic surveys have been conducted to decipher the age and structure of the oceanic basins and the evolution of the tectonic plates, and are therefore more focused on the seafloor spreading processes at mid-ocean ridges.

The purpose of this study is to understand the causes of the decaying seafloor spreading magnetic anomalies and their meaning in terms of the thermodynamic processes at subduction zones. Our work includes the measurements, processing and combination of two different types of marine magnetic data to build high resolution marine magnetic anomaly grids; the design of a simple methodology to alleviate the effect of topography and isolate the variations of magnetization; and the analysis of these variations of magnetization. We investigate the magnetization of the oceanic crust both before and after subduction and extended our initial study area, the Japan subduction zone, to other subduction zones.

In the first section, we analyze the magnetic structure of the oceanic crust after subduction to constrain the thermal structure of the subducting slab in Japan Trench using improved magnetic anomaly map derived from both scalar and vector magnetic anomaly data, coupled with a better knowledge of the slab geometry. We identify two steps in the anomaly disappearance: first the magnetization of extrusive basalt is rapidly erased between 9-12 km, where titanomagnetite reaches its blocking temperature between 150-350°C, then the magnetization of deeper crustal layers slowly decreases down to ~20 km, reflecting the progressive slab heating toward the Curie temperature of magnetite, 580 °C.

In the second section, we analyze the magnetic structure of the oceanic crust before subduction and show that a systematic loss of ~20 % in the amplitude of the magnetic anomalies arises between the outer rise and the trench on old ocean crust approaching the Japan and Kuril subduction zones. We discuss this decay with support of other geophysical observations, namely higher heat flow and seismic velocity changes observed toward the trench, to conclude that the flexure of the lithospheric plate approaching subduction induces

normal faults, rejuvenated hydrothermal circulation, alteration of the magnetic minerals of the extrusive basalt and possibly deeper crustal layers, and finally a decrease of magnetization.

In the third section, we try to generalize our observations to other subduction zones. Before subduction, a loss of magnetization between the outer-rise and the trench occurs in old oceanic crust, caused by rejuvenated hydrothermal circulations and alteration of magnetic minerals. Conversely, such a loss of magnetization is not observed for young oceanic crust because the flexure remains very limited. After subduction, both exhibit a fast decay of magnetization due to thermal demagnetization of titanomagnetite in the extrusive basalt, followed by a much slower one due to thermal demagnetization of magnetite in the deeper crust. However, the fast decay is more rapidly achieved in young oceanic crust due to the differences of thermal structure.

Overall, magnetic anomalies in subducting oceanic crust decay as an effect of flexure, normal faulting and hydrothermal alteration before subduction, and thermal demagnetization of the different magnetic minerals after subduction. The sea water injected in the oceanic crust before subduction is trapped by the sediment cover after entering subduction and may significantly heat up the slab through thermal blanketing, adding to the thermal gradient and possibly heat released by serpentinization of the mantle wedge. The speed of thermal demagnetization is modulated by the lithosphere thickness, the hydration rate, and therefore the age of oceanic crust.

Acknowledgements

Since I began studying geophysics for B.Sc in 2004, I have been always attracted by this field and for the first time, the magnetic survey was introduced to me while I was staying at King Sejong Station, Antarctica as a geophysicist of the overwinter party of Korea Antarctic research program. This experience triggered me to continue my master's and finally PhD.

First of all, I really appreciate Dr. Jerome Dyment. He recognized my potential during the workshop between Seoul National University and IPGP and gave me a chance to apply for the Ecole Doctoral STEP-UP program. I also thank him for his very helpful supervision and for giving me a lot of chances for the field experiences (e.g the Danakil field trip, the MAGOFOND4, and the MIRAGE cruise). Also, Professor Sang-Mook Lee, master's supervisor, gave me a lot of advice and encouragement.

I thank my colleagues in Geosciences Marines at IPGP. Especially, Dr. Yujin Choi, she gave me a lot of encouragement. Also, particularly Aline Robin, Dr. Manon Bickert, Benjamin Wheeler, Venkata Vadhineni, Jie Chen, Dr. Andreina Garcia, without them, I would have a lot of problems in surviving and in finishing my PhD degree. They helped me to understand cultural differences and to overcome language problems.

I would like to especially thank the jury members: Professor Nobukatsu Seama, Professor Philippe Huchon, Professor Marcia Maia and Dr. Satish Singh and my every annual meeting committee: Dr. Philippe Huchon and Dr. Helene Carton for their helpful discussion and their encouragements.

I am grateful to my colleagues and friends in Korea and particularly Jiweon Seo, who always trusted and supported me in Korea during my PhD degree. In the end, I would like to dedicate this thesis with the greatest appreciation and respect to my father and mother who have given me strong supports and love from behind.

Contents

Chapter 1.

General introduction

1.1 Motivation

Marine magnetic anomalies (Vine and Matthews, 1963) are essential to study the oceanic crust formed by seafloor spreading at mid-ocean ridges. Thanks to the frequent reversals of the geomagnetic field "frozen" by the magnetic mineral of the new oceanic crust, they allow deciphering the structure and age of ocean basins to reconstruct their evolution and the Earth plate tectonic history. The breakthrough of magnetic sensors and global positioning as well as the improving geomagnetic polarity time scale result in more precise seafloor spreading magnetic anomalies and structure of the oceanic basins by quantitative and combined analysis with other information (e.g. seismology, bathymetry, heat flow, gravity, rock samples from drilling, dredge and ophiolite).

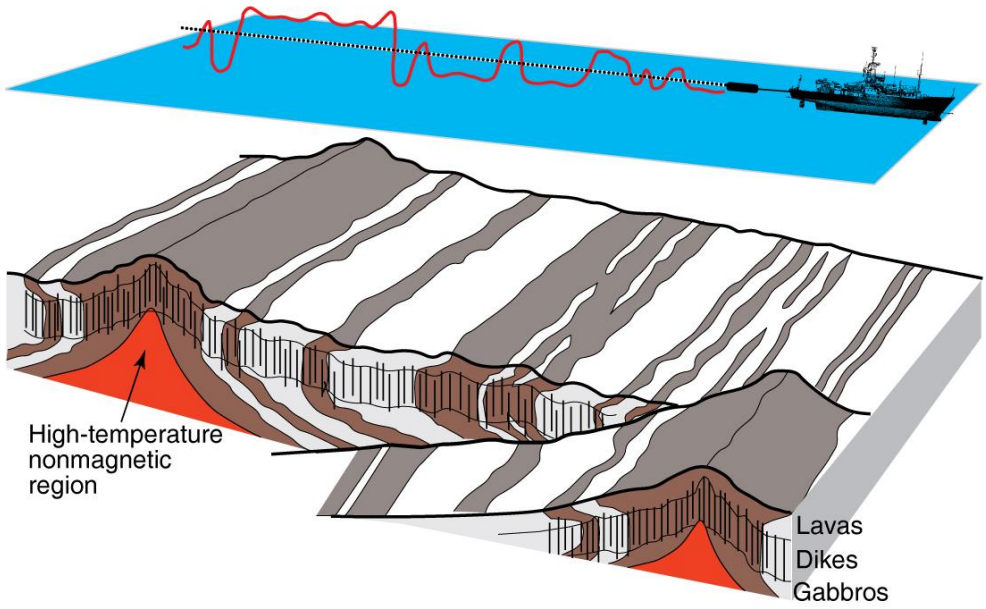

Figure 1-1. 3-D schematic illustration of ocean crust showing spreading centers (Gee and Kent, 2007). Grey and white areas indicate the normal and reverse geomagnetic polarity recorded by oceanic crust. The red solid curve is the magnetic anomaly. Magnetization polarity boundaries are expected to slope toward ridge in the extrusive basalt layer due to continuous emplacement of lavas, to be vertical in the sheeted dikes, and to slope away from ridge in the gabbro layer due to their progressive cooling.

Layer		Remanent magnetization (A/m)	Major magnetic mineral	Tc. (°C)	
2	2A	20-3	Titanomagnetite	100-350	Upper crust
	2B	1	Magnetite	580	
3		0.6	Magnetite	580	Lower crust
Serpentinite (0.72)		5	Magnetite	580	Upper Mantle
Serpentinite (1.5)		5	Magnetite	580	

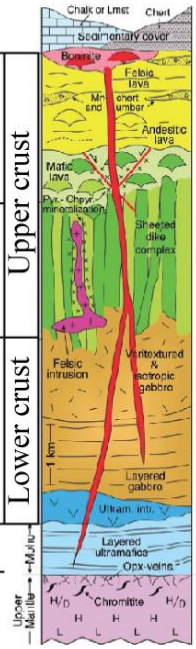

Figure 1-2. Magnetic characteristics of each oceanic crust layer (Harrison, 1987 ; Gee and Kent, 2007). The schematic illustration of oceanic crust structure (right) is slightly modified from Direk and Furnes (2014). The extrusive basalt layer 2A exhibits stronger intensity in remanent magnetization and low Curie temperature compared to the deeper oceanic crust layers.

Detailed magnetic studies combined with other methods have revealed the magnetic structure of the oceanic crust, made of four main layers (Figure 1-2). The extrusive basalt layer (Layer 2A), 0.5-1km thick, is rapidly quenched by seawater and its magnetic mineral is titanomagnetite with various Ti content and oxidation state (Curie temperature Tc 100-350°C, Zhou et al., 2001; Gee and Kent, 2007). The sheeted dykes or intrusive dolerite layer (Layer 2B), the gabbro layer (Layer 3), and the serpentinized peridotite layer all have magnetite as their magnetic mineral (Tc 580°C). The Natural Remanent Magnetization (NRM) carried by these layers varies: the extrusive layer bears a strong NRM (> 10 A/m) at the ridge axis which decays to ~3 A/m for old oceanic crust. It is the main contributor to the lineated marine magnetic anomalies observed at sea-surface. Conversely, the dolerite and gabbro bear a weaker NRM (~1 to 1.5 A/m) and the serpentinized peridotite a variable NRM (0 to 6 A/m) depending the degree of serpentinization (Harrison, 1987; Figure 1-2). The thermal evolution of the deeper magnetized layer controls the acquisition of their magnetization, explaining the anomalous skewness by the slanted shape of magnetization patterns in the deeper oceanic crust layer created at slow and intermediate spreading rates (Dyment and Arkani-Hamed,

1995). The acquisition of magnetization by serpentinization of ultramafic rocks in the lower crust and possibly the uppermost mantle at temperatures between 200 and 300°C is delayed with respect of the acquisition of thermoremanent magnetization in extrusive basalt, explaining the hook shape of some magnetic anomalies (Dyment et al., 1997).

Many marine magnetic studies contributed to understand oceanic crust structures. However, very few studies used them to study subduction zones. Whether the magnetic signature of structures created by subduction is diverse, complex, and interpreted in somewhat ad hoc or divergent ways, the magnetic signature of the subducting plate does not originally differ from that of oceanic basins, which magnetic structure and properties are now well constrained. This allows considering the magnetic anomalies observed on subducting plates to constrain the additional effects of subduction on these anomalies.

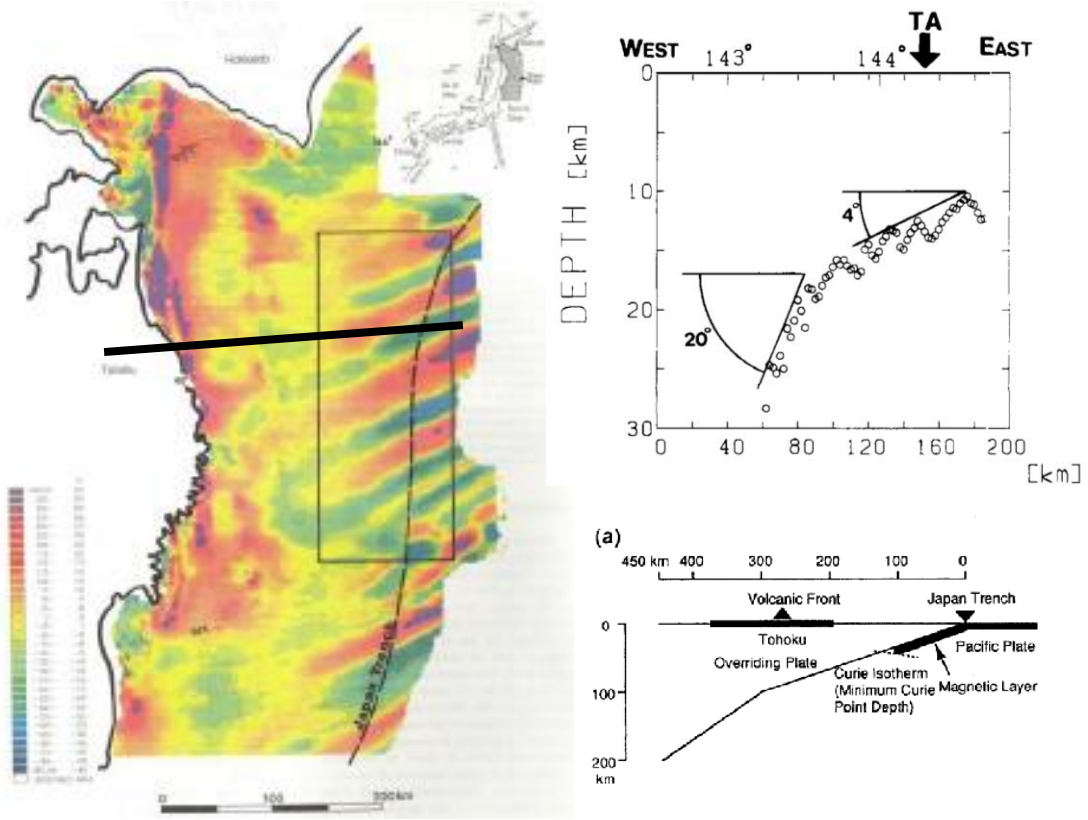

Figure 1-3. The previous magnetic study of Okubo et al. (1991) for seafloor spreading magnetic anomaly in the subducted oceanic crust. A, magnetic anomaly map in Japan Trench. B, estimated slab slope angles from wavelength variation of seafloor spreading magnetic anomaly. C, Schematic illustration of Curie isotherm depth of the subducting oceanic lithosphere.

1.2 Subduction zones

Subduction zones are convergent plate boundary in which at least one lithospheric plate is oceanic and disappear beneath the other plate. The oceanic crust formed at mid-ocean ridges is progressively covered by sediments, as time goes, and the existing faults and cavities are sealed, stopping the hydrothermal circulation. This is confirmed by the decay of magnetization within the first 10 million years observed at all spreading centers followed by a relative stability (Dyment et al., 2015). Before subduction, the flexure of the oceanic plate generates new faults parallel to the trench and re-open existing faults of proper trend resulting in increasing the permeability of the crust to seawater.

The subducting oceanic plate slides under the overriding plate along a basal detachment fault called decollement, which structure is formed by high pressure on the boundary between the subducted sediment layer on the oceanic crust and the overriding plate: the friction creates the megathrust zones where the large earthquakes are triggered.

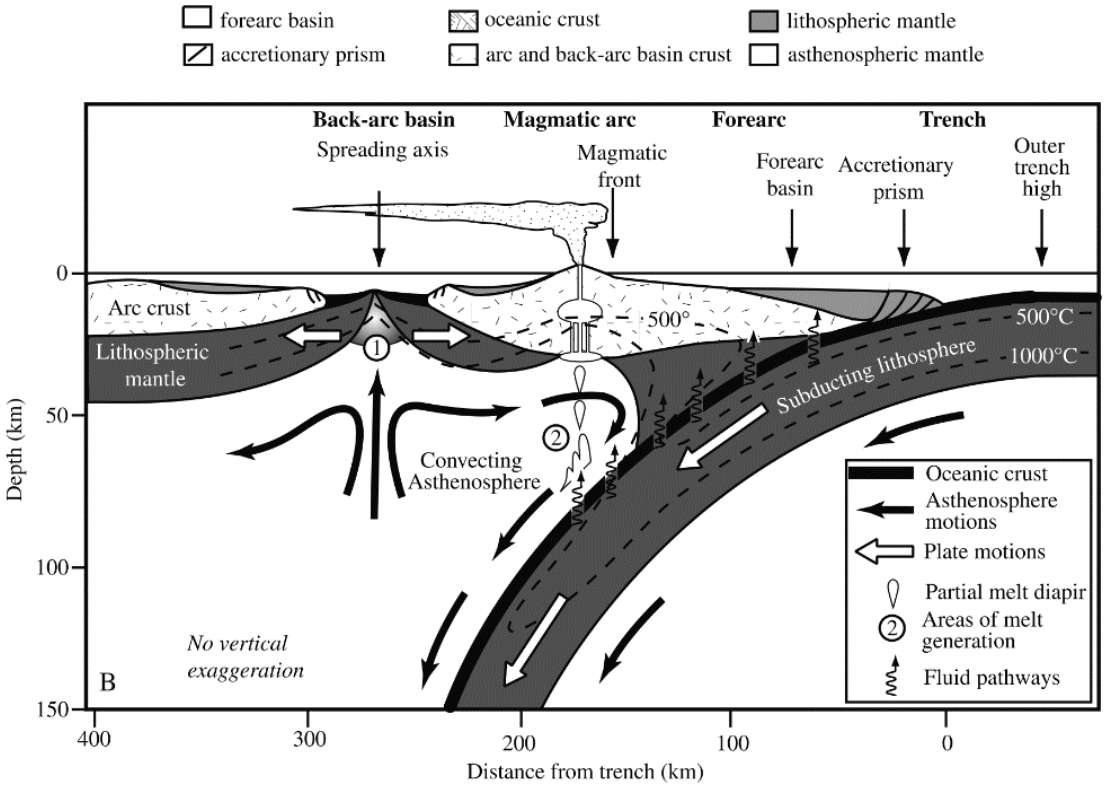

Figure 1-4. Schematic illustration of subduction zone (Stern, 2002).

Subsequently, the subducting oceanic plate starts to emit plenty of seawater when the plate reaches high pressure and high temperature, resulting in partial melting in the overlying mantle. In this process, the mantle becomes hydrated and serpentinizes. Lighter partially molten rocks rise to the surface and form the volcanic arc (Marsh and Leitz, 1979). As a result, the converging tectonic processes outcome tremendous natural hazards such as earthquakes, tsunamis and volcanic eruptions.

In the subduction zone, two distinctive magnetic anomaly signals are observed: (1) seafloor spreading magnetic anomalies of the subducting slab with strong NRM intensities are erased when the increasing temperature pass the Curie temperature of its magnetic minerals, and (2) landward magnetic anomaly belt generated by induced magnetization of the serpentinized fore-arc mantle which contains high susceptibility magnetic minerals.

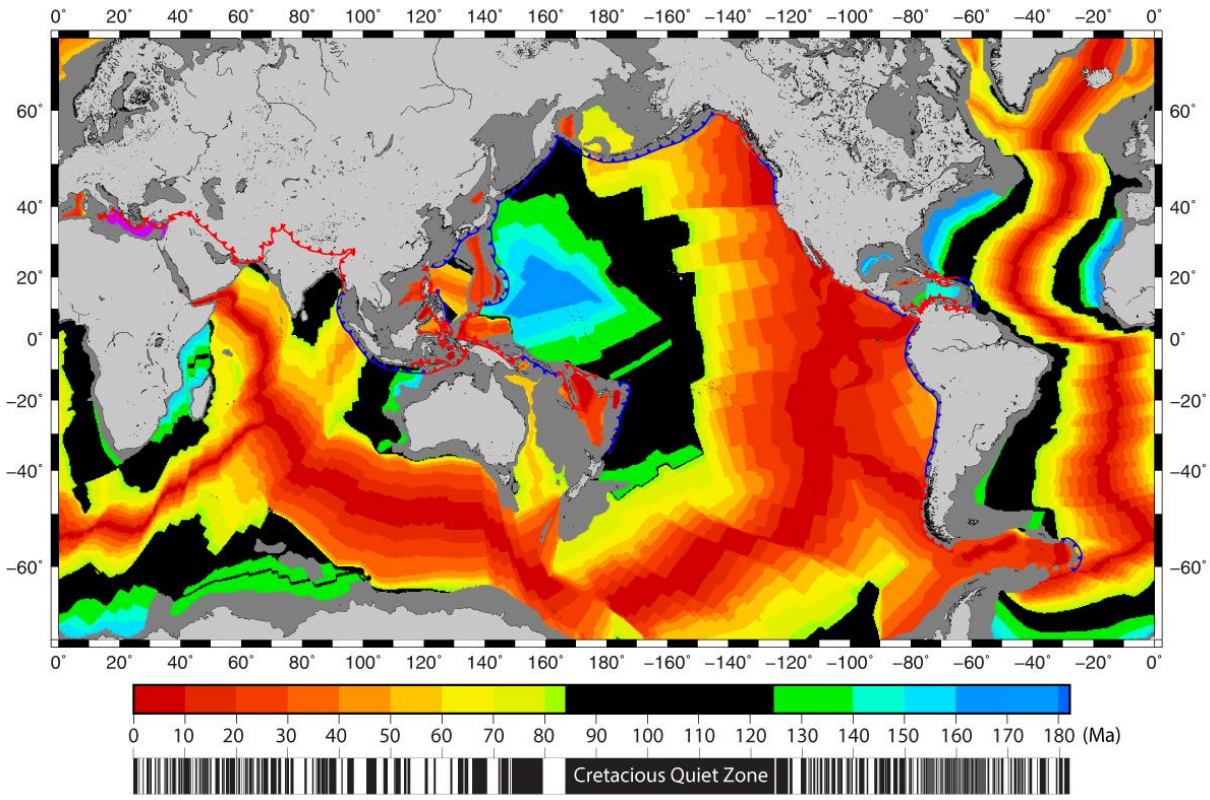

Figure 1-5. The world seafloor age map (Müller et al., 2008). The blue solid lines indicate the boundary of active subduction zones and red solid lines, inactive subduction zones.

1.3 Research framework

This work focuses on the analysis of fading seafloor spreading magnetic anomalies in subduction zones and the causes of this decay. To address this problem, we selected subduction zone areas following several criteria: (1) dense marine magnetic data, (2) no perturbation from other tectonic structures, and (3) strike of the anomaly oblique to the trench. The three criteria aim to observe the amplitude variations of seafloor spreading magnetic anomalies before and after subduction alleviating possible biases related to paleomagnetic field intensity variation with time, by studying the same sets of anomalies. The Japan-Kuril Trench area fits all conditions for a detailed analysis. We later extend the analysis to four other subduction zones.

To build better high-resolution magnetic anomaly maps, we include shipboard three-component magnetometer (STCM) data to complement proton precession magnetometer (PPM) data in areas where the later are not available and designed a new crossover algorithm to combine these two types of marine magnetic data (See appendix A). PPM are preferred over STCM data because the PPM sensor measures absolute magnetic field, whereas the STCM sensor measures relative variations of vector magnetic field which, despite complicated correction of the ship induced and remanent magnetization effects, is still affected by viscous remanent magnetization (VRM) progressively acquired by the ship while following a constant heading.

We took advantage of a high-resolution magnetic anomaly map and designed an original analytic method to alleviate the effect of topography and isolate the variations of magnetization along individual magnetic anomalies. This method, which differs from that used by Okubo et al. (1991) in the same area, was applied on magnetic anomalies having entered subduction in the Japan Trench (Chapter 2) and approaching the Japan-Kuril Trench (Chapter 3). It is later applied to four other subduction zones for comparison and generalization (Chapter 4).

Chapter 2.

Fading Magnetic Anomalies, Thermal Structure and Earthquakes in the Japan Trench

2.1 Abstract

Early magnetic studies of the Japan Trench showed that seafloor spreading magnetic anomalies progressively fade away and disappear during subduction, reflecting the increasing distance to magnetized sources and the removal of their remanent magnetization with alteration and increasing temperature. An improved magnetic anomaly map derived from both scalar and vector magnetic anomaly data, coupled with a better knowledge of the slab geometry in one hand, of the magnetic structure of the oceanic crust on the other hand, allow us to constrain the thermal structure of the subducting slab. We, for the first time, identify two steps in the anomaly disappearance: first the magnetization of extrusive basalt is rapidly erased between 9-12 km, where titanomagnetite reaches its blocking temperature between 150-350°C, then the magnetization of deeper crustal layers slowly decreases down to ~20 km, reflecting the progressive slab heating toward the Curie temperature of magnetite, 580 °C. The resulting slab temperatures are higher than predicted by most thermal models. Recent observations and models suggest rejuvenated hydrothermal activity triggered by lithospheric flexure before subduction that may significantly heat up the subducting oceanic crust through thermal blanketing and possibly serpentinization, with consequences on the depth of the seismogenic zone.

2.2 Introduction

Subduction is a major geodynamic process that leads to the consumption of oceanic lithosphere, the creation of volcanic arcs and the largest volcanic edifices on Earth, and the generation of natural disasters such as earthquakes and tsunamis resulting in major damages and casualties. Many geophysical studies have been conducted over the Japan Trench to understand the structure of the subducting plate. Detailed slab geometry models Slab 1.0 and

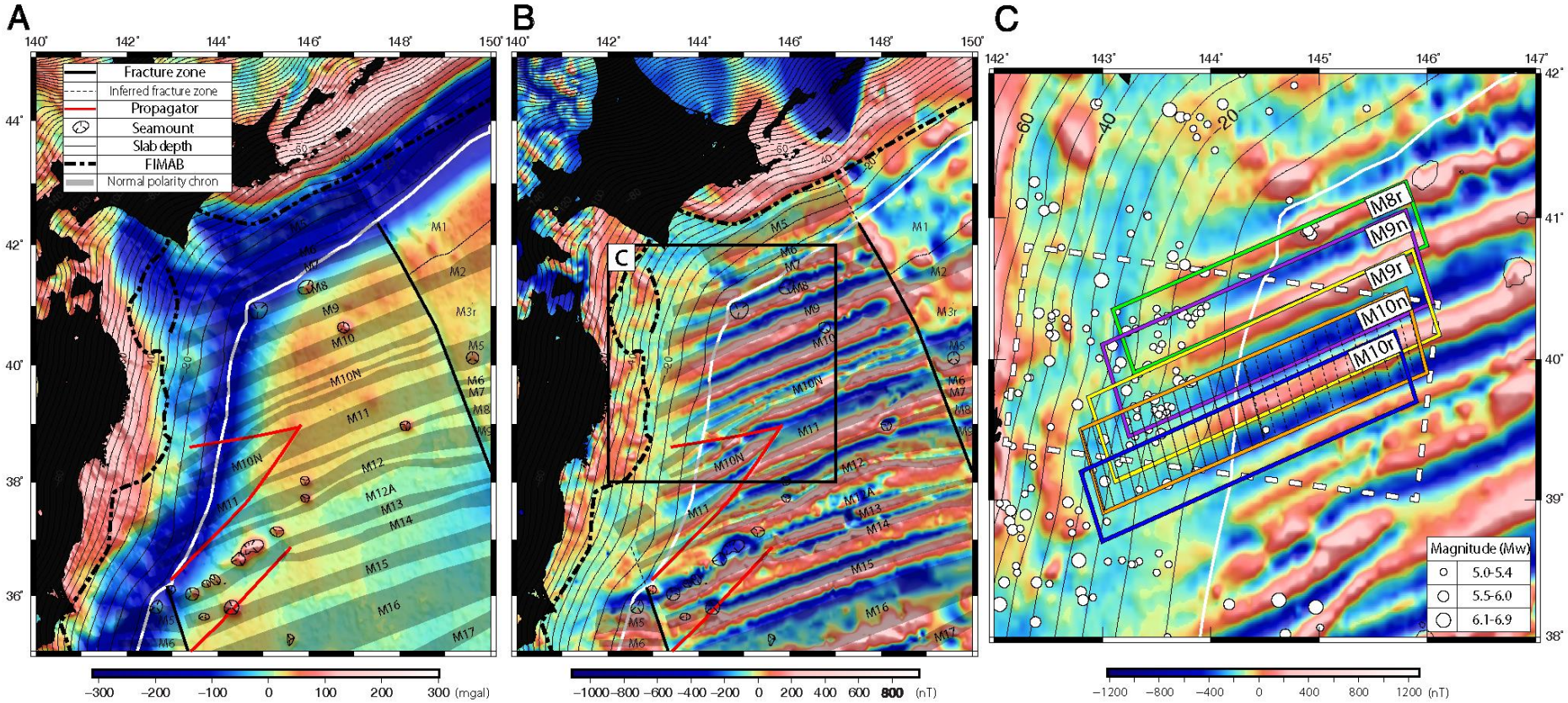

Figure 2-1. A: Free-air gravity anomaly map (Sandwell et al., 2014), B: Magnetic anomaly map in NE Japan, and **C:** Magnetic anomaly map after reduction to the pole (RTP) in detailed area of investigation. The white circles indicate earthquake epicenters (1970-2018) obtained from the Global CMT data base (Dziewonski et al., 1981). The contours in the maps indicate the slab geometry at 5 km depth interval (Hayes et al., 2012). The magnetic anomalies on the oceanic plate align along a regular ENE-WSW direction, only disrupted by propagators (red lines) and fracture zones (black solid lines). Grey-shaded numbered blocks mark the normal polarity intervals. Magnetic anomalies start to fade at the trench (white line) and disappear at ~20 km depth. The Japanese islands are shown in black and the ocean-ward limit of the Fore-arc Induced Magnetic Anomaly Belt (FIMAB) by a thick dashed line in **A** and **B**. The color boxes in **C** indicate the magnetic anomalies suitable for this study. The earthquakes plotted in Figure 2-3B lie within the white dashed box.

Slab 2 (Hayes et al., 2012; 2018) have been developed based on active seismic profiles and seismicity studies. Thermal structure models have been proposed based on heat flow surveys (Hyndman and Peacock, 2003; van Keken et al., 2012; Kawada et al., 2014; Wada et al., 2015). A pioneer study of magnetic anomalies on a subducting plate has shown that, from the Japan Trench landward, the magnetic anomalies decrease in amplitude and their short wavelength content attenuates (Okubo et al., 1991), as a result of increasing distance between the magnetized sources and the observation, thermal demagnetization and continuous oxidation of magnetic minerals within the extrusive oceanic crust (Okubo et al., 1991; Kido and Fujiwara, 2004). Today, the structure of the slab is well constrained (Hayes et al., 2012; 2018), moreover, the magnetic structure of the oceanic crust is better understood (e.g., Dyment and Arkani-Hamed, 1995; Gee and Kent, 2007). Based on this information, the magnetic anomalies over the Japan Trench offer an independent means to access to the slab thermal structure. To address this problem, we take advantage of a unique scalar and vector marine magnetic dataset to build an improved high-resolution magnetic anomaly map. We identify two steps of thermal demagnetization, corresponding to the two major magnetic minerals of the oceanic crust layers, which constrain the thermal structure at shallow depths within the subduction system.

2.3 Geological settings of North-West Pacific

The oceanic crust in the North-Western Pacific plate off Japan was formed about 125-140 Ma at the Pacific-Izanagi plate boundary (Nakanishi et al., 1989). The area is covered by pelagic sediments 1.6 km thick and subducts beneath the Japan islands at a speed of 70-90 km/Ma (Seno, 2017). A thicker and wider accretionary prism is observed in the northern Japan Trench (Kodaira et al., 2017). The free-air gravity anomaly locally delineates seamounts and fracture zones (Fig. 2-1A). In the whole area, it displays a negative anomaly associated to the trench and a positive anomaly on the flexural bulge ~150 km seaward. This bulge reflects the bending of the subducting plate and induces horsts and grabens as the plate approaches the trench (Tsuru et al., 2002; Kodaira et al., 2017).

2.4 Data and methods

Two different sets of marine magnetic data were gathered. Scalar magnetic data (i.e., total field vector intensity) acquired by proton precession magnetometer (PPM) were obtained

from DARWIN of Japan Agency for Marine-Earth Science and Technology (2016), GEODAS of National Center for Environmental Information (2007) and Nautilus of Institut Français de Recherche pour l'Exploitation de la MER (2014). Vector magnetic data (i.e., total field vector components) acquired by shipboard three component magnetometer (STCM), mostly on Japanese research vessels, were obtained from JAMSTEC (DARWIN data base). The International Geomagnetic Reference Field (IGRF) model (Thébault et al., 2015) was subtracted from the PPM data. The STCM data were corrected for the ship magnetic effect and motion by the method of Isezaki (1986). To minimize the misfit at cross over points, a modified cross over error analysis technique was applied both to the PPM data and to the STCM data (see Supplementary information). We reduced the corrected magnetic anomaly grid to the pole (RTP) assuming a 53.6° inclination and -7.6° declination (IGRF averaged over 20 years), 33° paleoinclination and 11° paleoazimuth (average value for the study area from the global grids of Dyment and Arkani-Hamed, 1998).

High resolution bathymetric data were obtained from Global Multi-Resolution Topography (GMRT; Ryan et al., 2009). The top of the magnetic source, i.e. of the extrusive basalt layer, for the subducting plate was computed by merging and correcting different grids. The World sediment thickness grid (Divins, 2003) was subtracted from the bathymetry grid, and the resulting grid was merged with Slab 1.0 (Hayes. et al., 2012; for a discussion on the choice of Slab 1.0 see Supplementary Information) validated by published seismic profiles (e.g., Tsuru et al., 2002; Kodaira et al., 2017). The geometrical misfit between the two grids along the trench boundary was erased and re-interpolated using the Partial Differential Equation (PDE) surface method (D'Errico, 2005).

We carefully selected magnetic anomalies showing no tectonic or volcanic local complexities such as fracture zones, propagators, or seamount. Anomalies older than M10r and younger than M8 are therefore discarded (Fig. 2-1). We extracted profiles from the magnetic grid across the selected anomalies and considered separately the anomaly profiles before and after subduction, i.e. located East and West of the Japan Trench. The anomaly profiles before subduction were inverted to equivalent magnetization assuming a 500-m-thick magnetized source layer with no vertical variation of magnetization (Parker and Huestis, 1974). The equivalent magnetization shows little variation among profiles and has been averaged (Fig. 2-2A). We use this average equivalent magnetization and the inferred top of the magnetic source layer along the anomaly profiles after subduction (Fig. 2-2B) to compute synthetic magnetic anomalies along these profiles (Fig. 2-2C). These modeled anomalies

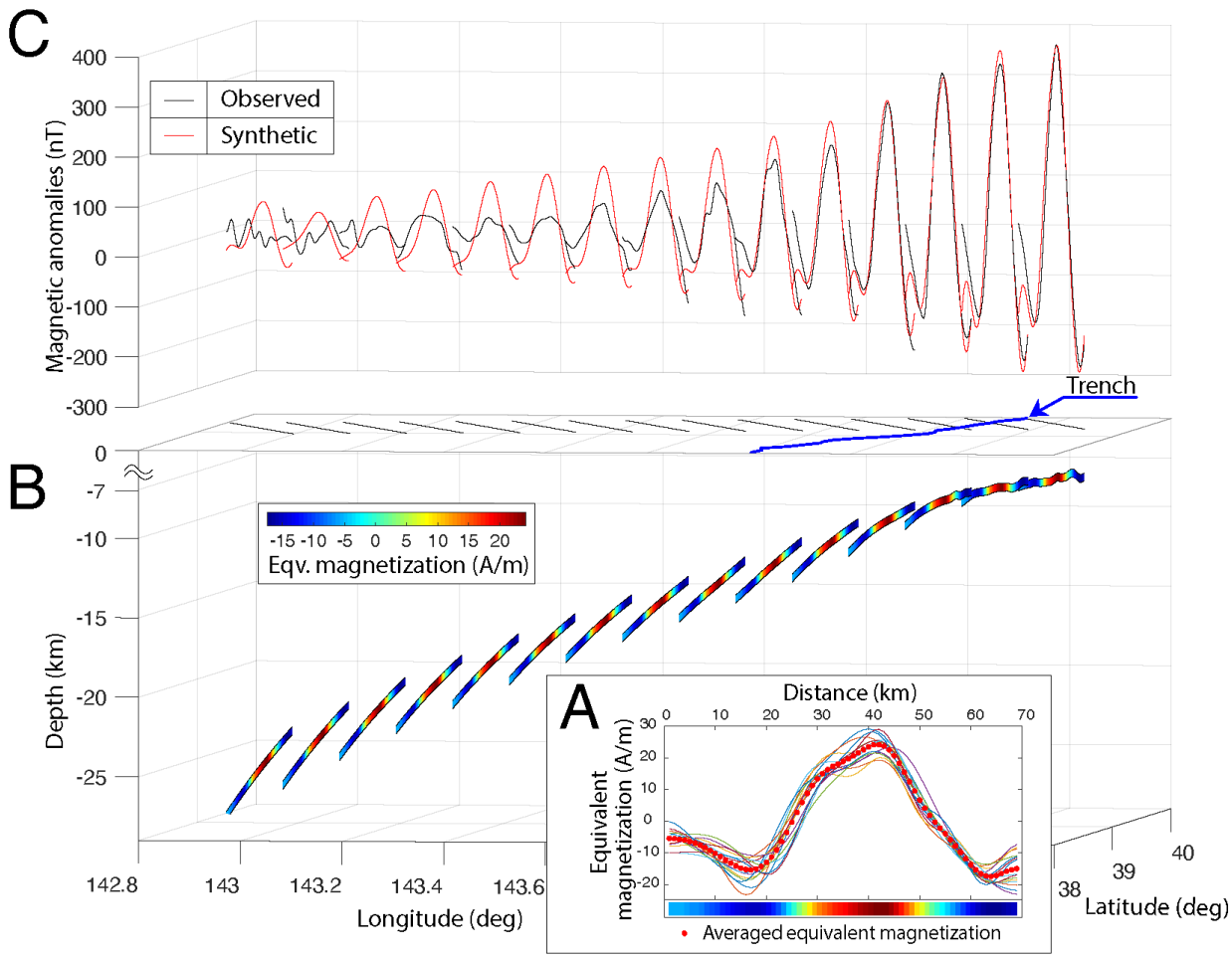

Figure 2-2. A: Equivalent magnetization inverted from profiles across magnetic anomaly M10n before subduction (location: see Fig. 2-1C, black dashed lines in orange box). Red dotted curve indicates the average equivalent magnetization adopted for further modeling. **B:** Three-dimensional view of the source layer and magnetization intensity (color) used to model the synthetic magnetic anomalies. Black solid lines on top indicate location of the profiles (location: see Fig. 2-1C, black solid lines in orange box). Blue solid line on top is the Japan Trench. **C**: Three-dimensional view of the observed (black) and synthetic (red) magnetic anomalies across magnetic anomaly M10n after subduction (location as above). Comparison of the observed and synthetic anomalies show that demagnetization is required to explain the difference of anomaly amplitudes west of 144°E.

represent the contribution of the subducting plate at the sea-surface if the magnetic structure of the plate remains unchanged. Comparison of these synthetic anomalies with the observed ones gives us the opportunity to estimate how the magnetic structure of the plate has been changed (Fig. 2-2C).

The ratio of peak to trough anomaly amplitudes of the observed and synthetic anomalies, hereafter named RAM (Remaining Amount of Magnetization), provides an estimate of the remaining fraction of magnetization in the subducting plate: when it is close to 1, demagnetization remains negligible, whereas when it tends to 0, demagnetization is almost complete. We expect demagnetization to progress as a function of depth, and display RAM as a function of the depth to the top of the magnetized layer under the maximum (resp. minimum) of the observed positive (resp. negative) anomalies (Fig. 2-3).

2.5 A new magnetic anomaly map on the japan trench area

We compiled both scalar and vector marine magnetic data available in the study area and merged them into a unique scalar magnetic anomaly map (Fig. 2-1B). Many gaps in the scalar anomaly coverage could be filled with the vector data. The resulting map shows two types of anomalies. Near the Japanese Islands, a strong positive anomaly (FIMAB in Fig. 2-1) is caused by the induced magnetization of serpentinite in the fore-arc mantle (Okubo and Matsunaga, 1994; Hyndman and Peacock, 2003; Blakely et al., 2005) and, possibly, of the volcanic arc. On the Pacific plate and subducting slab, alternating positive and negative lineated anomalies are caused by the remanent magnetization of the oceanic crust. Magnetic anomalies M5 to M17 (~124.6-139.7 Ma; Malinverno et al., 2012) are identified between two NNW-SSE-trending fracture zones depicted on the free-air gravity anomaly (Fig. 2-1A), confirming the interpretation of Nakanishi et al., 1989).

In our study area, only anomalies M8r-M10r (129.0-130.8 Ma) are suitable for a detailed analysis as they are linear and only disrupted by a few isolated seamounts. They display a clear seafloor spreading magnetic signal before and after subduction (Fig. 2-1A). Conversely, anomaly M5 is still recognizable but totally subducted, while anomalies M6-M7 are only partially subducted beneath the southern Kuril Trench, roughly parallel to the magnetic anomaly trend. The presence of propagating rifts (Nakanishi, 2011) and the Joban seamount chain affect anomalies M10n1-M15 south of 38°40'N. During this period the (half) spreading

rate was 70-80 km/Ma and the studied oceanic crust was formed at a fast spreading center (Nakanishi et al., 1989).

2.6 Magnetic structure of the oceanic crust and progressive demagnetization

The amplitude of the slab magnetic anomalies continuously decreases landward and the anomalies disappear beyond 20 km depth below sea level (bsl) (Fig. 2-1C). The increasing depth of the magnetized source preferentially attenuates the shorter anomaly wavelengths of the anomaly, as does demagnetization of the oceanic crust induced by fluids (alteration) and increasing temperature (thermal demagnetization). To separate the effects of increasing depth and demagnetizationthese effects, we compute synthetic magnetic anomalies assuming unchanged magnetic structure of the subducting plate. The observed anomalies decrease faster than the synthetic ones (Fig. 2-2C). Indeed, the RAM decays rapidly, by 20% per km, between 9-12 km bsl, and more slowly, by 2% per km, beyond (Fig. 2-3A).

The observation of two distinct depth intervals with contrasted RAM decay is in good agreement with our knowledge of the magnetic structure model of oceanic crust formed at fast spreading centers, where two magnetic layers are distinguished (Dyment and Arkani-Hamed, 1995). The shallower one, less than 1~1 km thick (Karson, 2002), is made of extrusive basalt which magnetic mineral is titanomagnetite with various Ti content and oxidation state (Curie temperature Tc 100-350°C, Zhou et al., 2001; Gee and Kent, 2007), the deeper one, ~5 km thick, is made of dolerite, gabbro and serpentinized peridotite in which magnetic mineral is magnetite (Tc 580°C) is the dominant magnetic phase. The Natural Remanent Magnetization (NRM) carried by these layers varies: the extrusive layer bears a strong NRM (> 10 A/m) at the ridge axis which decays to ~3 A/m for old oceanic crust. It is the main contributor to the lineated marine magnetic anomalies observed at sea-surface. Conversely, the dolerite and gabbro bear a weaker NRM (~1 to 1.5 A/m) and the serpentinized peridotite variable NRM (0 to 6 A/m) depending the degree of serpentinization (Harrison, 1987). We, therefore, suggest that the sudden decay of RAM between 9-12 km bsl corresponds to the thermal demagnetization of the extrusive basalt layer and the slow decrease beyond 12 km bsl to that of the deeper layers (Fig. 2-3B). Observed magnetic anomalies beyond 18 km bsl are very low and their shape does not match that of the synthetic ones, precluding the calculation of RAM.

Their short wavelength content is not consistent with the expected depth of subducting slab, suggesting the presence of shallower sources in the upper plate continental crust.

2.7 Thermal structure and earthquakes in the shallow subducting oceanic crust

A global compilation over subduction zones suggests that, apart for local effects, heat flow over oceanic lithosphere entering subduction does not significantly deviate from that of normal oceanic lithosphere (Stein, 2003), whereas a more recent study supports higher heat flow over oceanic lithosphere approaching subduction (Harris et al., 2017). Conversely, heat flow over the fore-arc basin is generally low (Stein, 2003; Yamano et al., 2014). Heat flow measurements on the Pacific plate off the Japan Trench range between 50 and 100 mW/m2, significantly higher than the ~50 mW/m2 expected for oceanic lithosphere of this age (Yamano et al., 2014).

Estimating the slab thermal structure is difficult because the hydrothermal circulation in the accretionary prism and overriding continental crust is hard to quantify. Proposed models consider constraints such as the age of oceanic lithosphere, rate of convergence, shear heating and dip of the slab (van Keken et al., 2012; Wada et al., 2015). However, strong uncertainties remain in the shallow subduction zones on the effectiveness of hydrothermal circulation, the permeability of the igneous crust, and its evolution with depth. Consequently, models propose a wide variety of temperature ranges for the shallow subducting slab. For instance, the obtained temperatures are as low as ~100-200 °C from the deformation front to 20 km depth (Hyndman and Peacock, 2003; van Keken et al., 2012; Wada et al., 2015), a consequence of the rapid convergence of old oceanic crust (van Keken et al., 2012). Our study suggests that the Curie temperature of titanomagnetite, within the range 150-350°C, is reached by the extrusive basalt layer at 9-12 km bsl, and the Curie temperature of magnetite, 580°C, is reached by the deeper crustal layers when the slab surface is at 20 km bsl (i.e. at ~22-26 km bsl considering the initial depth of these layers). These temperatures are significantly higher than those predicted by most published models. They agree better with the background thermal gradient of 26.29° ± 0.13°C/km measured on the overriding plate near the trench (Fulton et al., 2013), which predicts 170°C at 10 km bsl (6.5 km below seafloor) and 460°C at 20 km bsl (17.5 km bsf).

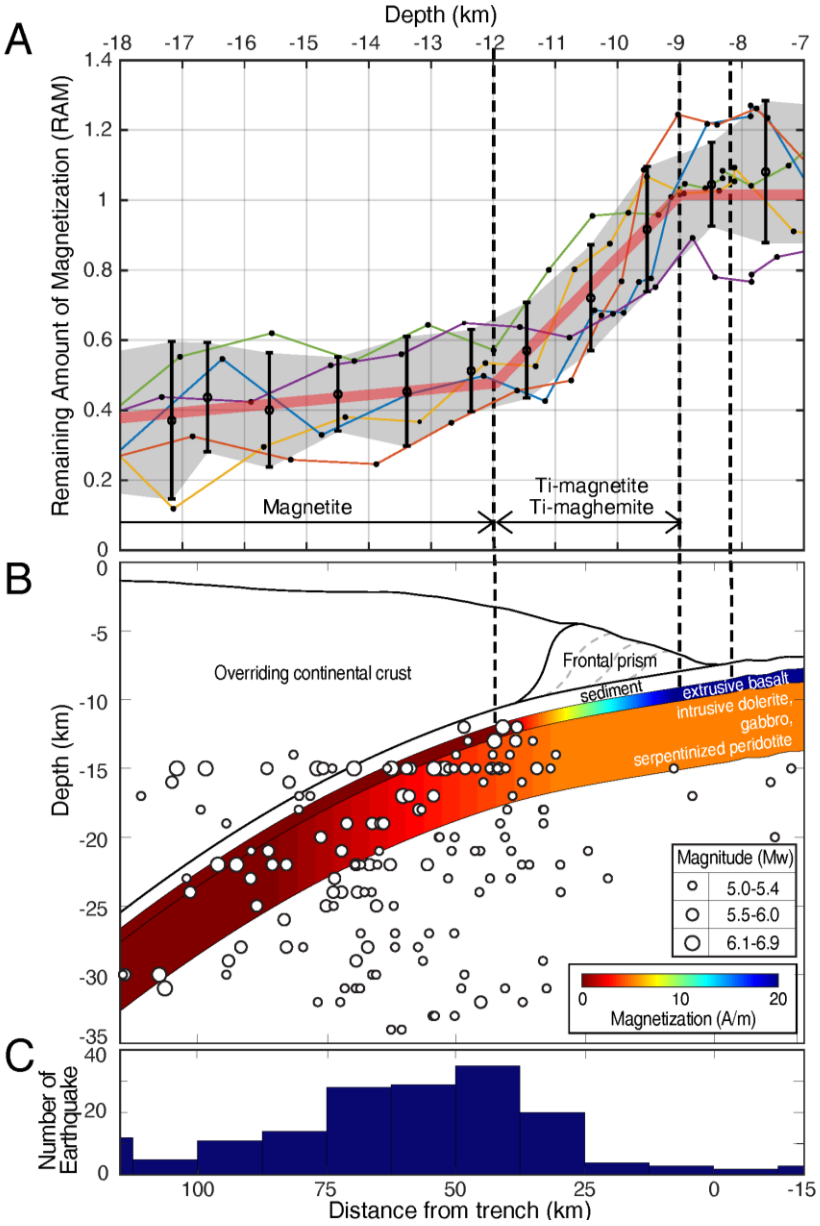

Figure 2-3. A: Remaining Amount of Magnetization (RAM) versus depth of the top of the magnetic layer for the subducting plate. Colored lines correspond to a magnetic anomaly shown by a similarly colored box on Fig. 2-1C. Averaged RAM within 1 km depth intervals are shown by circles with error bars (σ=1), and confidence limits by the shaded area. Thick red line summarized the RAM variation with depth: (1) between 7-9 km, i.e. before and immediately after subduction, the RAM is equal to 1; (2) between 9-12 km, the RAM decays rapidly as a result of alteration and/or thermal demagnetization of the extrusive basaltic layer; and (3) beyond 12 km, the RAM decreases slowly, reflecting the thermal demagnetization of the deeper crust. **B:** Schematic illustration of decaying magnetization in the different layers of the oceanic crust based on the result in A. Earthquake hypocenters are shown by circles of size proportional to magnitude. The magnetization of the extrusive basaltic layer decreases rapidly and disappears between 9-12 km depth; the magnetization of the deeper oceanic layers slowly decays and disappears at ~20km depth. **C:** Number of earthquakes per 12.5 km-intervals versus distance from the trench. The number of earthquakes sharply increases 25 km landward from trench (~10 km depth) and suddenly decreases 75 km landward from trench, where the slab depth is ~ 18 km.

A recent study explains the high heat flow before subduction by rejuvenated hydrothermal activity induced by the flexural bending of the lithosphere and associated normal faults (Kawada et al., 2014). After entering subduction, the convecting fluid mines heat from depth but is prevented to transfer this heat upward by the thick sediments of the accretionary prism, the subducted pelagic sediments, and possibly an impermeable decollement surface, warming up the subducting oceanic crust through thermal blanketing (e.g., Granot and Dyment, 2019). Additional heat may be provided by serpentinization, i.e. the hydration of mantle rocks by the percolating fluid, an exothermic transformation most active between 100 and 400°C (MacDonald and Fyfe, 1985) reported in various active tectonic contexts involving the oceanic crust – slow seafloor spreading (Kelley et al., 2001), compressive deformation (Delescluse and Chamot-Rooke, 2008), and subduction (Grevemeyer et al., 2018). Conversely, the frictional heat generated by recurring megathrust earthquakes, although reaching high temperatures (Yang et al., 2016) for a short time at a very local scale, remains negligible if the estimate of Fulton et al. (2013) is considered.

A warmer subducting oceanic crust has implications on the rheology of the subducting slab. The brittle-ductile transition in basalt occurs at 550 ± 100°C (e.g., Violay et al., 2012). If our inference on the Curie temperatures are correct, this depth is reached at ~20 km, explaining why most earthquakes of magnitude stronger than 5 are observed at depths < 20 km, as Fig. 2-3C suggests despite the poor vertical resolution of epicenter determinations.

2.8 Acknowledgement

We thank Jeff Gee, Ingo Grevemeyer, and an anonymous reviewer for their helpful comments. We also thank Koichiro Obana for providing precise earthquake catalogs even though we could not use them due to their limitation in deeper area. HC has been supported by an Ecole Doctorale STEP'UP Fellowship. We thank all scientists and crews who collected the marine geophysical data used in this study. This is IPGP contribution 4089.

2.9 Supplementary materials

2.9.1 Supplementary method :

Crossover correction for scalar and vector magnetic anomalies

Reliable marine magnetic data are generally acquired by deploying a proton precession magnetometer (PPM), which provides absolute measurements of the field vector intensity that can be immediately used after removing a core field model. To try to access the three components of the field vector and, in some cases, to avoid the deployment of a PPM, shipboard three-component magnetometers (STCM) have been installed on research vessels, mostly in Japan. As a result, large amounts of STCM data are available around the Japan Trench and cover areas where PPM surveys have not been conducted so far (Fig. 2-S1). However, STCM data requires some heavier processing to remove the ship magnetic effect and recover the magnetic field in proper geographical coordinates (Isezaki, 1986). Despite correction of the induced and remanent magnetization of the ship, other magnetic effects remain that prevent merging the magnetic anomalies obtained from STCM data, which are only relative, together or with those derived from the absolute PPM data (Fig. 2-S2A and B).

We built our magnetic map of the Japan Trench by first considering the absolute PPM data, then including the relative total field computed from the STCM data. The PPM data gathered from different cruises and databases are leveled (for instance using X2SYS, a crossover analytic tool available in GMT; Wessel, 2010). In the next step, the corrected PPM data are used as a reference to tie the STCM surveys at their intersections. To do so, we first attempt to apply a constant leveling to individual cruise, but erroneous linear trends remain along STCM tracks (Fig. 2-S2C). These errors may result from the accumulation of viscous magnetization by the ferromagnetic ship body as the ship keeps the same heading. This effect is not taken into account by Isezaki (1986). Viscous magnetization is difficult to estimate for a cruise with changing headings. To approximate its effect by a linear trend, we split the STCM survey tracks in straight segment lines.

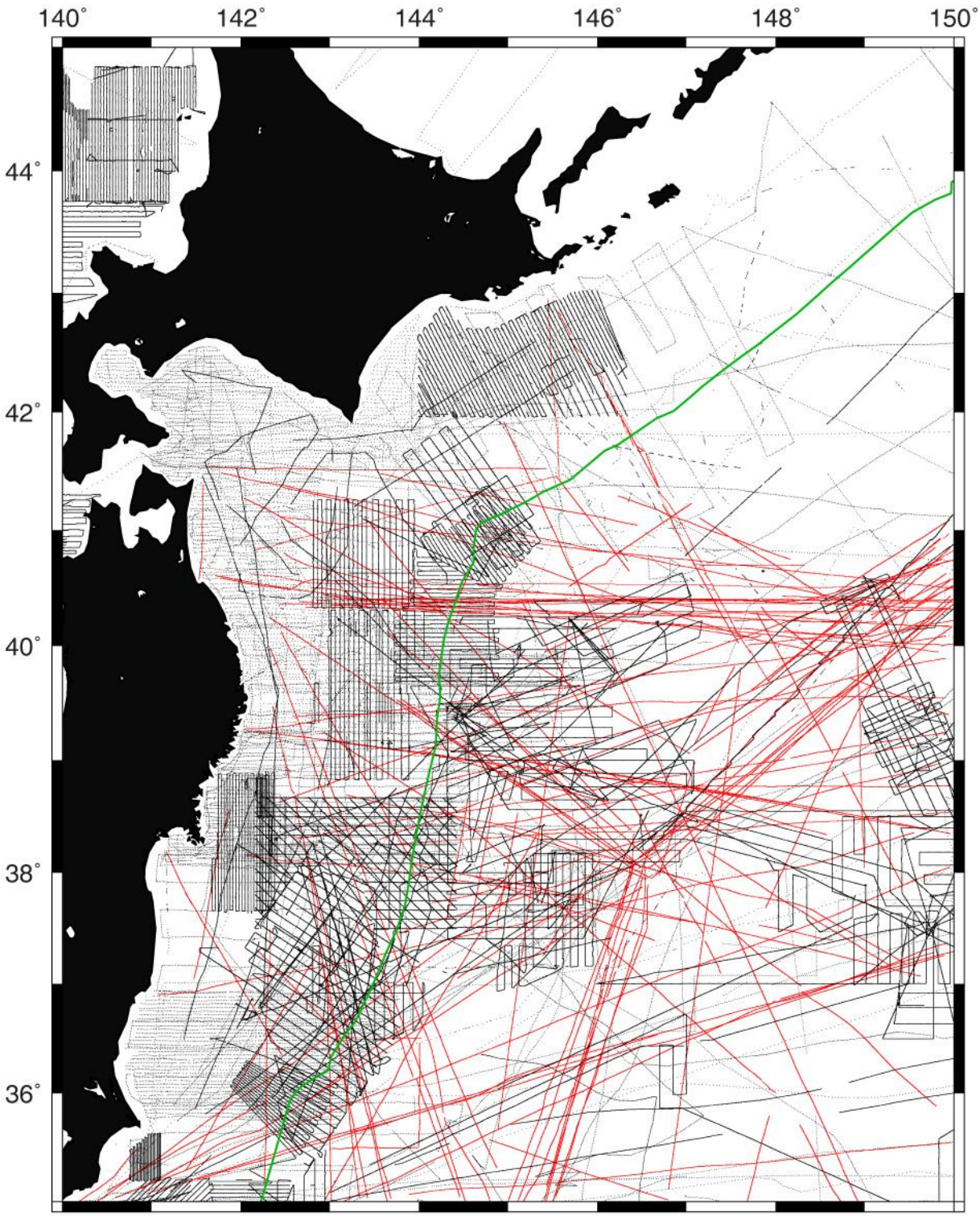

Figure 2-S6. Marine magnetic surveys NE of Japan. Red solid lines display the STCM survey tracks, black solid lines the PPM survey tracks. The green solid line shows the Japan and Kuril trenches.

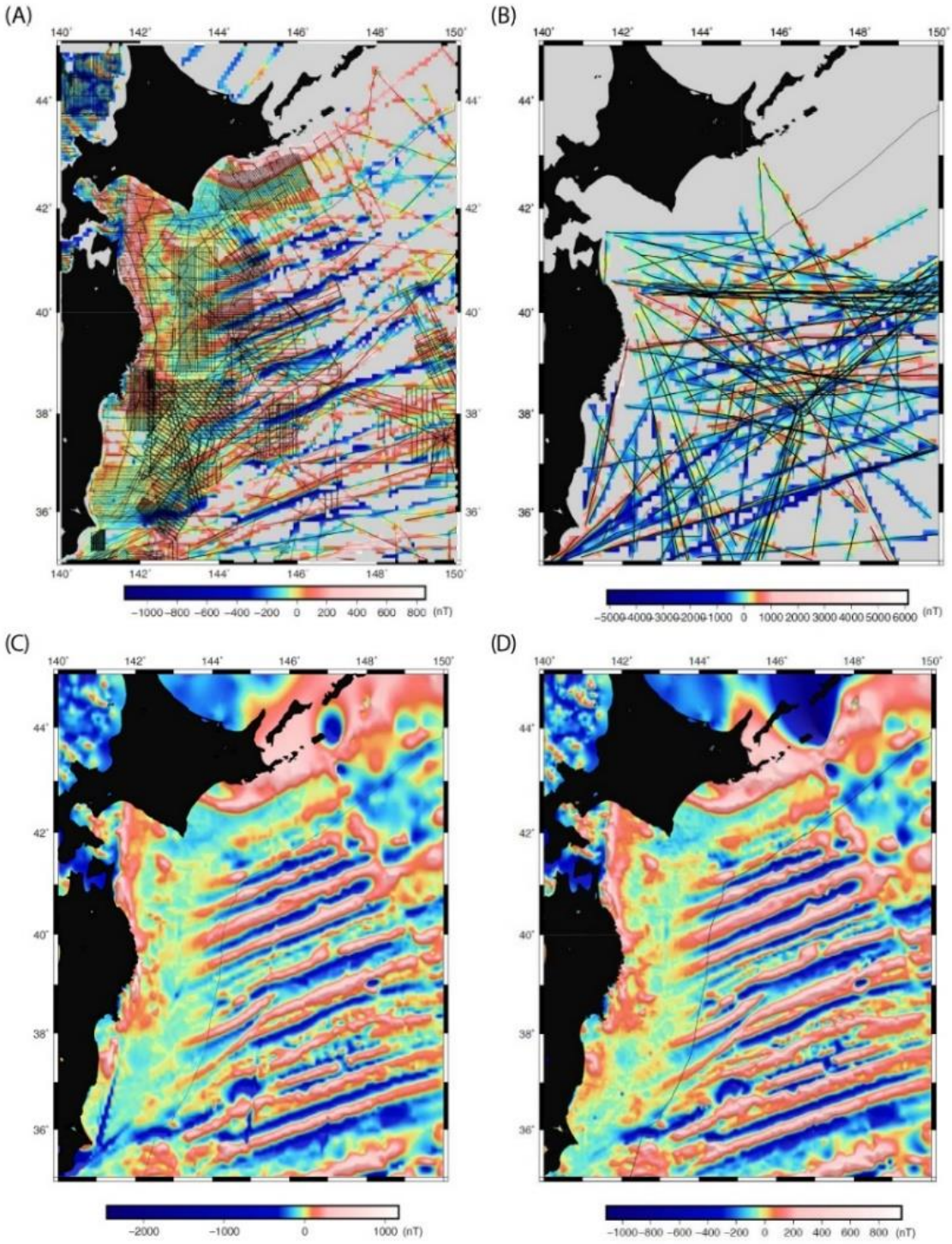

Figure 2-S2. (A) Magnetic anomaly grid from the leveled PPM data; (B) Magnetic anomaly grid from the corrected STCM data; (C) Magnetic anomaly grid after leveling the corrected STCM data to adjust them to the leveled PPM data; (D) Magnetic anomaly grid after leveling and de-trending the corrected STCM data to adjust them to the leveled PPM data.

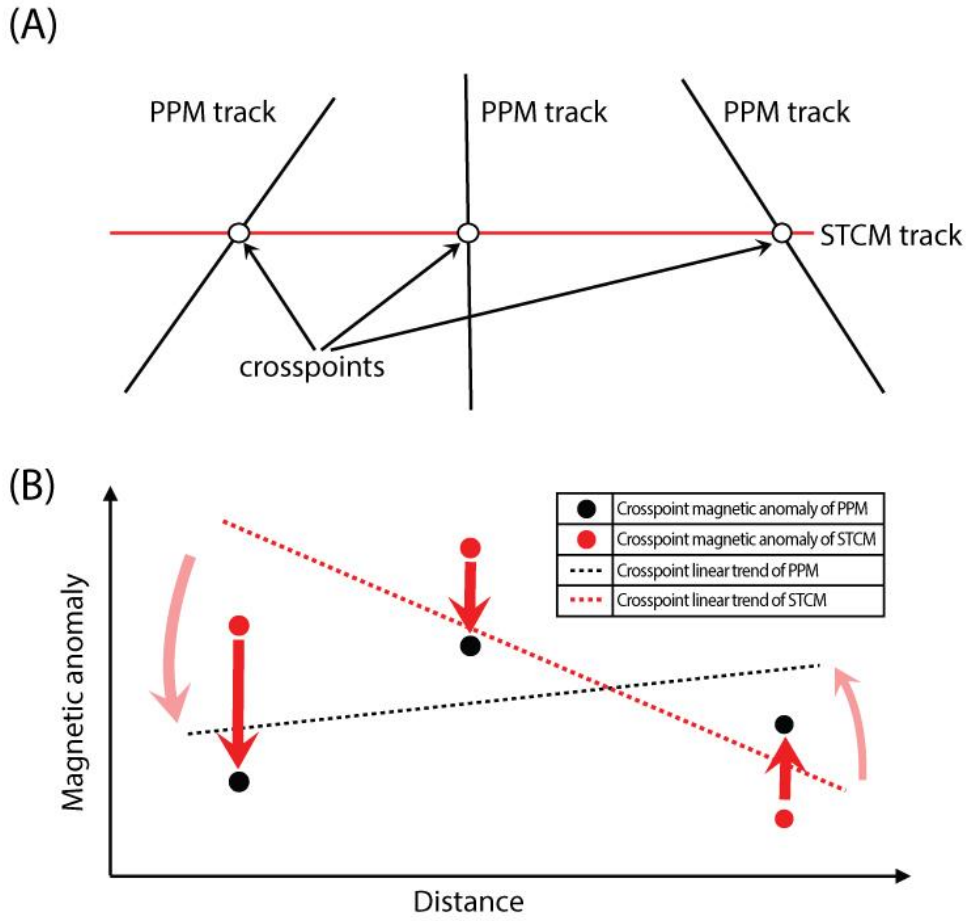

Figure 2-S3. Schematic explanation of crossover method. The method is applied to de-trend the STCM data to adjust them to the PPM data.

We apply a linear regression method at crossover points between the considered STCM segment and the PPM data. We determine the crossover points and average separately the PPM and STCM values for each crossover point within 1 arc-minute radius. If only one crossover point exists or if there are only two and the distance between them is less than 20 km, we discard the STCM segment. We compute separate linear trends from the PPM and STCM values at the crossover points of the segment to evaluate the residual trend, i.e. the difference between the linear trends from STCM values at crossover points and from PPM values at the same points and remove it from the STCM data (Fig. 2-S3). This method properly eliminates the misfit between the STCM and PPM data, as shown by an example with real data (Fig. 2-S4).

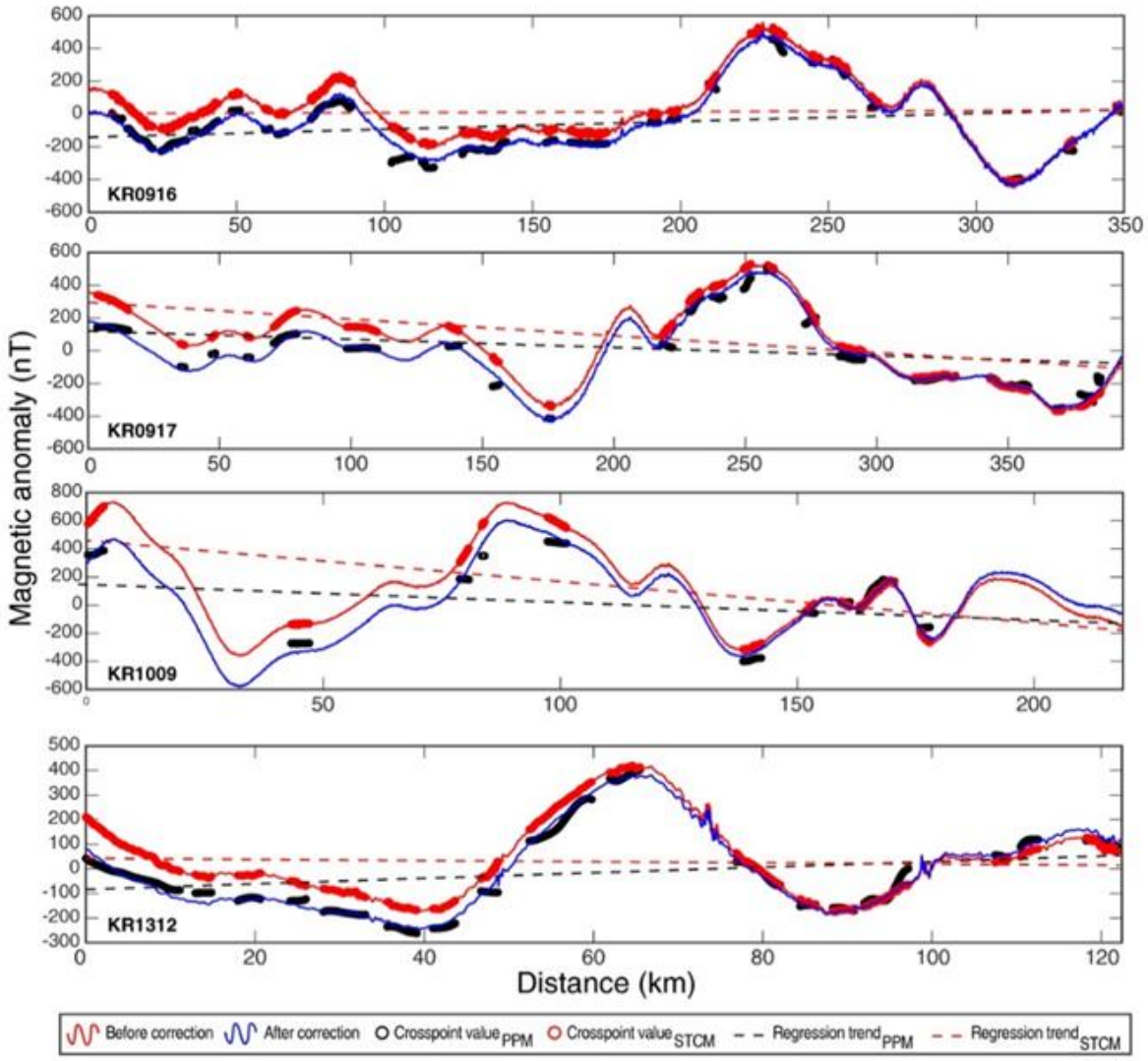

Figure 2-S4. Method to de-trend the STCM data to adjust them to the PPM data applied to real data. Red solid line, STCM data affected by the ship viscous magnetization approximated by a linear trend; Red circles, STCM at crossover points; Red dashed line, linear regression of STCM at crossover points; Black circles, PPM at crossover points; Black dashed line, linear regression of PPM at crossover points; Blue solid line, corrected STCM data after removing the linear trend from STCM at crossover points and adding the linear trend on PPM at crossover points.

The histogram of the misfits shows the significant improvement obtained by de-trending the STCM data along straight segments compared to the simple leveling of the STCM data cruise by cruise and to the initial data (Fig. 2-S5). The standard deviation (1σ) is 104.9 nT, 68.9 nT and 49.2 nT for the original data, the leveled data using the conventional crossover analysis method, and our crossover algorithm including de-trending of the data.

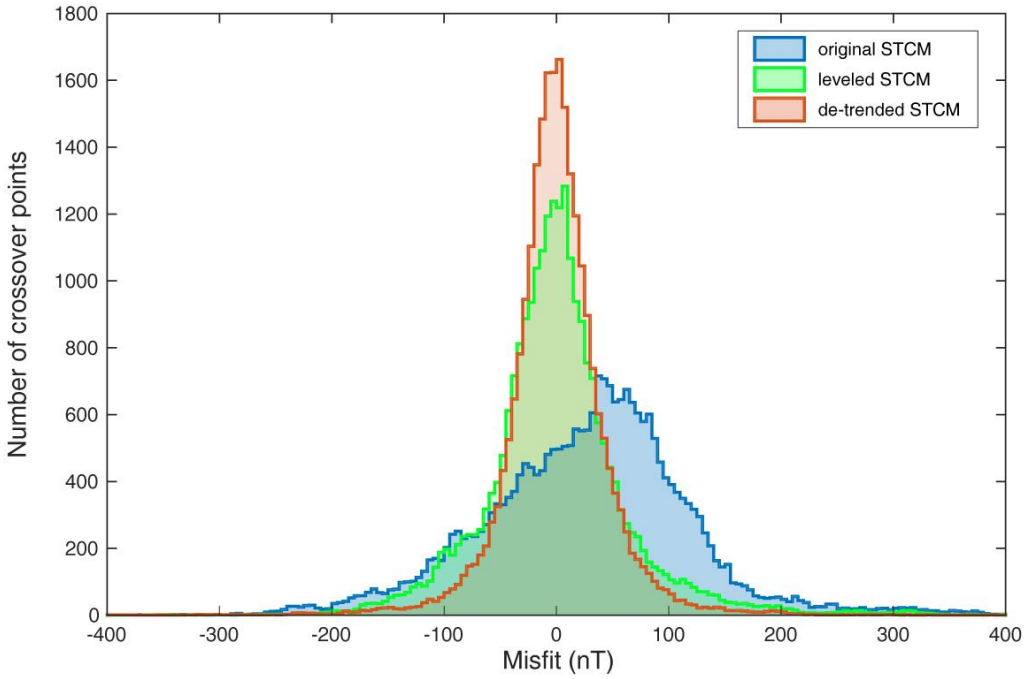

Figure 2-S5. Histogram of the misfits between leveled PPM data and various sets of STCM data. Blue, initial STCM data; Green, STCM data leveled cruise by cruise; Red, STCM data de-trended along straight segments.

We analyze the relationship of the residual trends obtained from R/V Kairei and R/V Mirai with the ship heading (Fig. 2-S6). Despite significant scatter, the residual trend shows a symmetrical distribution that can be approximated by a sine function of the ship heading. Although this is verified for datasets from both R/V Kairei and R/V Mirai, the residual trends for these two ships show opposite signs.

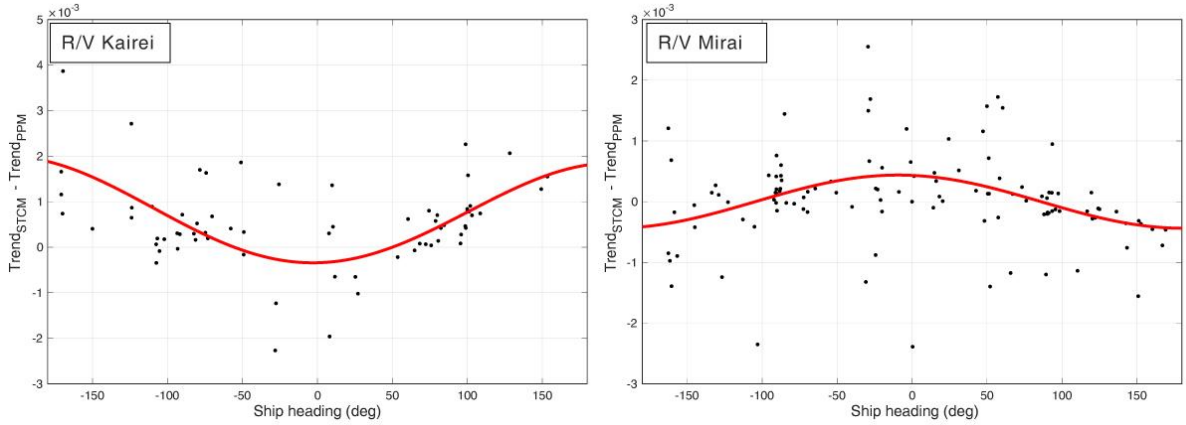

Figure 2-S6. Relationship of the residual trend with the ship heading. Black dots, data from R/V Kairei (left) and R/V Mirai (right). Red solid lines, best fitting Sine functions.

To understand these observations, let consider the ship as a big magnet (Fig. 2-S7). In mid-latitudes, such a magnet produces a dipolar anomaly with a positive lobe toward the Equator and a negative lobe toward the pole (see Dyment and Arkani-Hamed, 1998; Fig. 2-1B, for examples). We can therefore suspect that the STCM is located forward on R/V Kairei (resp. backward on R/V Mirai) to sample the negative (resp. positive) lobe when the ship is heading North. When the ship is heading in different directions, the STCM is sampling different parts of the ship magnetic anomaly. Instead of the anomaly - as it would be in a very similar way if we were discussing the effect of induced magnetization, Figure 2-S6 and 2-S7 are considering the linear trend of the anomaly created by viscous magnetization. These figures offer a way to model and possibly correct the ship viscous magnetization in future surveys.

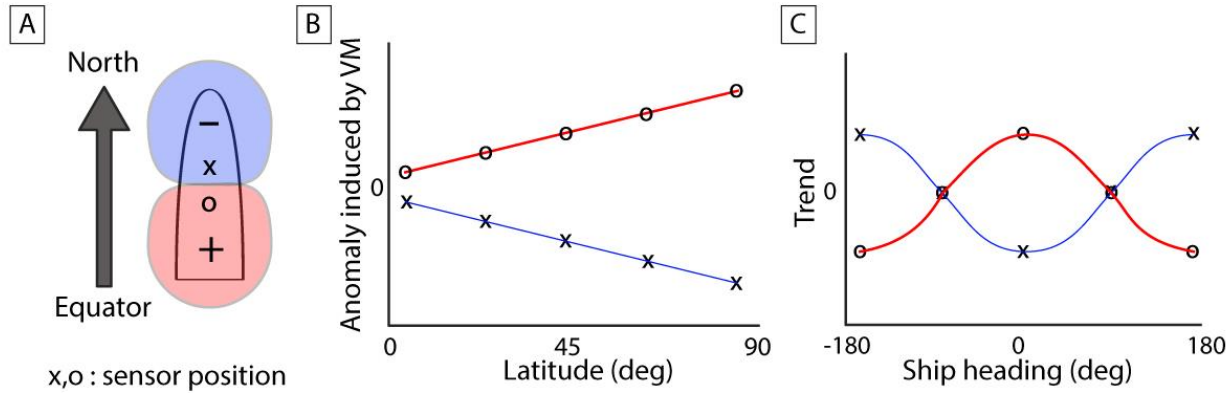

Figure 2-S7. (A) Schematic illustration of the magnetic anomaly of a ferromagnetic ship body when the ship is heading to the north at northern mid-latitudes. “X” and “O” signs mark the location of the STCM sensor on R/V Kairei and R/V Mirai, respectively. (B) Expected magnetic field variations trlated to the acquisition of viscous magnetization, following Fig. 2-S7A. (C) Predicted relationship of the residual trend with the ship heading for R/V Kairei (blue) and R/V Mirai (red).

2.9.2 Supplementary discussion:

Uncertainties in the slab geometry

Currently, two open-source slab grids, Slab1.0 (Hayes et al., 2012) and Slab2 (Hayes et al., 2018), are widely used for various geophysical analysis. A careful analysis of Fig. 2-3A (see main text) reveals that the maximum gradient of the remaining amounts of magnetization (RAM) is not observed at the exact same depths for the five investigated magnetic anomalies. These small discrepancies may result from uncertainties in the slab geometry. In order to choose the best slab geometry grid, we compared the two grids to recently published seismic sections in the study area (Kodaira et al., 2017) and observed a good coincidence between the seismic sections and Slab1.0, and significant discrepancies reaching 4 km with Slab2 (Fig. 2-S8).

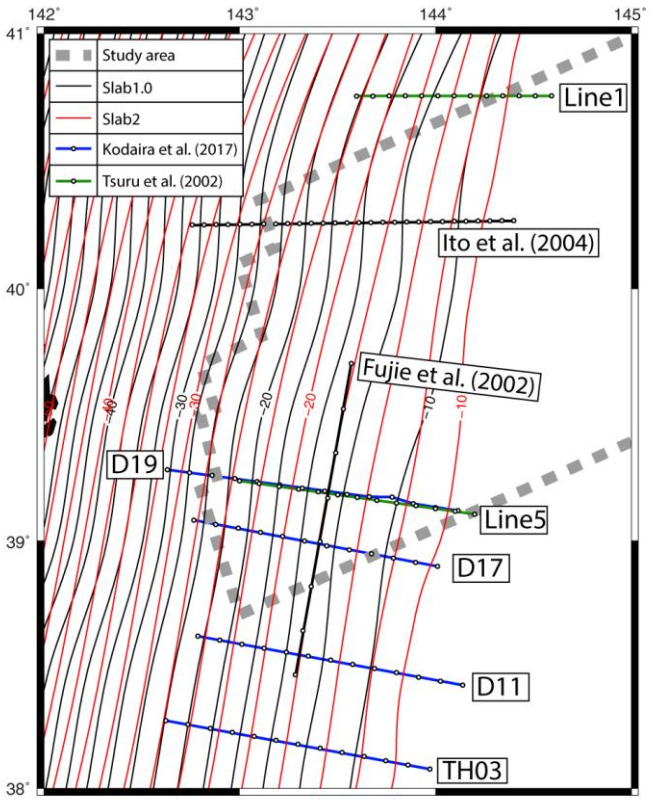

Figure 2-S8. Comparison between the two slab grids and published seismic profiles. Black solid lines indicate the grid contour of Slab1.0 (Hayes et al., 2012); Red solid lines indicate the grid contour of Slab2 (Hayes et al., 2018). The interval of grid contour depths is 2.5 km. Blue solid lines with black circles indicate active seismic lines of Kodaira et al. (2017). Green solid lines with black circles indicate active seismic lines of Tsuru et al. (2002). Black solid lines with black circles indicate survey tracks used in Fujie et al. (2002) and Ito et al. (2004).

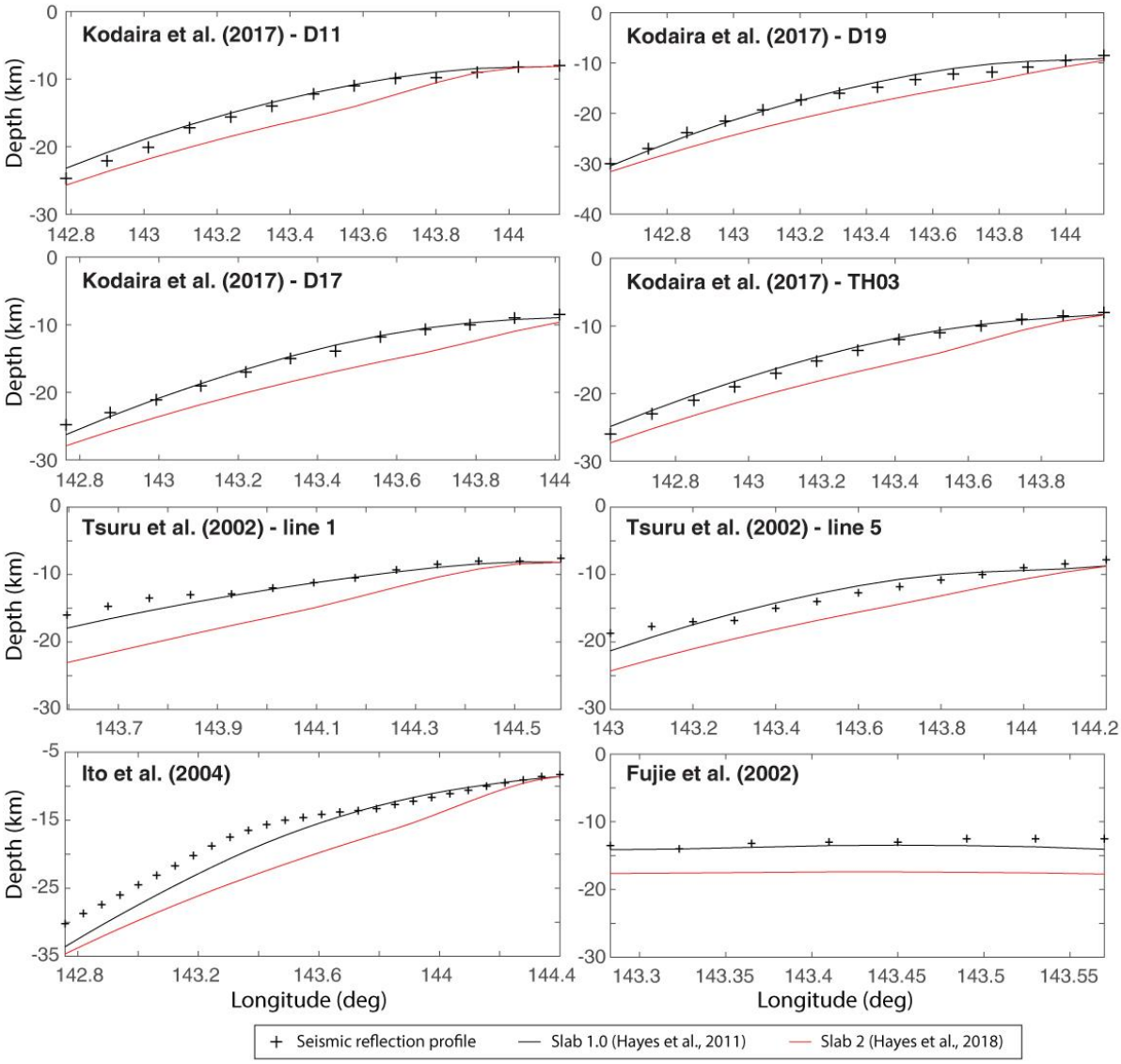

Figure 2-S9. Comparison between slab geometry from seismic data (black crosses) and the two Slab grids along each seismic line (black solid line from Slab1.0, red solid line from Slab2). Slab1.0 agrees well with the seismic profiles whereas Slab2 is systematically deeper.

Fig. S9 shows the slab depth along the four seismic lines. Comparison between depths from the seismic profiles and the two slab grids shows unambiguously that Slab1.0 has much smaller misfits (usually less than ± 2 km) than Slab2, which predicts generally a deeper slab and larger misfits (2 to 5 km). We suspect that the degraded slab geometry in Slab2 results from improper digitization of Figure 1B of Kodaira et al. (2017), which extends in longitude from 142°E to 144.75°E. This fractional eastern bound may have misled the digitizer. We therefore decided to use Slab1.0 in our analysis.

2.9.3 Supplementary discussion:

Effect of a dipping slab on the inclination and declination of magnetization, consequences on the amplitude of magnetic anomalies

The slope of the subducting oceanic lithosphere gradually increases with depth. This increasing slope causes a progressive change in the direction of the remanent magnetization vector. Slight changes in this direction may generate significant effect on the synthetic magnetic anomalies, affecting the determination of the Remaining Amount of Magnetization (RAM; see Data and Methods section). In this appendix, we examine this effect for the Japan Trench area and compare the amplitude of modeled anomalies considering, or not, the tilt induced by the slab geometry.

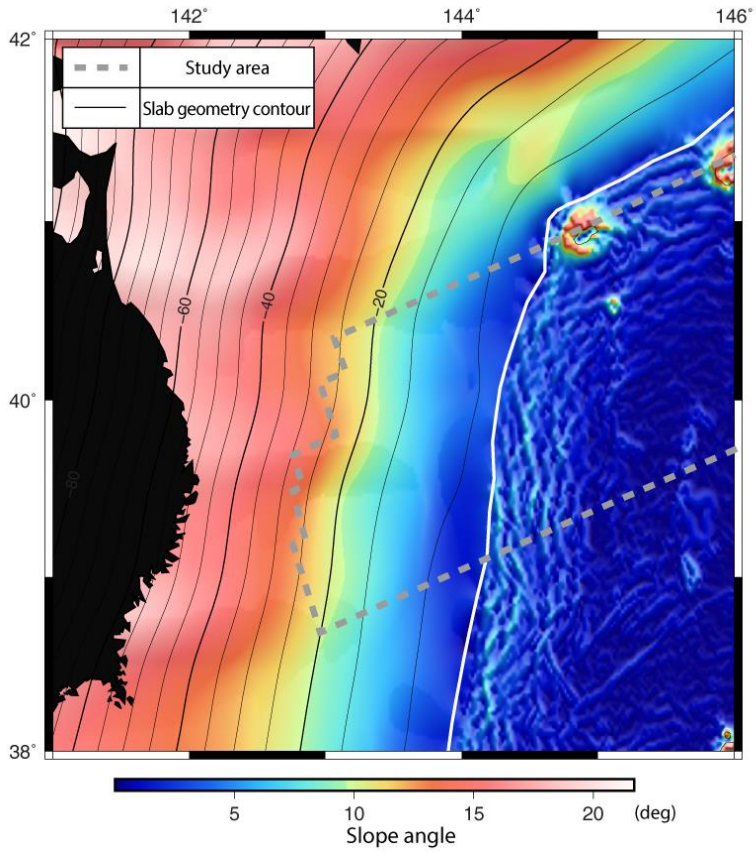

Figure 2-S10. Tilt angle grid of subducting oceanic crust based on Slab1.0. Gray dashed line indicates study area in the main text. Black solid lines indicate the grid contour of Slab1.0 (Hayes et al., 2012). The interval of grid contour depths is 5 km. White solid line describes the location of Japan Trench.

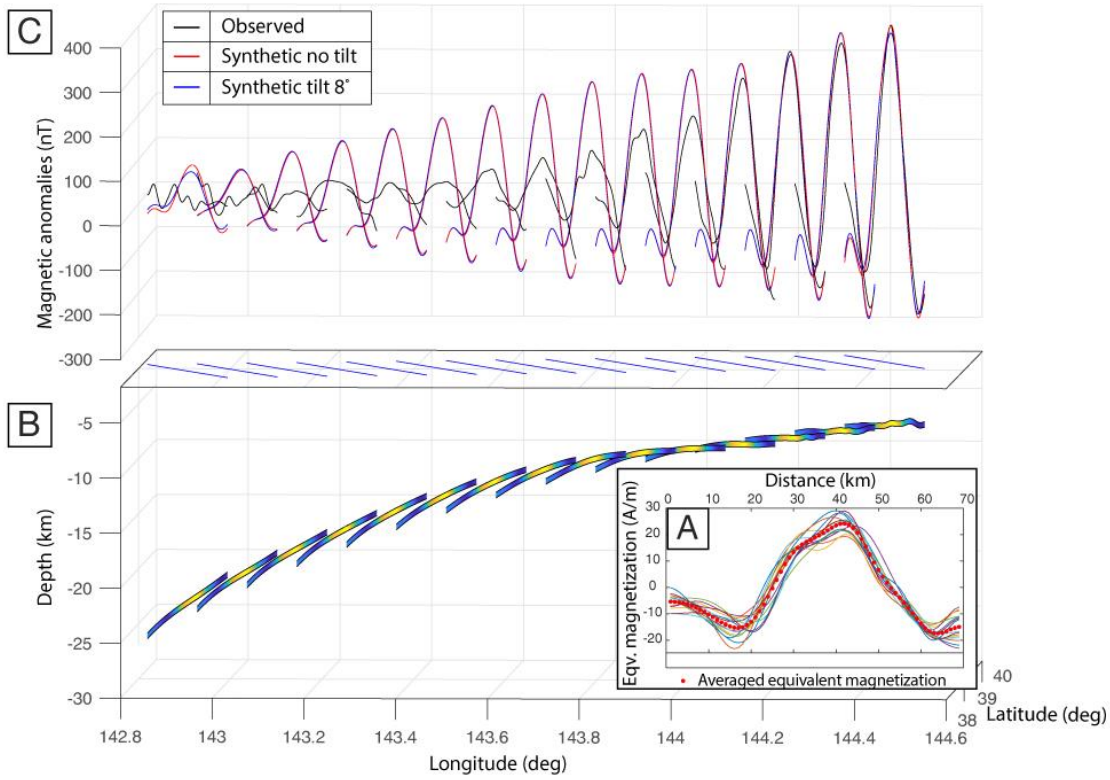

Figure 2-S11. **A:** Equivalent magnetization inverted from profiles across magnetic anomaly M10n before subduction (location: see Fig. 1C, orange box). Red dotted curve indicates the average equivalent magnetization adopted for further modeling. **B:** Three-dimensional view of the source layer and magnetization intensity (color) used to model the synthetic magnetic anomalies. Blue solid lines on top indicate location of the profiles. **C**: Three-dimensional view of the observed (black), synthetic magnetic anomalies with no tilt (red) and with a tilt of 8° (blue) across magnetic anomaly M10n after subduction.

The slope of the source geometry, shown in Figure S10, increase from a bit less than 3° west of the Japan Trench to 10° at 20 km bsl, where the seafloor spreading magnetic anomaly disappear. To check the effect of tilting the magnetization vector beneath 12km bsl, we used a 82° inclination and 103° azimuth (respectively a 90° inclination) to forward-model reduced-to-the-pole magnetic anomalies taking the tilt into account (respectively not taking the tilt into account). We compared the difference of these synthetic anomalies (Fig. S11) and the difference of the RAM deduced from these anomalies (Fig. S12). These difference are negligible and do not affect the result of our study.

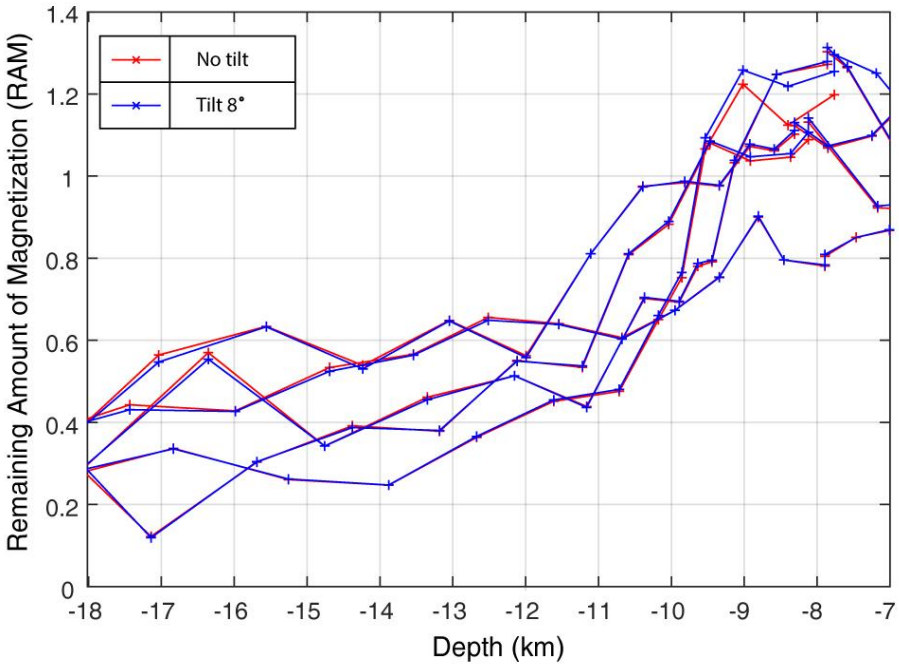

Figure 2-S12. Remaining Amount of Magnetization (RAM) versus depth of subducting slab surface. Blue (respectively red) crosses and solid lines indicate the RAM considering (respectively not considering) the tilt of the remanent magnetization vector. The result shows no significant change in RAM values.

Chapter 3.

Decreasing magnetization, lithospheric flexure and rejuvenated hydrothermalism off the Japan-Kuril subduction zone

3.1 Abstract

Seafloor spreading magnetic anomalies formed at mid-ocean ridges initially display strong amplitudes that decay within the first 10 million years as a result of pervasive hydrothermal circulation and alteration. The amplitudes do not vary much for older oceanic crust, suggesting that the thickening sediments hinder heat advection. Here we show, however, that a systematic loss of ~20 % in the amplitude of the anomalies arises between the outer rise and the trench on old ocean crust approaching the Japan and Kuril subduction zones. We interpret this decay as reflecting the opening of normal faults and fissures caused by extension on the outer flexural rise, and the subsequent renewed circulation of seawater into the oceanic crust, resulting in additional alteration of the magnetic minerals. This interpretation is supported by higher heat flow and seismic velocity changes observed toward the trench.

3.2 Introduction

The part of the Pacific plate subducting into the Japan and Kuril subduction zones has been formed at fast spreading rate (70-80 km/My) between Chrons M5 and M17 (e.g., Nakanishi et al., 1989), 124.6-139.7 Ma (Geomagnetic Polarity Time Scale of Malinverno et al., 2012), and is subducting at a rate of 70-90 km/My (Seno, 2017). It is covered with 0.5-1.0 km-thick pelagic sediments (Tsuru et al., 2002; Fujie et al., 2016). Satellite-derived free-air gravity anomaly (Sandwell et al., 2014; Figure 1a) clearly show the Japan and Kuril trenches and two NNW-SSE-trending major fracture zones. A positive, long-wavelength free-air gravity anomaly (~50 mgal) marks the outer rise structure, due to the flexure of the thick oceanic lithosphere approaching subduction zone, ~140 km seaward from the Japan Trench and ~120 km from the Kuril Trench. (Fig. 3-3D). Recent seismic and electro-magnetic studies suggest

that the normal faults induced by lithospheric flexure at the subduction zone causes increasing hydration of the oceanic lithosphere (Ranero et al., 2003; Key et al., 2012; Fujie et al., 2018).

Magnetic anomalies formed by seafloor spreading initially exhibit strong intensities that decay within the first 10-15 million years as a result of pervasive hydrothermal circulation and alteration (Dyment et al., 2015). The alteration of the magnetic minerals only takes place where seawater meets the oceanic rocks along cracks and faults (Zhou et al., 2001). After 10-15 Ma, 1) the temperature cools down and the hydrothermal circulation decreases, 2) there is no further generation of cracks and faults, 3) sediments make more difficult the influx of additional seawater, and 4) the existing paths for hydrothermal circulation get gradually clogged (e.g., Lister, 1972; Hutnak and Fisher, 2007). As a result, the magnetic minerals that are accessible to the hydrothermal fluid are fully altered, but those that are out of reach are still bearing a significant magnetization: there is no alteration of additional material and the magnetization of the oceanic crust becomes quite stable, until the magnetic anomaly finally disappear in subduction zones (Okubo et al., 1991).

In a previous work (Choe and Dyment, 2020), we studied the decay of marine magnetic anomalies associated to the subducting slab in the Japan Trench area to evaluate quantitatively the effects of the increasing distance to the magnetic source and thermal demagnetization of the slab (Okubo et al., 1991; Kido and Fujiwara, 2004) using the well-defined slab geometry. While analyzing the same magnetic anomalies prior subduction for reference, we noted that the magnetic anomaly amplitude seems to decrease while approaching the subduction zone. Such a decrease may be due to a deepening basement (i.e. increasing distance to the magnetized source), a geological process, or a combination of both effects.

In this paper we confirm the systematic decrease of seafloor spreading magnetic anomalies approaching the Japan and Kuril subduction zones by analyzing a high-resolution magnetic anomaly map compiled from the unique scalar and vector marine magnetic anomaly dataset available on the area. We ascribe this decrease to rejuvenated hydrothermal circulation and the associated low-temperature alteration induced by flexure-related normal faults and fissures.

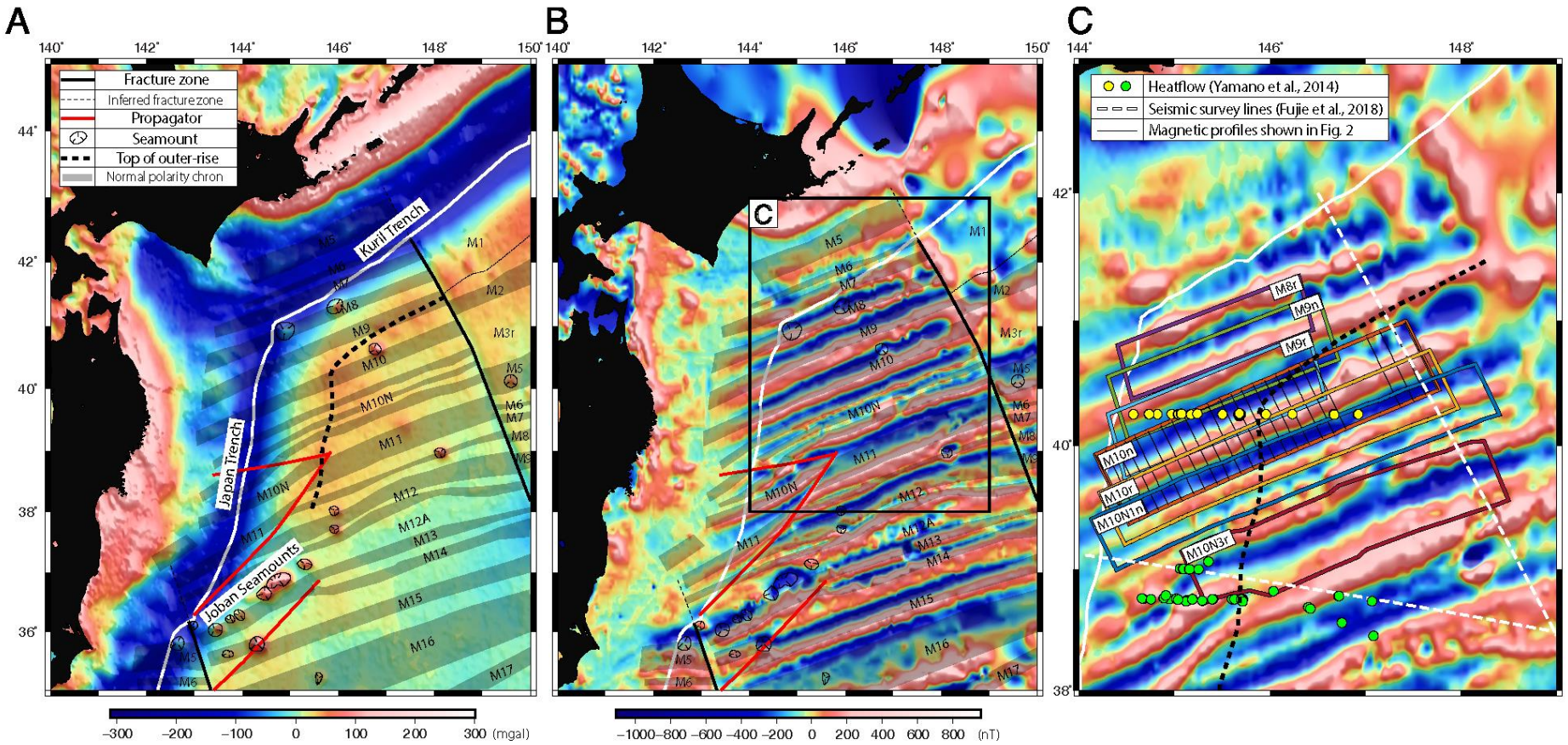

Figure 3-1. A: Free-air gravity anomaly map (Sandwell et al., 2014). **B:** Magnetic anomaly map in NE Japan. **C**: Magnetic anomaly map after reduction to the pole (RTP) in detailed area of investigation. The magnetic anomalies on the oceanic plate trend ENE-WSW, only disrupted by propagators (red lines) and fracture zones (black solid lines). Grey-shaded numbered blocks mark the normal polarity intervals. The Japanese islands are shown in black and the top of outer rise structure by a thick dashed line in **A** and **C**. The color boxes in **C** indicate the magnetic anomalies suitable for this study. Yellow and Green dots indicate heat flow measurements from two different survey lines from Yamano et al. (2014). White dashed lines indicate seismic profiles from Fujie et al. (2018). The profile across Japan Trench is used in Fig. 3-3C.

3.3 Data and Methods

In order to make high resolution marine magnetic anomaly map, we collected available magnetic data from the DARWIN database of the Japan Agency for Marine-Earth Science and Technology (JAMSTEC, 2016), the Nautilus database of the Institut Français de Recherche pour l'Exploitation de la MER (IFREMER, 2014), and the GEODAS database of the National Center for Environmental Information (NCEI, 2007). The data obtained by proton precession magnetometer (PPM) were subtracted the International Geomagnetic Reference Field (IGRF) model (Thébault et al., 2015). We applied the method of Isezaki (1986) to correct the data acquired by Shipboard Three Component Magnetometer (STCM) for the ship induced and remanent magnetization and motions. To combine both the PPM and the STCM data, the crossover correction algorithm of Choe and Dyment, (2019) was applied. We reduced the corrected magnetic anomaly grid to the pole (RTP) assuming 53.6° inclination and -7.6° declination (IGRF averaged over 20 years), 33° paleoinclination and 11° paleoazimuth (average value for the study area from the global grids of Dyment and Arkani-Hamed, 1998). Each anomaly profile was inverted to equivalent magnetization assuming a 0.5 km thick magnetized source layer with no vertical variation of magnetization (Parker and Huestis, 1974).

We downloaded the bathymetric grid as part of the Global Multi-Resolution Topography (GMRT; Ryan et al., 2009) from the Interdisciplinary Earth Data Alliance (IEDA) and the World sediment thickness grid (Divins, 2003) from NCEI. To compute the top of the magnetic source, i.e. of the extrusive basalt layer, the sediment thickness grid was subtracted from the bathymetry grid.

To observe a systematic decay of the seafloor spreading magnetic anomalies on oceanic crust approaching to the subduction zone, we set the outer flexural rise from the satellite free-air gravity anomaly map (Sandwell et al., 2014) showing a clear flexural rise undisturbed by seamounts or fracture zones (Fig. 3-1C) and computed distances in the WGS84 reference system. We then plotted the ratio of peak to trough anomaly amplitudes of each studied magnetic anomaly versus the distance to the outer flexural rise (Fig. 3-3A).

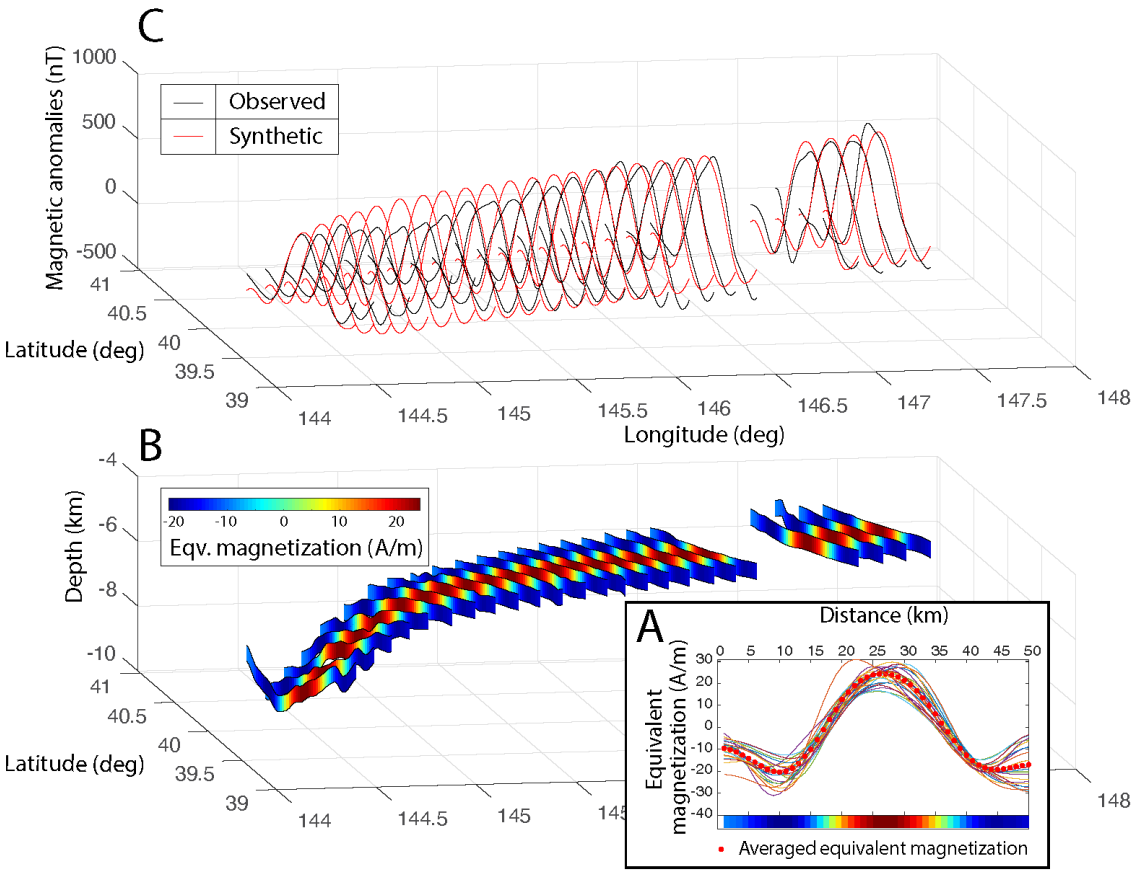

Figure 3-2. A: Equivalent magnetization inverted from profiles across magnetic anomaly M10n before subduction (location: see Fig. 3-1C, orange box). Red dotted curve indicates the average equivalent magnetization adopted for further modeling. **B:** Three-dimensional view of the source layer and magnetization intensity (color) used to model the synthetic magnetic anomalies. **C:** Three-dimensional view of the observed (black) and synthetic (red) magnetic anomalies across magnetic anomaly M10n after subduction (location as above). Comparison of the observed and synthetic anomalies show that the anomaly decreases from 146°E while approaching trench.

3.4 Magnetic structure of the subducting plate before entering the japan-kuril trench

The Pacific plate and associated subducting slab display NNE-SSW magnetic anomalies of Early Cretaceous age (see above). The southern Kuril Trench is roughly parallel to these anomalies, with anomaly M5 (124.58-126.05 Ma) recognizable although totally subducted whereas anomalies M6 and M7 (127.2-128.54 Ma) are only partially subducted. Conversely, the Japan Trench is oblique to anomalies M8 to M11 (128.5-132.67 Ma), which are

progressively fading away after passing the Trench to disappear ~100-120 km landward (Okubo et al., 1991). These observations result both from the increasing distance to the magnetized source and to thermal demagnetization of the oceanic magnetic layers (Choe and Dyment, 2019). On the plate prior subduction, the magnetic anomalies are slowly fading away while approaching the trench. To evaluate quantitatively the amplitude variation of these anomalies, we selected data showing clear seafloor spreading magnetic anomalies both in amplitude and wavelength (i.e. 20-40 km), in areas of dense data coverage. Profiles perturbed by local complexities such as seamounts, propagators and fracture zones are discarded.

Investigating the same anomaly reduces possible biases related to paleomagnetic field intensity variation with time. We limited our study to magnetic anomalies M8r to M10Nr (129.0–132.0Ma) off the Japan Trench. We compared the observed magnetic anomaly profiles to synthetic ones computed by assuming that (1) the basement is the top of a 0.5 km-thick magnetized extrusive basalt layer, and (2) the magnetization is the average of all equivalent magnetization profiles inverted from the observed anomaly profiles with the same local geometry. Figure 3-2 presents the example of magnetic anomaly M10 (133.45-133.49Ma), which shows a good fit between the observed and synthetic anomalies East of the outer rise and an increasing misfit between the outer rise and the trench (Fig. 3-2C). We computed the ratio of peak to trough anomaly amplitudes of the observed and synthetic anomalies, hereafter named RAM (Remaining Amount of Magnetization). Figure 3-3A represents the RAM versus the distance to the closest outer rise for all anomalies and, despite some scatter, shows a significant decrease of the RAM toward the trench. We averaged the RAM at 25 km intervals and adopted the corresponding standard deviation as the uncertainty (Fig. 3-3A). The average RAM is constant at 0.93 East of the outer rise and decreases exponentially to 0.7 from the outer rise to the trench (Fig. 3-3A).

The decreasing RAM reflects a loss of magnetization occurring between the outer rise and the trench and can be attributed to two main processes, the alteration and thermal demagnetization of magnetic minerals.

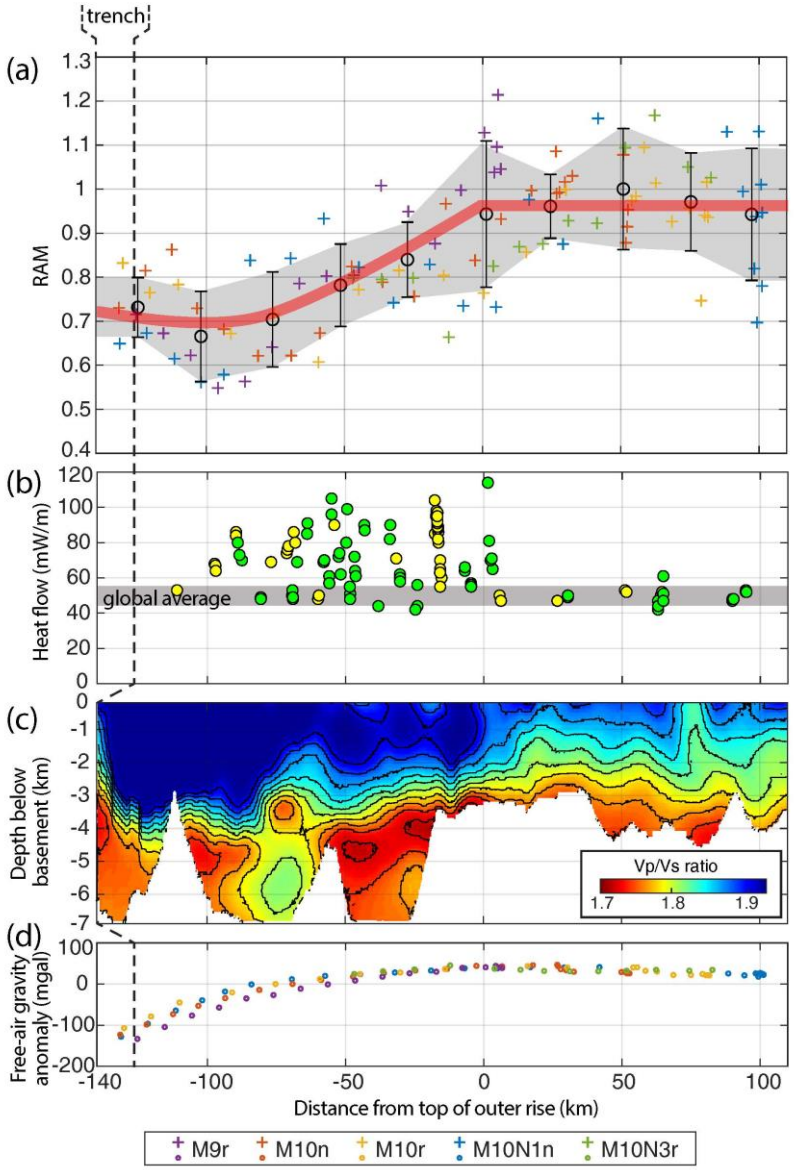

Figure 3-3. Comparison of the Remaining Amount of Magnetization (RAM) to other geophysical data versus distance to the top of outer rise. **A**: RAM. Colored cross signs and dots in **A** and **D** correspond to a magnetic anomaly shown by a similarly colored box on Fig. 3-1C. Averaged RAM within 25 km distance intervals are shown by circles with error bars, and confidence limits by the shaded area. Thick red line summarized the RAM variation with distance from top of outer rise. **B**: heat flow data (Yamano et al., 2014). Yellow and Green dots are shown in Fig. 3-1C. **C**: Vp/Vs ratio grid from depth below basement (Fujie et al., 2018). Before approaching the top of outer rise, the RAM is close to 0.92, the heat flow converges to global average and Vp/Vs ratio shows low values. Between top of outer rise to trench, on the other hand, heat flow and Vp/Vs ratio increase and the RAM decays rapidly as a result of alteration and hydrothermal circulation of magnetic mineral. **D**: free-air gravity anomaly.

3.5 Decay of magnetization before subduction: alteration as the main process

Two major processes can be inferred to explain the decay of marine magnetic anomalies between the outer rise and the trench. The first one, thermal demagnetization, relates the loss of magnetization to an increase of temperature: the magnetic minerals are heated beyond their Curie temperature and loose their magnetization (Okubo et al., 1991). The second process, alteration, considers that hydrothermal circulation oxidizes the magnetic minerals which transform to less or non-magnetic minerals (Tivey et al., 1993; Dyment et al., 2015).

Moreover, recent heat flow data show values close to the global average (~50Wb/m^2) East of the outer rise and scattered, in average higher values between the outer rise and the trench (Yamano et al., 2014; Fig. 3-3B). The higher heat flow observed over the oceanic crust approaching the trench suggests high temperatures that may support thermal demagnetization of titanomagnetite, the magnetic bearer of extrusive basalt that exhibits a strong magnetic intensity but a low Curie temperature (150-350°C; Zhou et al., 2002; Gee and Kent, 2007). However, a recently published thermal structure model (Kawada et al., 2014) concluded that the additional hydrothermal circulation which causes the higher and more scattered heat flow measurements of Yamano et al. (2014) only heats up the oceanic crust at 1.5 km depth by 40°C, insufficient to reach the Curie temperature and significantly demagnetize the plate. We therefore consider that thermal demagnetization only plays a minor role in the observed decay of the marine magnetic anomalies before entering subduction.

Recent active seismic reflection profiles show that the Vp/Vs ratio strongly increases and the high Vp/Vs layer thickens up to 3.5km-deep below seafloor (bsf) from the outer rise to the trench as the hydrothermal activity and subsequent alteration significantly increase (Fujie et al., 2018; Fig. 3-3C). These results and the heat flow measurements (Yamano et al., 2014) support rejuvenation of the hydrothermal circulation within the old oceanic crust. Seawater penetrates the pelagic sediments and the crust along normal faults and fissures opened by the flexure of the oceanic lithosphere at the outer rise as it is observed in most subduction zones (Contreras-Reyes et al., 2008; Shillington et al., 2015; Fujie et al., 2018).

The decay of RAM is therefore most likely caused by the flexure of the lithosphere approaching the trench, the resulting normal faulting and fissuring, the associated rejuvenated hydrothermal circulation, and finally the alteration of the magnetic minerals (Fig. 3-4). It is

interesting to note that the decay seems to attenuate from the outer rise to the trench, as does the increasing crustal hydration estimated from Vp/Vs values (Fig. 3-3C). Both the crustal hydration and the magnetic mineral alteration are fast when the faults and fissure open, and tend to saturate with time, when hydrated and altered minerals cover the cracks and their vicinity. For this reason, the RAM decay is much more subdued near the trench (Fig. 3-3A).

3.6 An integrated magnetization model of the subducting plate

This study and our previous work (Choe and Dyment, 2019) offer an integrated view on the magnetic structure of the Pacific Plate before and after entering subduction in the Japan-Kuril Trench. Here we show that, after passing the outer rise, the magnetic anomaly amplitude decreases by roughly 20% due to the alteration of magnetic minerals induced by rejuvenated hydrothermal circulation. From our previous study, half of the remaining 80% is further erased between 9-12 km depth of the slab surface below sea level (bsl) due to the thermal demagnetization of the extrusive basalt layer above the Curie temperature of titanomagnetites (150-350°C). The last 40% are finally removed between 12-20 km depth of the slab surface bsl by thermal demagnetization of the deeper crust above the Curie temperature of magnetite (580°C; Gee and Kent, 2007).

Heat flow, Vp/Vs structure, and magnetization decay concur in supporting rejuvenated hydrothermal circulation and the subsequent alteration as an important process on the plate before subduction. As a consequence, the crust entering subduction is already very altered, and it is therefore unlikely that the drop of magnetization observed between 9 and 12 km may be due to any vigorous hydrothermalism and alteration. Thermal demagnetization appears as the only process able to generate such a magnetization drop. A major difference between the oceanic crust before and after subduction is, the heat mined by hydrothermal circulation before subduction is released to the ocean as the hydrothermal system is open; the thermal structure is only marginally affected, as noted by Kawada et al. (2014). Conversely, after subduction, the hydrothermal system is closed. The seawater trapped in the thick aquifer of Kawada et al. (2014) continues to mine the heat from depth but cannot escape due to the overlying accretionary prism, pelagic sediments and the possibly impermeable decollement surface, resulting in the same fluid convecting and heating the oceanic crust by thermal blanketing (Granot and Dyment, 2019). As a result, the heat flow measured on the seafloor is low (Kawada et al., 2014; Yamano et al., 2014).

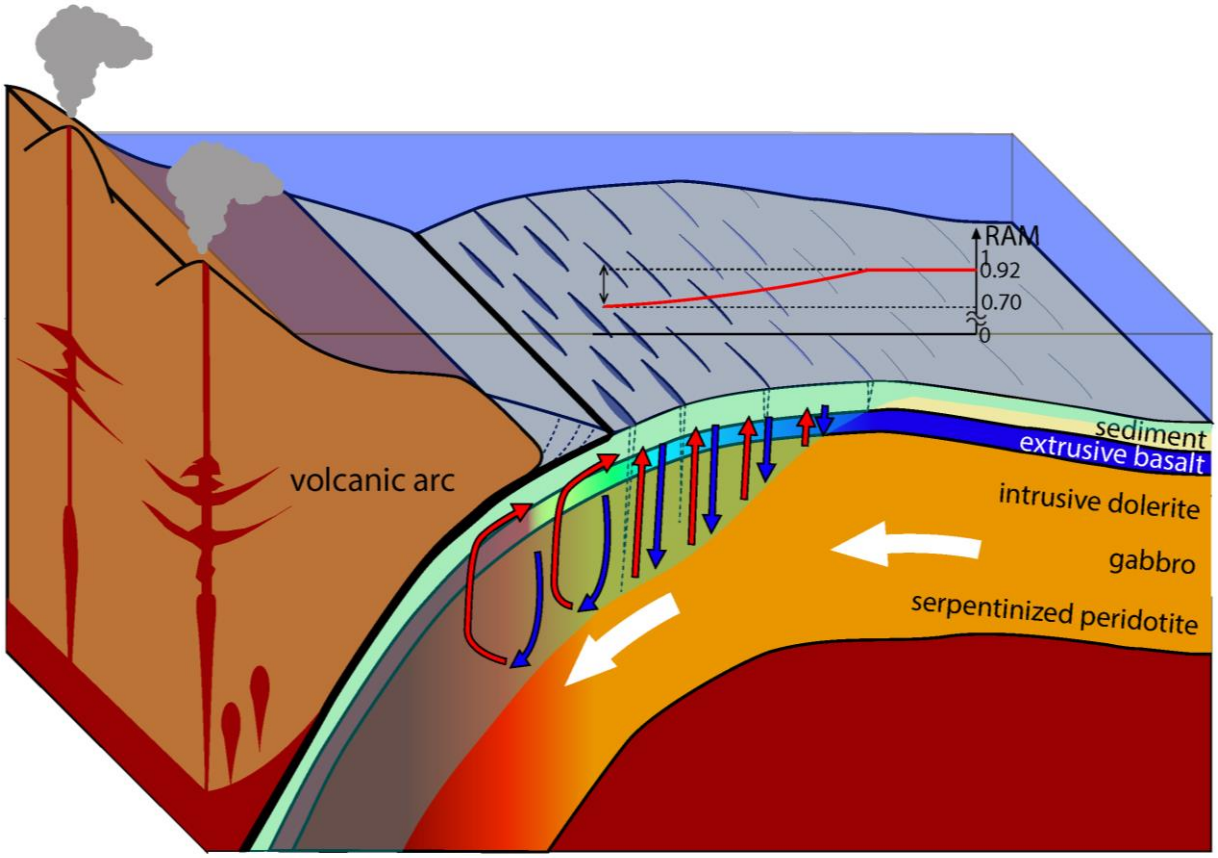

Figure 3-4. Schematic illustration of the processes shaping the magnetic structure of the subducting plate. Red solid line describes the RAM decrease shown in Fig. 3-3A. Blue and red arrows describe hydrothermal activity in the oceanic crust. Before subduction, normal faults induced by the bending of old oceanic lithosphere causes seawater penetration and active hydrothermal activity, and in turn oxidation of the magnetic minerals and crustal magnetization reduction. Once entered in subduction, the heat mined by hydrothermal circulation does not escape to the ocean as a result of thermal blanketing by the accretionary prism, the pelagic sediments and the possibly impermeable decollement surface, making the temperature increase and the magnetization of the extrusive layer then the deeper crust fade away as their magnetic minerals pass their Curie temperature.

Our study underlines the major role of fluid circulation, alteration, and more generally of thermodynamics in shaping the Japan-Kuril Trench before and after subduction. In predicting a warmer subduction zone, these results have consequences on the depth and location of the seismogenic zone, which knowledge is important to assess the seismic risk in the area (Choe and Dyment, 2019). Magnetic anomalies reflect thermal processes and can be used as a tool to address these processes. Our inferences on the thermodynamics of subduction zones should be confirmed by a rigorous thermal model that is beyond the scope of this paper.

3.7 Acknowledgement

We thank Nobukazu Seama and an anonymous reviewer for their helpful comments, as well as Editor Monika Korte for her efficient handling of this paper. HC has been supported by a fellowship of Ecole Doctorale STEP'UP. We thank all scientists and crews who collected the marine geophysical data used in this study. This is IPGP contribution xxx. The marine magnetic data used in this study are available at the NCEI (GEODAS database https://www.ngdc.noaa.gov/mgg/geodas/trackline.html), JAMSTEC (DARWIN database https:// http://www.godac.jamstec.go.jp/darwin/e) and IFREMER (Nautilus https://www.flotteoceanographique.fr/en/Cruises/Research/Oceanographic-campaigns-data)

Chapter 4.

The two categories of fading marine magnetic anomaly in subduction zones

4.1 Abstract

Magnetic anomalies in subduction zones progressively lose their amplitudes and disappear as a result of various processes. Before subduction, the alteration of magnetic minerals is induced by the rejuvenated hydrothermal circulation in new cracks and pre-existing normal faults opened by the flexure of the oceanic lithosphere. After subduction, thermal demagnetization affects the various magnetic minerals of the oceanic crust when the increasing temperature of the subducting slab pass their Curie temperature. Previous studies of these processes focused on the Japan Trench area, where magnetic data are dense, and other subduction zones have not been investigated. Here we attempt to generalize the previous observations and classify the patterns of fading magnetic anomalies in five subduction zones. We find that the major difference is controlled by the age of the lithosphere and related physical property variations. Two categories can be defined: the first one, the Japan-Kuril subduction zone, shows decay before and after subduction, whereas the other one, the Cascadia subduction zone, displays no decay before subduction as a result of no flexure on the young Juan de Fuca plate.

4.2 Introduction

The oceanic crust formed by seafloor spreading at mid-ocean ridges initially exhibits a strong remanent magnetization. The magnetic structure of the oceanic crust comprises two main layers bearing distinctive magnetic minerals with different Curie temperature (i.e. the temperature at which it acquires and loses its magnetization): titanomagnetite with varying titanium content predominates in the extrusive basalt, and magnetite in the deeper layer.

Strong hydrothermal circulation cools the oceanic crust in its early stages and results in the alteration of its magnetic minerals. However, pelagic sediments progressively cover the oceanic basement, fill up the existing faults and cavities, and hinder the hydrothermal circulation and associated alteration. This is confirmed by the decay of magnetization within the first 10 million years observed at all spreading centers, followed by a relative stability (Dyment et al., 2015). Recent geophysical studies, on the other hand, observe that the hydration of the oceanic crust (Fujie et al., 2018; Shillington et al., 2015) and the heat flow (Yamano et al., 2014) progressively increases in old Pacific oceanic crust approaching the Japan Trench. A recent geothermal model speculates that rejuvenated hydrothermal circulation induced by the bending oceanic lithosphere increases the heat flow before subduction in Japan Trench (Kawada et al. 2014). In a previous magnetic study in the Japan-Kuril subduction zone, Choe and Dyment (2019b) find that magnetic anomalies in the NW Pacific plate loses 20% of their amplitude between the outer rise and the trench due to the alteration of magnetic minerals of the oceanic crust by the rejuvenated hydrothermal circulation. After subduction, the slab progressively loses its magnetization while its magnetic minerals pass their Curie temperature, in two steps characterizing titanomagnetite and magnetite (Choe and Dyment, 2019a).

In this paper, we attempt to generalize these results to other subduction zones. We investigate five subduction zones selected on several criteria (See data and methods; Fig. 4-1). We observe two distinctive decreasing patterns depending the age of the subducting oceanic lithosphere and related physical property variations. Before subduction, the magnetization progressively decreases between the outer rise and the trench for old subducting oceanic lithosphere. Conversely, no decay is observed for young oceanic lithosphere. After subduction, both exhibit the fast decay related to thermal demagnetization of titanomagnetite in the extrusive basalt and the more progressive decay due to thermal demagnetization of magnetite in the deeper crust, although it happens earlier on the young lithosphere due to its stronger thermal gradient.

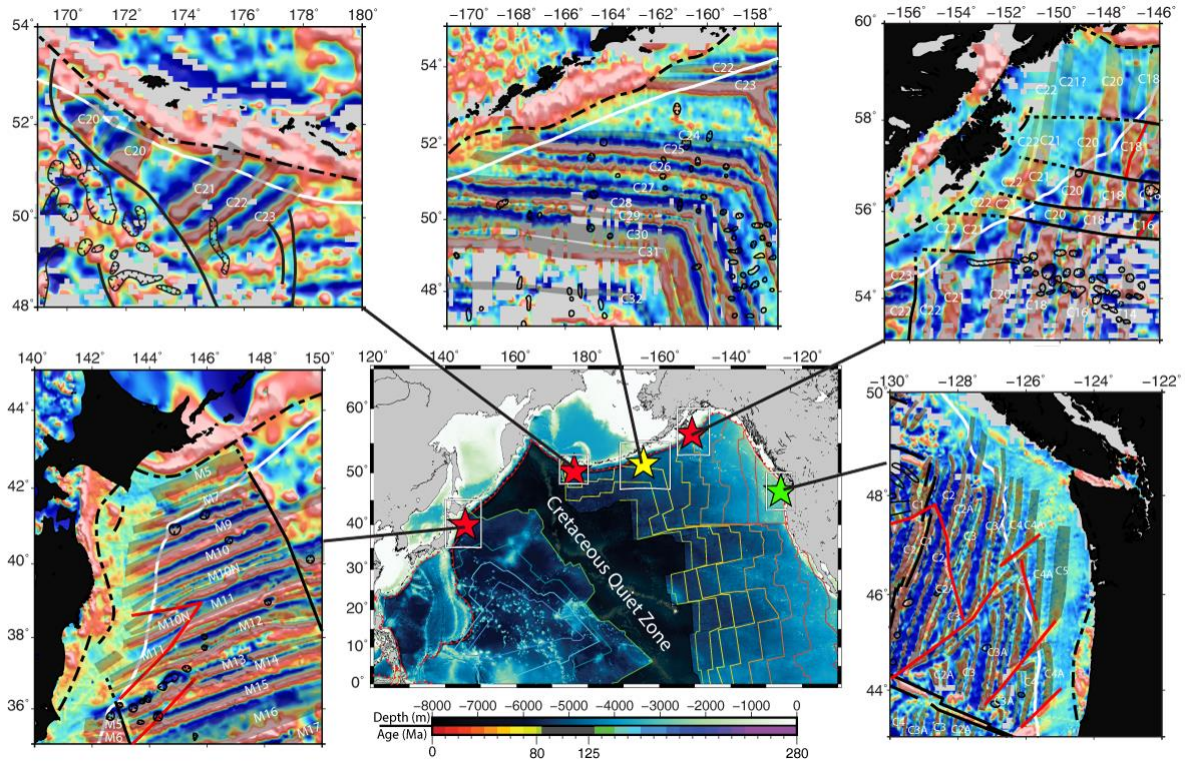

Figure. 4-1 Five selected study area. The grid in the center displays bathymetry from ETOPO1 Global Relief Model (Amante and Eakins, 2009). Colored lines indicate the age of oceanic crust (Müller et al., 2008). The stars display the location of the areas, with red stars: old oceanic crust displaying clear flexure, yellow star: same but the magnetization of the extrusive basalt is almost totally erased before subduction due to the absence of thick sediments, and green star: young oceanic crust. Black solid lines in the magnetic anomaly map indicate fracture zones and dotted lines: estimated fracture zones on slabs from the magnetic anomaly map; dashed lines: induced magnetic anomalies from fore-arc mantle; red solid lines: propagating rifts.

4.3 Data and Methods

4.3.1 Selection of study area

To choose the areas where we investigate the detailed variations of the magnetic anomalies at subduction zones, we adopted the following criteria: (1) the marine magnetic data are sufficiently dense to accurately constrain magnetic anomaly variations; (2) the magnetic anomalies exhibit an oblique strike with respect to the trench; (3) the amplitudes and wavelengths (>20km) of the magnetic anomalies are consistent; and (4) the magnetic anomalies perturbed by transform or non-transform offsets, seamounts or oceanic plateaus are excluded. Consequently, five areas are chosen for further analysis (Fig. 4-1).

4.3.2 Magnetic data collection and processing

We gathered data from JAMSTEC (Japan Agency for Marine-Earth Science and Technology; DARWIN data base: http://www.godac.jamstec.go.jp/darwin/e), NCEI (National Center for Environmental Information; GEODAS data base: www.ngdc.noaa.gov/mgg/geodas/) and IFREMER (Institut Français de Recherche pour l'Exploitation de la Mer; Nautilus data base: http://donnees-campagnes.flotteoceanographique.fr/). The International Geomagnetic Reference Field (IGRF) model (Thebault et al., 2015) is subtracted from the magnetic data obtained by proton precession magnetometer (PPM). The data collected by shipboard three-component magnetometer (STCM) are corrected by the method of Isezaki (1986). To minimize the crossover misfits between the PPM and the STCM data, we applied the crossover algorithm of Choe and Dyment (2019a). Afterwards, we reduced to the pole (RTP) the corrected magnetic anomaly grid assuming the direction of the current magnetic field from the IGRF and that of the magnetization vector from the paleoinclination and paleoazimuth grids of Dyment and Arkani-Hamed (1998).

RTP magnetic anomaly profiles perpendicular to each anomaly strike are inverted to equivalent magnetization by applying the method of Parker and Huestis (1978) and the inverted profiles are averaged to obtain a reference magnetization profile for each anomaly.

4.3.3 Basement geometry data and processing

High resolution bathymetric data were obtained from the Global Multi-Resolution Topography (GMRT) (Ryan et al., 2009) from the Interdisciplinary Earth Data Alliance (IEDA: www.gmrt.org/). To compute the top of the magnetized source, i.e. the basement, we subtracted the World sediment thickness grid (www.ngdc.noaa.gov/mgg/sedthick/sedthick.html) (Divins, 2003) to the bathymetry grid and merged the resulting grid with Slab 1.0 (Hayes. et al., 2012) to study the magnetic anomalies arising from the subducted slab. The geometrical misfit between the two grids along the trench boundary was erased and re-interpolated using the Partial Differential Equation (PDE) surface method (D'Errico, 2005) as applied in our previous study (Choe and Dyment, 2019a).

4.3.4 Remaining amount of magnetization

Investigating the same anomaly reduces possible biases related to paleomagnetic field intensity variation with time. We compared the observed magnetic anomaly profiles to synthetic ones computed by assuming that (1) the basement is the top of a 0.5 km-thick magnetized extrusive basalt layer, and (2) the magnetization is the reference magnetization as defined above. We computed the ratio of peak to trough anomaly amplitudes of the observed and synthetic anomalies. We plotted the RAM versus the minimum distance from the trench in each area as shown in Fig. 4-2. We averaged the RAM values with 25 km intervals to observe the variations before subduction and with 10km intervals after subduction with the corresponding standard deviation (σ=1) as the uncertainties. In the subducted part, unexpected short-wavelength anomalies are often observed for the deeper part of the slab (~20 km) and disagree with the corresponding long-wavelength synthetic anomalies. They are discarded for the calculation of RAM. Their short-wavelength content is inconsistent with the depth of the subducting slab, suggesting the presence of shallower sources in the upper plate continental crust.

4.4 Results

4.4.1 Magnetization loss in old oceanic lithosphere

The systematic loss of magnetization as subduction progresses in the five selected subduction zones can be sorted in two categories. The best example of the first one, the subducting oceanic lithosphere beneath the Japan-Kuril Trench, displays ENE-WSW magnetic anomalies of Early Cretaceous age between Chrons M5 and M17 (124.6-139.7 Ma according to the Geomagnetic Polarity Time Scale of Malinverno et al., 2012) at a fast spreading rate (half rate 70-80 km/My) and is subducting at a rate of 70-90 km/My (Seno, 2016). Whereas the southern Kuril Trench is roughly parallel to these anomalies, the Japan Trench is oblique and the anomalies are progressively fading away with a 20% amplitude loss between the outer-rise and the trench as a result of crust hydration after passing the outer rise, ~140 km seaward from the Japan Trench and ~120 km from the Kuril Trench (Fujie et al., 2018). The heat flow progressively increases in the same area, indicating a very active hydrothermal circulation (Yamano et al., 2014; Kawada et al, 2014). This activity and the associated alteration of the magnetic minerals lead to the observed loss of magnetization in the oceanic crust (Choe and Dyment, 2019b).

After subduction the RAM value rapidly decreases between 10-45 km horizontal distance landward from the trench (9-12 km depth) with a 40% amplitude loss, then slowly decreases between 45-100 km landward from trench (12-19 km depth) (Fig. 4-2).

4.4.2 Magnetization loss in young oceanic lithosphere

The second category only includes the Cascadia subduction zone, which involves the Juan de Fuca plate with NNE-SSW magnetic anomalies C1 and C4A (0-9 Ma according the Geomagnetic Polarity Time Scale of Cande and Kent, 1995) at intermediate spreading rate (half rate 20-48 km/My; Riddihough, 1984) and is subducting at a rate of 26-40 km/My toward ENE (Finley et al., 2019). The Cascadia Trench is oblique to the anomalies and the RAM does not decrease toward the trench despite some fluctuations interpreted as reflecting the normal aging of the oceanic crust and associated alteration of the magnetic minerals, and also possibly the presence of propagating rifts with higher iron content (e.g., Ravilly et al., 1998). No significant lithospheric flexure has developed for such a young oceanic plate

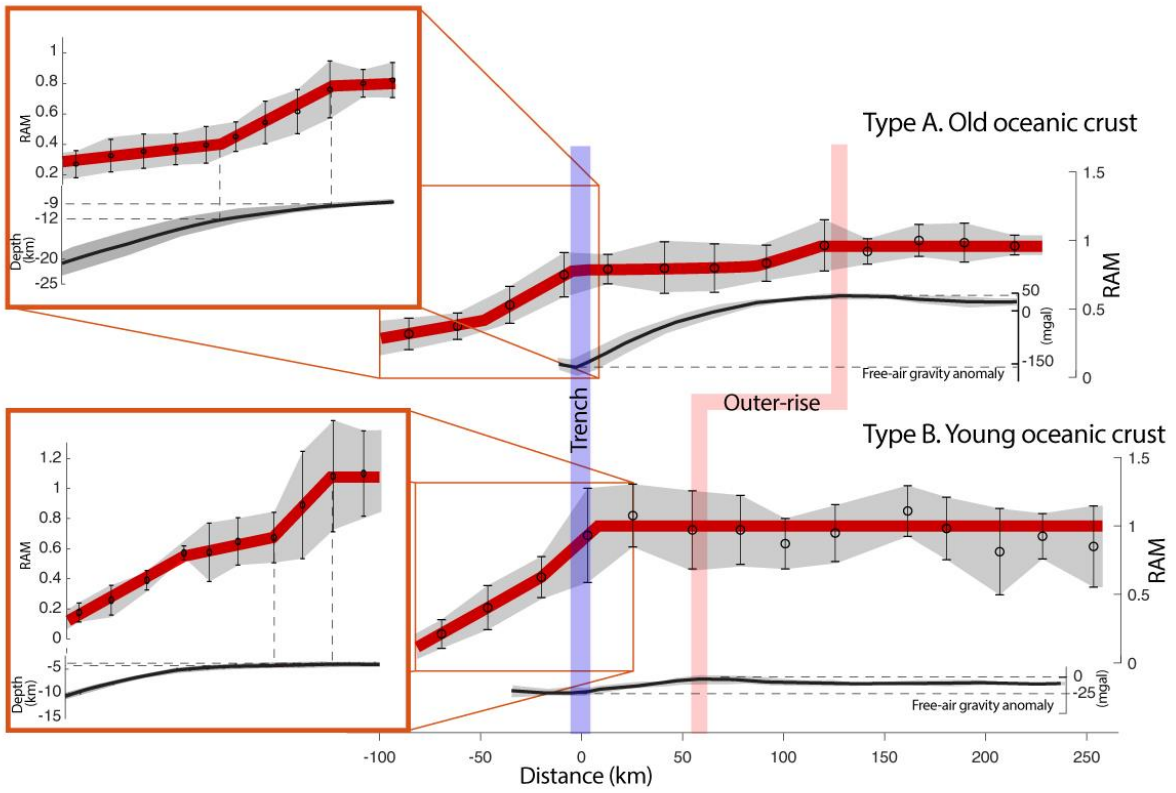

Figure. 4-2 Two categories in RAM decay. Type A, old oceanic crust in Japan-Kuril subduction zone shows 20% loss of amplitude between outer rise and trench due to hydrothermal circulation and the related alteration of magnetic minerals. The extrusive basalt layer magnetization disappears between 9-12 km; the deeper crust magnetization slowly decays and disappears at ~20km. Type B, young oceanic crust in Cascadia subduction zone shows no amplitude decrease before subduction, and the extrusive basalt layer magnetization disappears between 4-4.5 km (7 and -13 km away from the trench). The RAM rapidly decays between 13-78 km landward from the trench.

(Canales et al., 2017) and the slab shows a low angle typical of flat subduction. As a result, no subduction-related normal faults develop. Furthermore, the thick sediment deposits from the continental margin also hinder the hydrothermal activity, resulting in slowing down the alteration of the magnetic minerals.

After subduction, the RAM rapidly decays between 7 and -13 km horizontal distance from the trench (4-4.5 km depth) with 35% amplitude loss, and the amplitude slowly decreases between 13 and 78 km landward from the trench corresponding to 11 km depth of slab surface (Fig. 4-2). In this area, the observed heat flow exhibits between 110-140 mW/m (Johnson et al., 2012), and the sediment originated from both continent and ocean shows 1-1.5 km thickness. The blanket effect under the thick sediment layer and the observed high heat flow in the trench explain the more rapid (by comparison with the older crust) demagnetization of both the titanomagnetite of extrusive basalt and the magnetite of the deeper crust, even though the depth of the slab surface is very shallow.

4.5 Discussion

4.5.1 Comparison between the two categories

4.5.1.1 Before subduction

The two categories exhibit two major differences in their physical properties resulting from the age of oceanic lithosphere. One is the fact that normal alteration of the oceanic crust is still ongoing for young lithosphere whereas it is stopped for old lithosphere. As a result, the intensity of the magnetization is still varying and unstable in young lithosphere. The second difference is flexure and the thickness of the lithosphere. As it cools down over a long period of time, old oceanic lithosphere is thick and results in a large flexural bulge during subduction, with consequences as previously described. Conversely, the young oceanic lithosphere is thin and flexure is limited.

4.5.1.2 After subduction

The two steps of magnetization decay are observed for both categories: first the magnetization of extrusive basalt is rapidly erased where titanomagnetite reaches its blocking temperature between 150-350°C (Zhou et al., 2001; Gee and Kent., 2007), then the

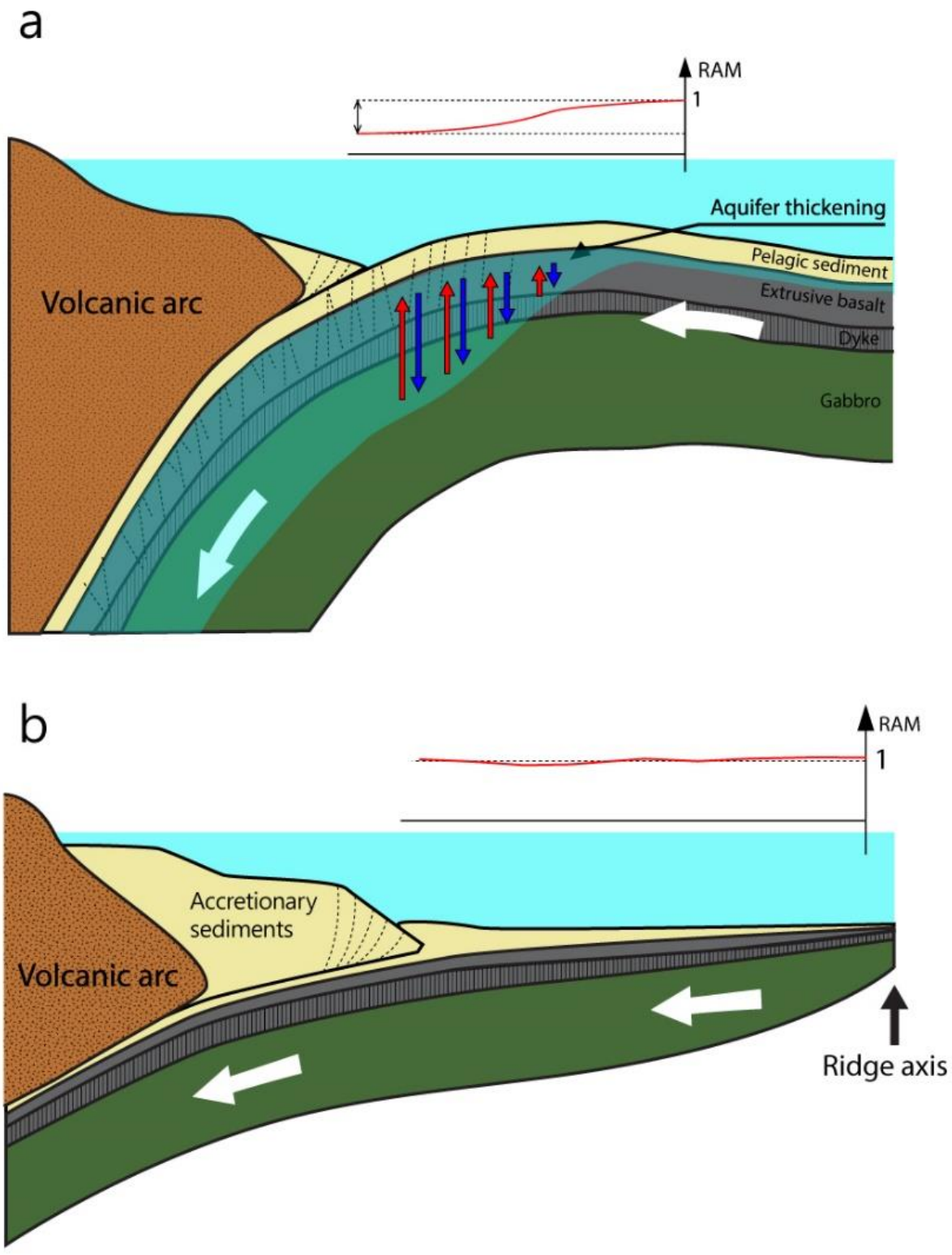

Figure. 4-3. Schematic illustration of the two categories.

magnetization of deeper crustal layers slowly decreases, reflecting the progressive slab heating toward the Curie temperature of magnetite, 580 °C (Gee and Kent., 2007). The amount of lost magnetization between the two subduction zones is similar. However, the distance over which the RAM decay for old oceanic lithosphere is twice longer than that for young oceanic lithosphere due to different thermal conditions. Old oceanic lithosphere has lower heat flow and larger heat capacity due to the crust hydration. Conversely, young oceanic lithosphere shows higher heat flow (Johnson et al., 2012) and relatively low heat capacity, and the thick sediment cover accelerates the slab warming up, leading to faster thermal demagnetization.

4.5.2 Discussion for the other subduction zones

The West Aleutian and South Alaska subduction zone show decaying patterns similar to that of the Japan-Kuril subduction zone and therefore belong to the same category. However, many fracture zones are observed on the subducting plates. The RAM decreases from the outer rise to the trench as for the first category, but unexpected variations observed in the South Alaska RAM pattern may be related to the stronger magnetization usually present at segments end in relation to magmatic differentiation (e.g., Ravilly et al., 1998).

We consider the Central Aleutian subduction zone as also belonging to the first category because the RAM progressively loses 50% of its amplitude before entering subduction. This decay continues after subduction until 9 km depth. This progressive decay is considered as representing the complete loss of magnetization in the extrusive basalt layer. The area is covered by very thin sediments (<300m) and the RAM progressively decay after the oceanic lithosphere is sharply bent. Less sediment cover and more flexure concur to make the fracturing and renewed hydrothermal circulation more pervasive, and therefore the crustal hydration and the associated alteration of the magnetic minerals more efficient.

By defining two categories related to the age of the subducting oceanic lithosphere we highlight the major role of fluid circulation, alteration, and thermodynamics before and after subduction. The analytic approach used in this study reflects thermodynamic processes and can be used as a tool to address these processes in other subduction zones. Our inferences on the thermodynamics of subduction zones should be confirmed by additional data such as heat flow observations, seismic velocities, etc. in many subduction zones and, more importantly, thermal models inclusive of realistic sediment covers, varying permeability related to the

extensive or compressive stresses, and hydrothermal circulation. Such a model beyond the scope of this paper.

4.6 Acknowledgement

HC has been supported by an Ecole Doctorale STEP'UP Fellowship. We thank all scientists and crews who collected the marine geophysical data used in this study. This is IPGP contribution xxx.

4.7 Supplementary materials

4.7.1 Japan-Kuril

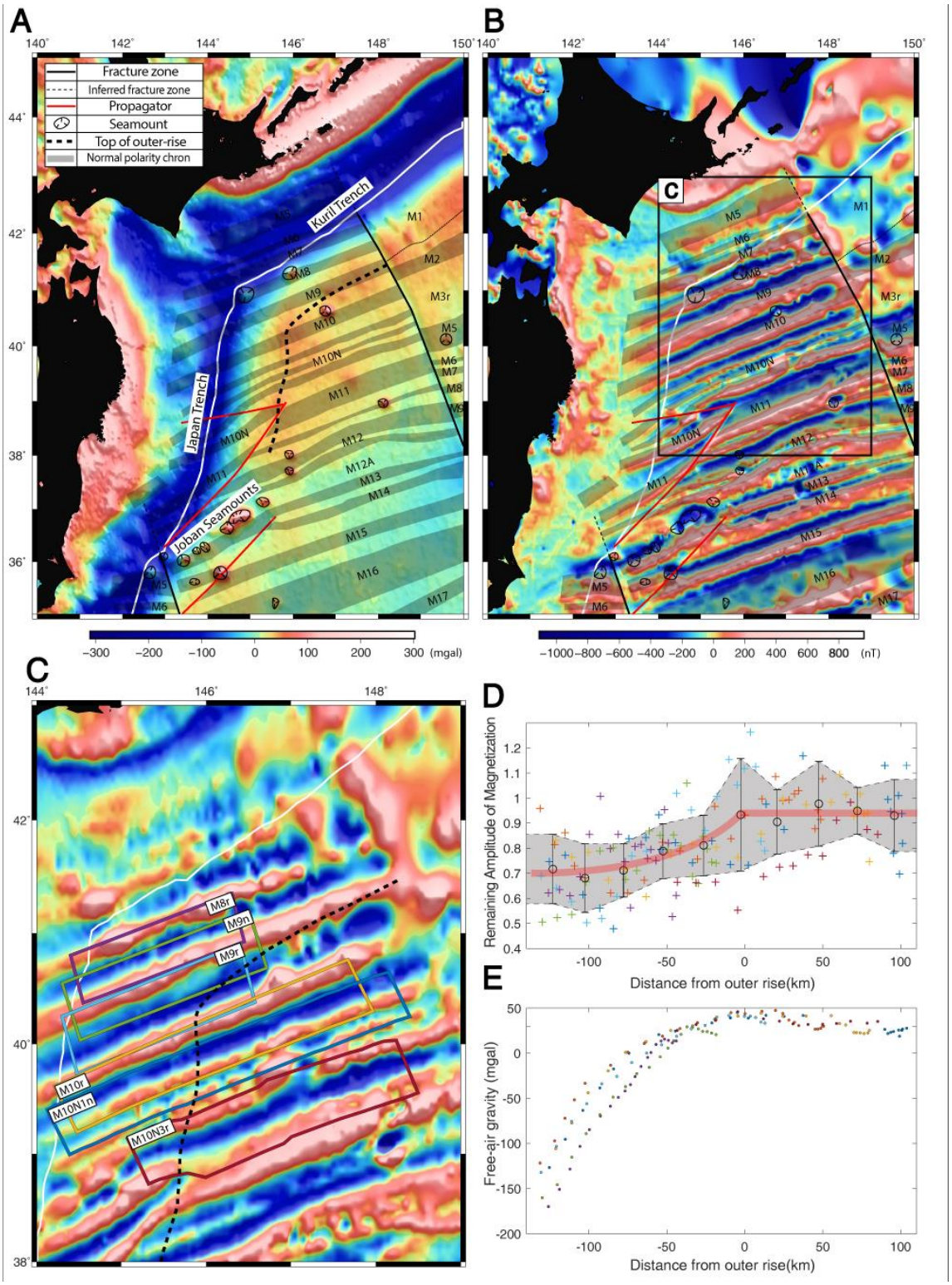

4.7.2 West Aleutian

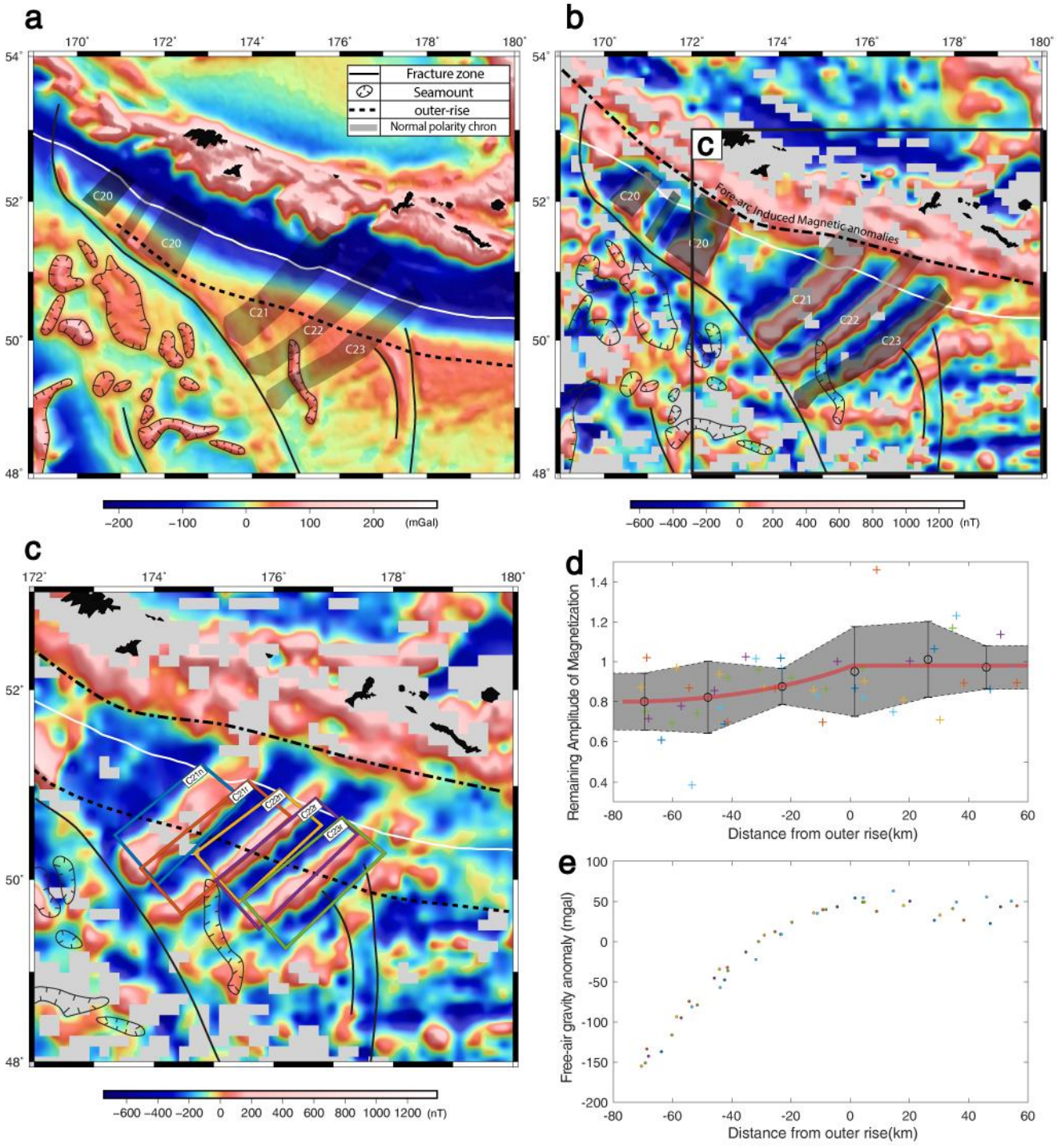

4.7.3 Central Aleutian

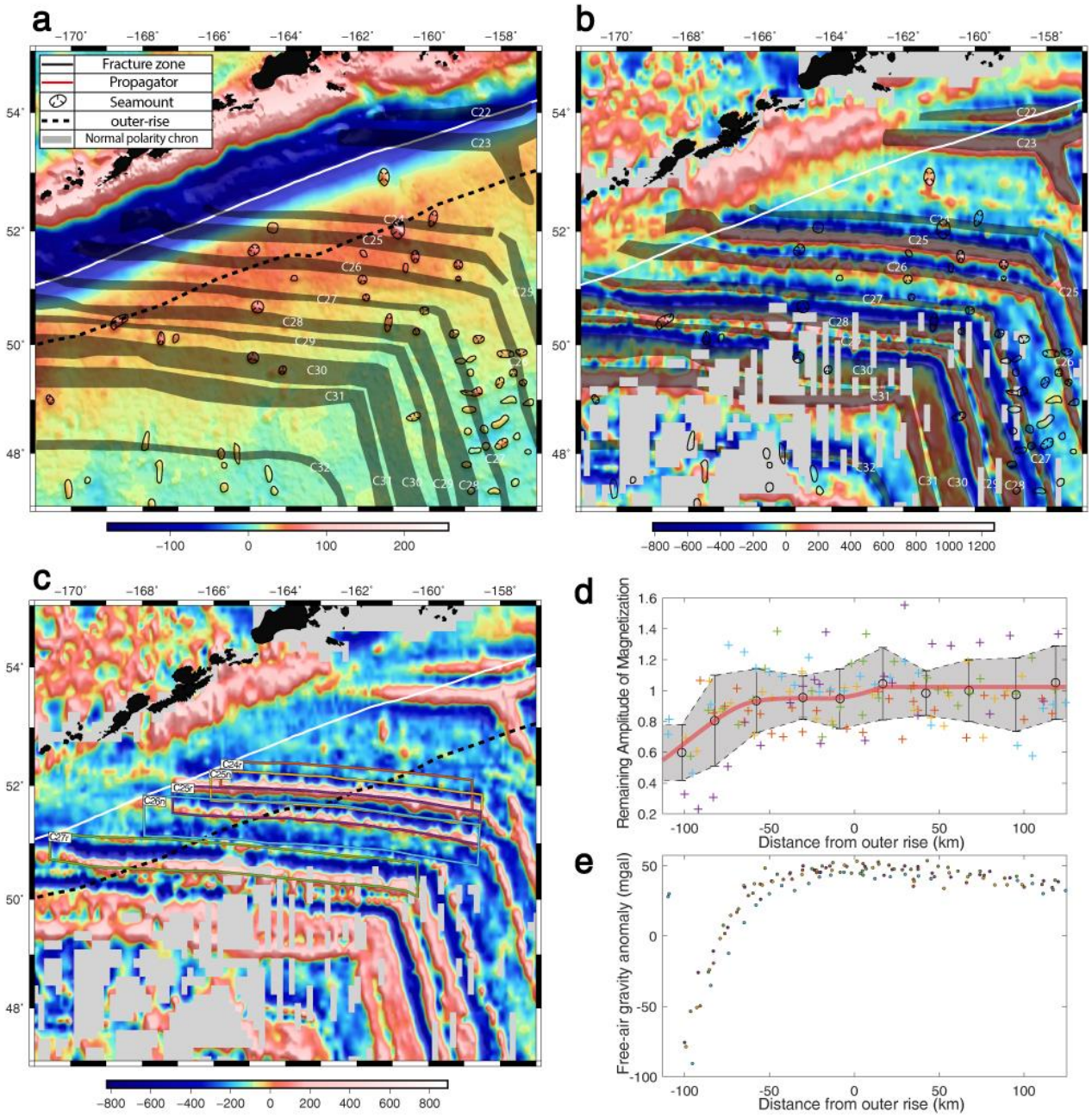

4.7.4 South Alaska

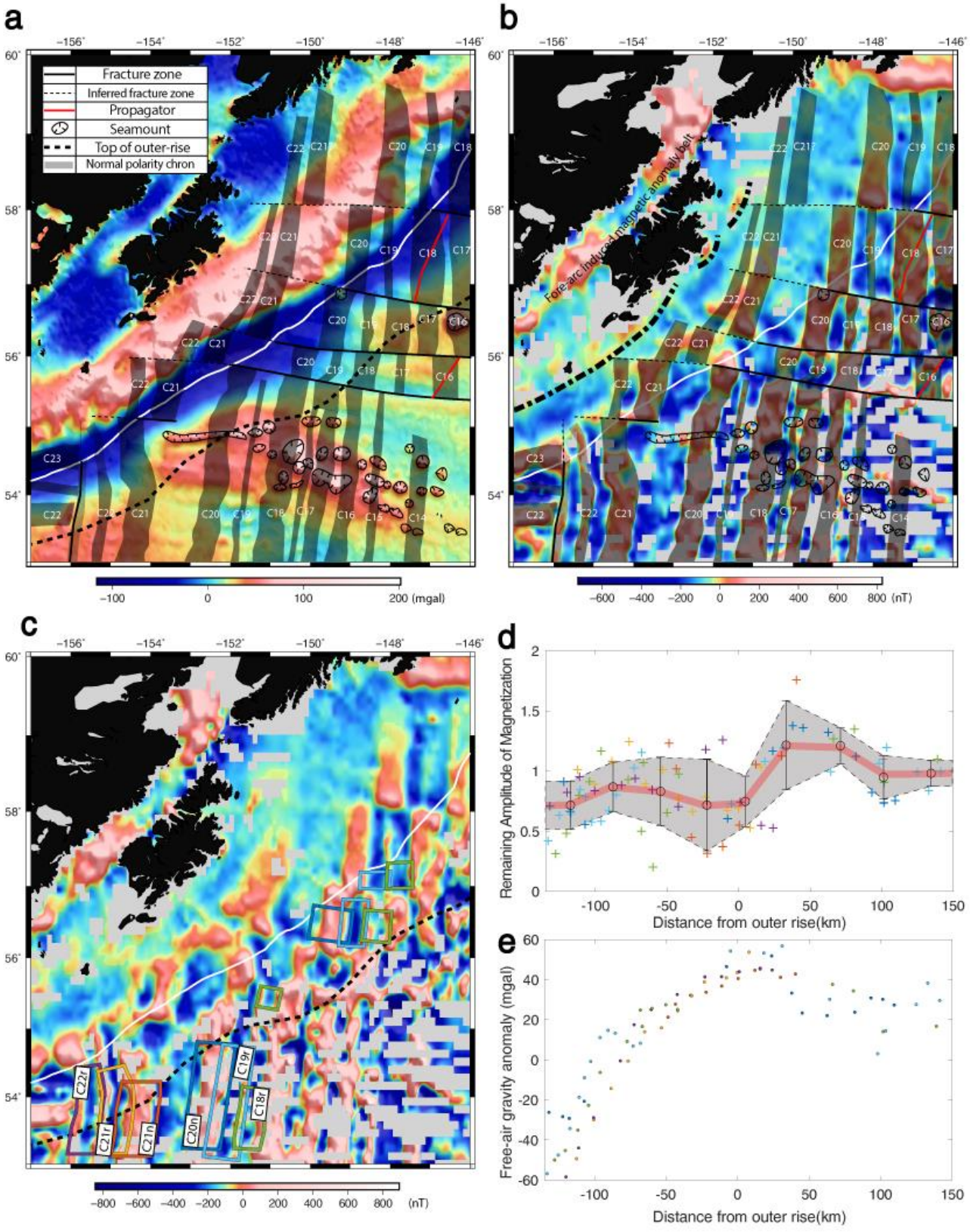

4.7.5 Cascadia

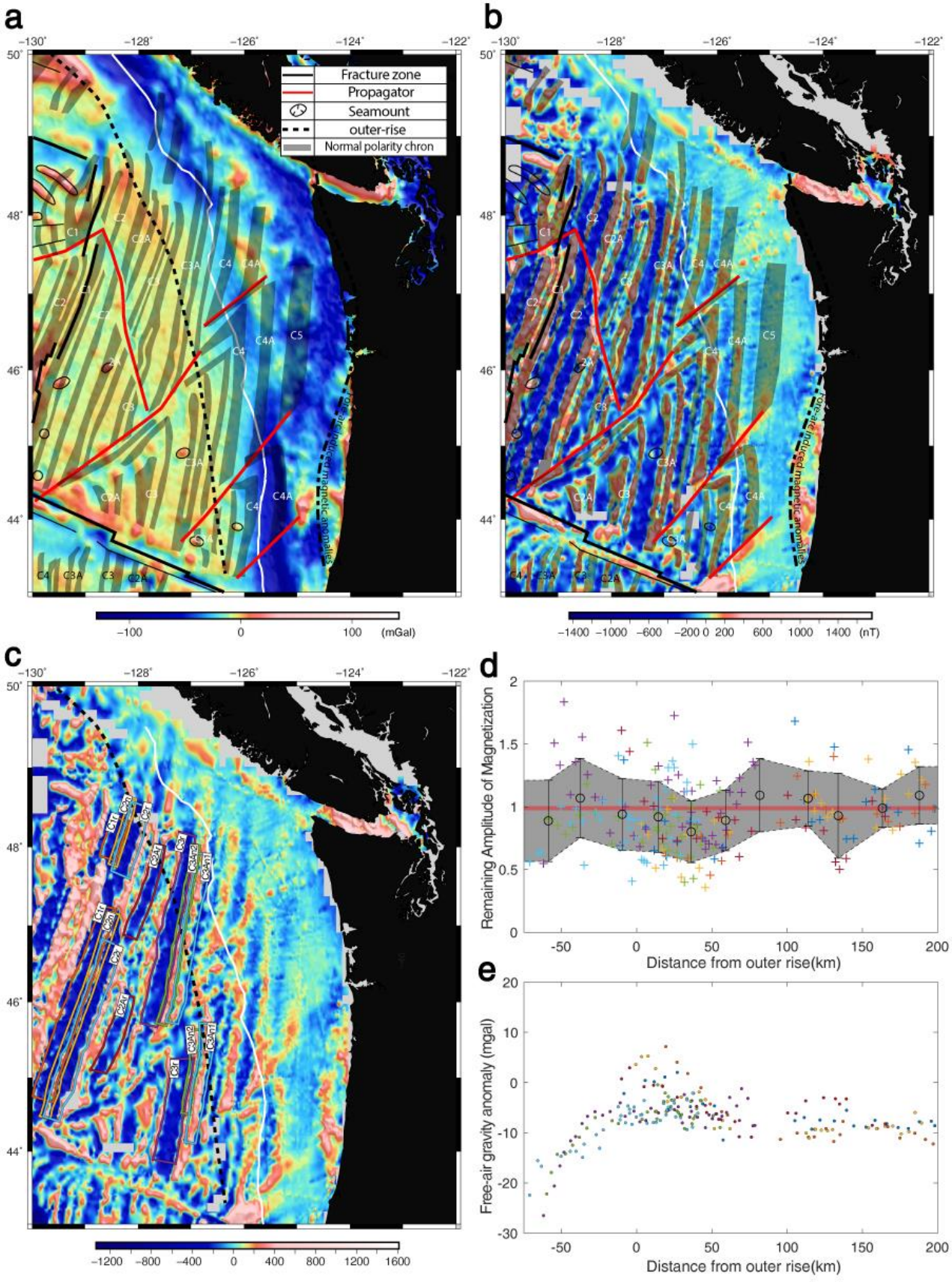

Chapter 5.

General conclusion

The purpose of this study is to confirm and quantify the decay of seafloor spreading magnetic anomalies at subduction zones and to understand its meaning in terms of physical processes. Our work includes the processing and combination of two different types of marine magnetic data to build high-resolution marine magnetic anomaly grids, and the application of an original method to eliminate the topographic effect and retain only magnetization variations. We investigate the magnetization of the oceanic crust both before and after subduction and extend our initial study area, the Japan subduction zone, to other subduction zones to show significant variations with the age of the subducting lithosphere.

5.1 New high-resolution magnetic anomaly map

High resolution marine magnetic anomaly grids are built to investigate the amplitude variations of magnetic anomalies in subducting oceanic crust. We collected and processed the available sea-surface magnetic data in the selected study area. In this work, a new crossover algorithm was developed to build high-resolution scalar magnetic anomaly maps using both the vector STCM and scalar PPM datasets. Furthermore, this method provides additional characteristics of the magnetized ship body with viscous magnetization depending on the navigating direction. To exploit the new anomaly map in terms of equivalent magnetization variations, we developed a new analytic method based on the ratio of peak to trough anomaly amplitudes of the observed and synthetic anomalies computed assuming a constant magnetization and the basement topography: variations this RAM (remaining amount of magnetization) eliminate the effect of the topography. Working on variations along the same anomaly and averaging the results reduces possible biases related to paleomagnetic field intensity variation with time. This quantitative analysis allowed us to observe (resp. confirm) the decreasing remanent magnetization intensity of the oceanic crust before (resp. after) entering subduction.

5.2 Decaying magnetic signals in subduction zones

We began to analyze decaying magnetic anomalies before and after subduction in the Japan-Kuril subduction zone where the denser marine magnetic data are available, and the oceanic crust shows clear and consistent magnetic anomalies. Then, we extended our study area to four other subduction zones.

The decaying magnetization intensity of the subducted oceanic crust could be constrained using the well-imaged slab geometry of the Japan Trench. Two distinct steps could be observed: first the magnetization of extrusive basalt is rapidly erased between 9-12 km, where titanomagnetite reaches its Curie temperature between 150-350°C, then the magnetization of deeper crustal layers slowly decreases down to ~20 km, reflecting the progressive slab heating toward the Curie temperature of magnetite, 580 °C. The magnetic analysis therefore allows us to constrain the thermal structure of the subducting slab.

Before subduction, we show that a systematic loss of ~20 % in the intensity of magnetization arises between the outer rise and the trench on old ocean crust approaching the Japan and Kuril subduction zones. It reflects the opening of normal faults and fissures before subduction, caused by extension on the outer flexural rise, and the subsequent rejuvenated circulation of seawater into the oceanic crust, resulting in the additional alteration of the magnetic minerals as confirmed by the increasing heat flow and the seismic velocity variations characteristic of increasing hydration of the crust toward the trench.

We attempted to generalize our results to other subduction zones and found that the age of the subducting lithosphere defines two categories. The first one, illustrated by the Japan-Kuril subduction zone, shows old oceanic lithosphere with progressive alteration of the magnetic minerals before subduction. Conversely, the Cascadia subduction zone presents young oceanic lithosphere and no decay before subduction, because flexure is very limited there. Both categories display two steps of thermal demagnetization after subduction.

5.3 Perspectives

Our study of the magnetic anomaly amplitude of the subducting slab questions the thermal models of subduction. The depth of demagnetization of the magnetic minerals suggested by our study are very different from that predicted by the existing thermal model. These

numerical models are based on old heat flow data measured on the seafloor. The initial conditions of these models assume the top of the basement to 0 degrees before entering subduction and only consider heat conduction. Thermal models based on more recent heat flow data in the Japan Trench and including the hydrothermal circulation suggest that the basaltic layer can be heated up to 40 degrees before entering subduction (Kawada et al., 2014).

To solve these misfits, direct heat flow and temperature observations of the subducted oceanic crust are required by drilling through the thick sediments and the decollement. How the heat dissipate through the thick sediments of the highly permeable accretionary prism and the thick consolidated pelagic sediments covering the subducting oceanic crust is of primordial importance, although it is hard to implement due to technical difficulties and astronomical costs.

Several seismic tomography studies estimate the temperature of the subducting oceanic crust by converting the relative seismic velocity variation to rigidity. However, the temperature for the brittle-ductile transition increases as the pressure increases, and the pressure within the slab can be significantly affected by the hydration of the crust. Therefore, temperature estimates using seismic study in the shallow part of the subduction zones are also showing uncertainties.

Considering the problems mentioned before, an effort is required to build a thermal model that takes into account thermal blanketing by thick sediment layer and the hydrothermal circulation in the crust that are expected to occur actively in the subducted oceanic crust. In addition, thermodynamic models constraining the seawater contents in the slab will help to estimate more realistic strain and stress in the slab.

In our study of the magnetic anomalies before subduction, the progressive loss of magnetization from the outer rise to the Japan-Kuril trench implies the active alteration of the magnetic minerals, which deliver Fe^{3+} and gain O^{-}. This alteration will have consequences in the chemical composition of the hydrothermal fluid that will partly be released in the ocean and partly entrained in the subduction. This rejuvenated hydrothermalism should be considered in the global chemical balance of the ocean and investigated. Iron has proven an excellent marker of hydrothermalism at mid-ocean ridges (as revealed, for instance, by the GEOTRACES program).

Our attempts to generalize our results from the Japan Trench to other subduction zones has revealed the importance of the age of the subducting lithosphere. However, all the studied areas were formed at fast- or intermediate-spreading, and the subducting oceanic crust formed at slow-spreading has not been investigated, to cite only this example. Therefore, further RAM analyses in other subduction zones may be required to better understand the effect of other characteristics of the subducting oceanic crust - for instance the spreading rate at which the subducting lithosphere was formed, the sediment thickness, the subduction speed, the slab angle, etc.). Because high-resolution magnetic data do not exist in these subduction zones, more magnetic surveys are needed to do so.

Appendices

Appendix 1

Sea-surface magnetic data processing

A1.1 Introduction

Magnetic data acquired from two different sensors are used in this study. However, since each magnetic sensor has its own characteristics, the methods used to process their data are different. In this appendix, I describe the principle of these two magnetic sensors and the correction applied to their data.

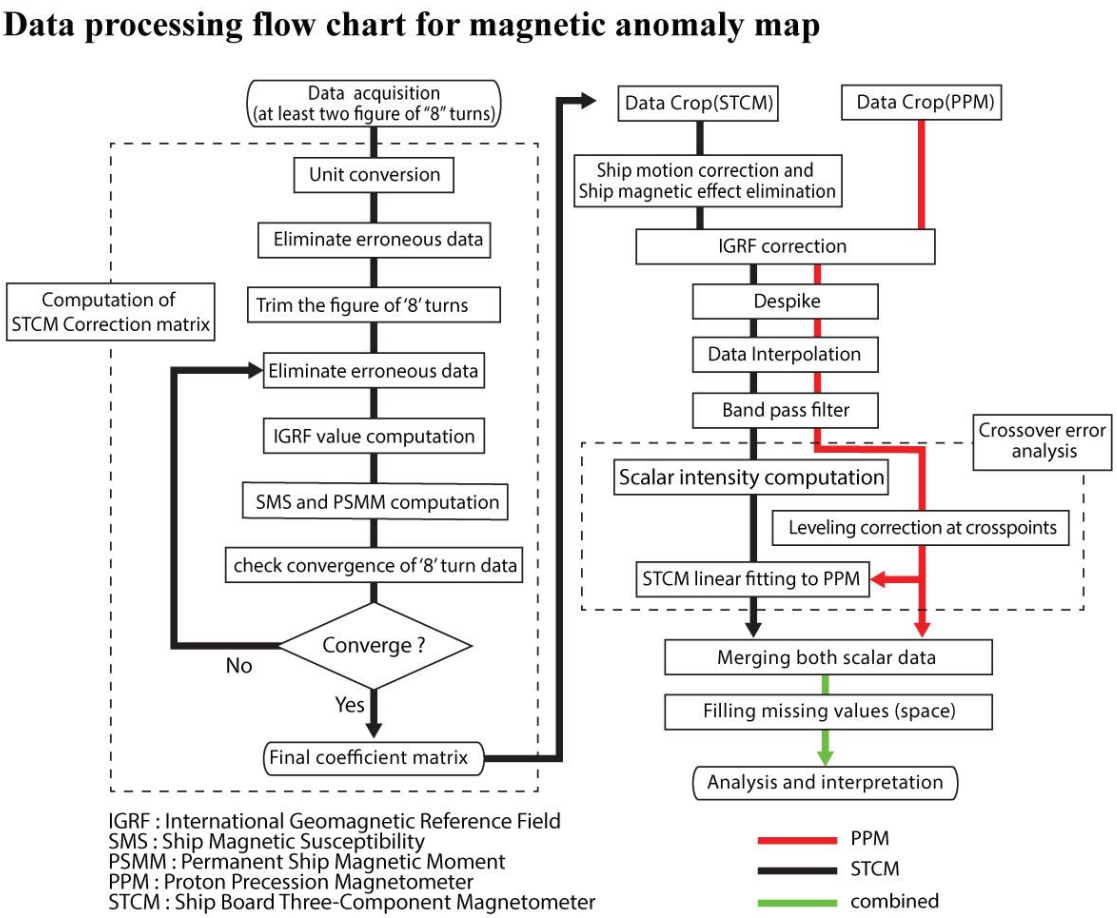

Figure A1-1. Magnetic data processing flow chart. Black solid line indicates the processing flow of magnetic data collected by shipboard three-component magnetometer, gray dashed line indicates the processing flow of the data acquired by proton precession magnetometer.

A1.2 Proton precession magnetometer

A Proton Precession Magnetometer (PPM) is an instrument collecting the scalar intensity of the local magnetic field from the precession of spinning protons in hydrocarbon fluid (e.g. kerosene). The spinning protons tend to be temporarily aligned by application of a uniform magnetic field generated by passing electric current through the coil in the box. Afterward, once the electric current is stopped, the aligned protons start precession to change direction to the local ambient magnetic field. As a result, the precession motion induces very small electric current in the coil from which we can deduce the absolute value of the ambient scalar magnetic field. This magnetometer has the advantage of providing high precision absolute values from which it is easy to compute the magnetic anomaly. However, it does not give access to the vector components (Figure. A1-2).

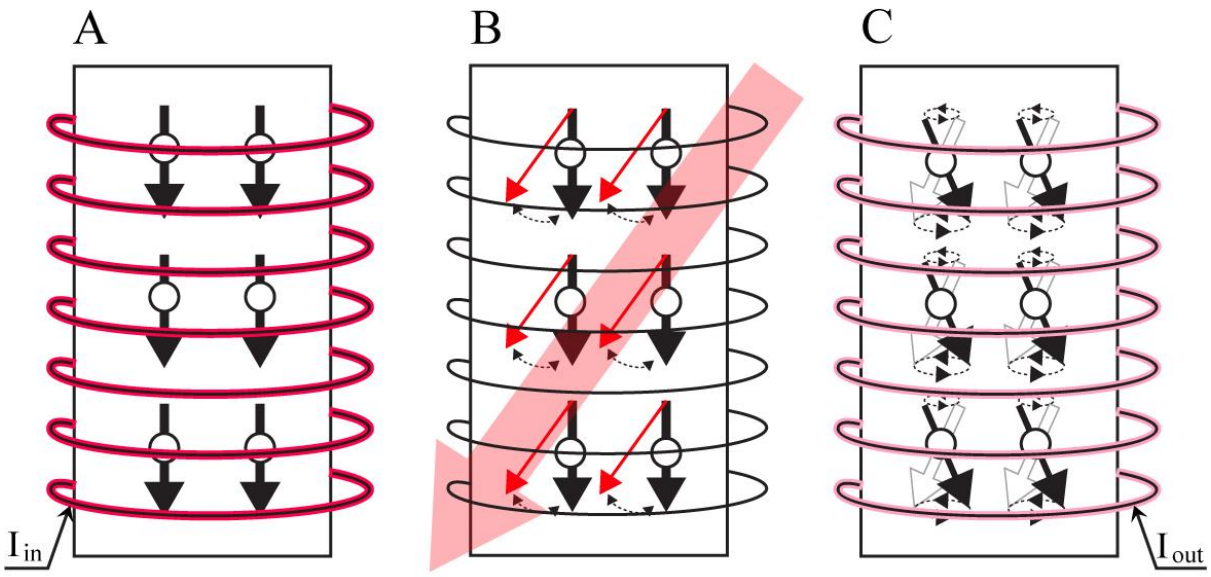

Figure A1-2. Schematic illustration of operating principle of PPM sensor. The PPM sensor consists of a proton-rich fluid in a container, surrounded by a coil. When current is passed through the coil, a magnetic field is induced and the protons in the fluid align themselves with the magnetic field (A). When the current is turned off, the protons try to align themselves with the Earth s magnetic field (B). They cannot do so instantly and precess at a certain frequency about an axis whilst trying (C). This precession frequency is directly proportional to the external magnetic field.

The intensity of the ambient magnetic field measured by the marine PPM includes the main geomagnetic field, originating in the Earth outer core, and the magnetic field resulting from the remanent magnetization of the oceanic crust, among others. Time variations of the field such as the secular variation (locally corrected by the crossover error analysis), the daily solar quiet diurnal variation of relatively low amplitude (sometimes modeled from nearby magnetic observatories and removed, or filtered as a long-wavelength), and the occasional high-frequency variations of external origin known as magnetic storms (which importance is evaluated from published geomagnetic activity indices), are not further considered. The magnetic susceptibility (and therefore the induced magnetization) is considered uniform within normal oceanic crust and produces no significant magnetic anomaly. A good way to remove the main field and the time-varying effects to get scalar residual magnetic anomaly ($\Delta\mathbf{B}$) is to subtract the earth magnetic field measured at a fixed location close to the survey area. However, most marine magnetic surveys cover too wide areas to apply such a technique. Most often, the International Geomagnetic Reference Field model (Thebault et al., 2015; $\mathbf{B}_{\mathbf{igrf}}$) is subtracted from the observed Earth magnetic field ($\mathbf{B}_{\mathbf{raw}}$):

$$\Delta\mathbf{B} = \mathbf{B}_{\mathbf{raw}} - \mathbf{B}_{\mathbf{igrf}}$$

A1.3 Shipboard three-component magnetometer

A shipboard three-component magnetometer (STCM) is made of 3 orthogonal fluxgate magnetometers, each measuring relative variations of the ambient vector magnetic field in one direction. The STCM is installed on the middle of the ship body. The fluxgate sensor is made of a magnetically susceptible core rolled within two wire coils. The relatively strong alternating electric current passing through the first coil drive the core magnetically saturated, which generate a current in the secondary coil. Fluctuations in the ambient magnetic field modify the magnetization in the core, which in turn affects the output currents in the secondary coil recorded by the instrument (Figure A1-3).

The STCM is permanently installed on the ship and allows acquiring magnetic data without deployment and manipulations, unlike the PPM which requires rear towing on the ship. However, since the STCM sensor records both the desired ambient local magnetic field

and the ship magnetic field caused by its induced and permanent magnetizations and is affected ship motion, the corrections are more complicated than with the PPM.

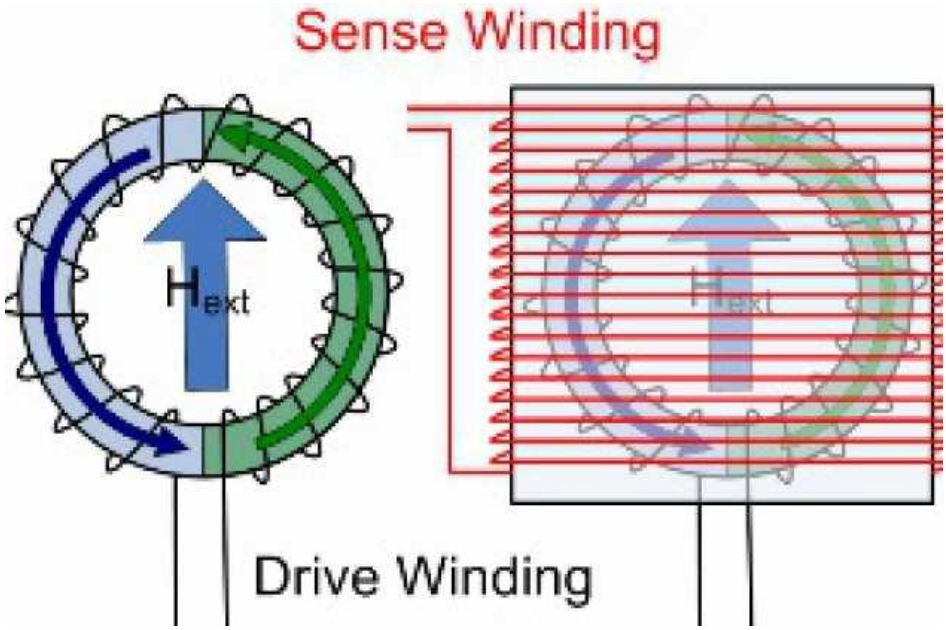

Figure A1-3. The schematic concept of a fluxgate magnetometer

The STCM data processing flow chart used in this study is shown in Figure A1-1. First of all, the erroneous data showing roll and pitch angles of ± 45˚ and yaw variation of 20 deg/sec are removed because the research vessel cannot abruptly change its orientations. In addition, the raw fluxgate data which absolute value exceeds 60000 nT for each horizontal component and 80000 nT for the vertical component are removed. The magnetization coefficient matrix is inverted from each cruise by the least square method from several "figure eight" turns (Isezaki, 1986).

The observed STCM data can be described as

$$\mathbf{H_{ob}} = \boldsymbol{F} + \boldsymbol{H_i} + \boldsymbol{H_p} \qquad (1)$$

where $\mathbf{H_{ob}}$ is the observed magnetic field, $\mathbf{F}$ is the Earth magnetic field, $\mathbf{H_i}$ is the induced magnetic field due to the magnetization of the ship under the influence of the ambient geomagnetic field, and $\mathbf{H_p}$ is the permanent magnetic field. $\mathbf{H_i}$ can be expressed as

$$\mathbf{H_i} = \boldsymbol{CF} \qquad (2)$$

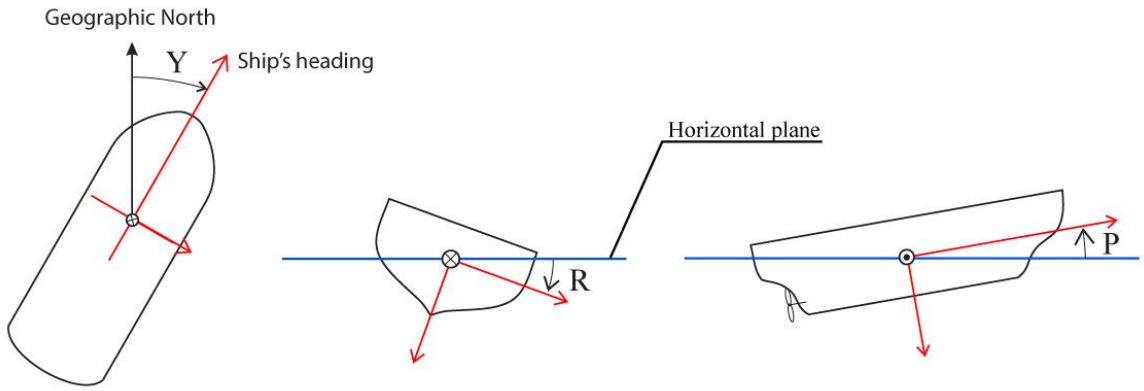

Figure A1-4. Definition of the ship's attitude angles (modified from Koenig, 2006)

where **C**, a 3x3 matrix, is the magnetic susceptibility tensor of the ship. The Earth magnetic field vector **F** can be described as **(RPY)F** where **R**, **P**, and **Y** are the operators of each 3X3 rotation describing the roll, pitch, and yaw. Because the vector $\mathbf{H_{ob}}$ is measured in the ship coordinate system, equation (1) becomes

$$\mathbf{H_{ob}} = (\boldsymbol{C}+\mathbf{1})\boldsymbol{RPYF} + \boldsymbol{H_p} \tag{3}$$

Now, the known values are $\mathbf{H_{ob}}$, **RPY**, and **F**. For easy computation, **(C+1)** can be simply expressed as **C**.

$$\mathbf{H_{ob}} = \boldsymbol{CRPYF} + \boldsymbol{H_p} \tag{4}$$

The goal is to compute the susceptibility of the ship, matrix **C**, and its permanent magnetization, vector $\mathbf{H_p}$, expressed as

$$\boldsymbol{C} = \begin{bmatrix} a_{11} & a_{12} & a_{13} \\ a_{21} & a_{22} & a_{23} \\ a_{31} & a_{32} & a_{33} \end{bmatrix} \text{ and } \boldsymbol{H_p} = \begin{bmatrix} H_{px} \\ H_{py} \\ H_{pz} \end{bmatrix} \tag{5}$$

The coefficients $\mathbf{a_{ij}}$ **(i,j = 1, 2, 3)** can be imaged by their relation to the induced ship field (Figure A1-5; König, 2006).

The known information $\mathbf{H_{ob}}$ and **RPYF** can be simply expressed as

$$H_{ob} = \begin{bmatrix} H_{obx1} & H_{oby1} & H_{obz1} \\ \vdots & \vdots & \vdots \\ H_{obxn} & H_{obyn} & H_{obzn} \end{bmatrix} \quad (6)$$

$$RPYF = \begin{bmatrix} F_{x1} & F_{y1} & F_{z1} \\ \vdots & \vdots & \vdots \\ F_{xn} & F_{yn} & F_{zn} \end{bmatrix}$$

Equation (4) can simply be rewritten **AX = H_{ob}** and **AX - H_{ob} = 0**. We compute the coefficient matrix by solving the linear equation by least square method. The two coefficients **C** and **H_p** are combined into one 3x4 matrix

$$X = \begin{bmatrix} a_{11} & a_{12} & a_{13} & H_{px} \\ a_{21} & a_{22} & a_{23} & H_{py} \\ a_{31} & a_{32} & a_{33} & H_{pz} \end{bmatrix} (3 \times 4)\ matrix \quad (7)$$

And **H_{pk} (k = x, y, z)** are constant values, so we can express the **RPYF** matrix as **A,**

$$A = \begin{bmatrix} F_{x1} & F_{y1} & F_{z1} & 1 \\ \vdots & \vdots & \vdots & \vdots \\ F_{xn} & F_{yn} & F_{zn} & 1 \end{bmatrix} (n \times 4)\ matrix \quad (8)$$

However, the inverse matrix of **A** does not exist since it is not a square matrix. Therefore, to compute the unknown coefficient matrix X, pseudo inverse (pinv) is applied as

$$\mathbf{X} = \mathbf{pinv(A)} \times \mathbf{H_{ob}} = (\mathbf{A^T A})^{-1} \mathbf{A^T H_{ob}} \quad (9)$$

Once the coefficient matrix **X** is determined from the Figure 8 turn data, the corrected magnetic field **H_{corr}** can be computed as

$$\mathbf{H_{corr}} = (RPY)^{-1} X H_{ob} \quad (10)$$

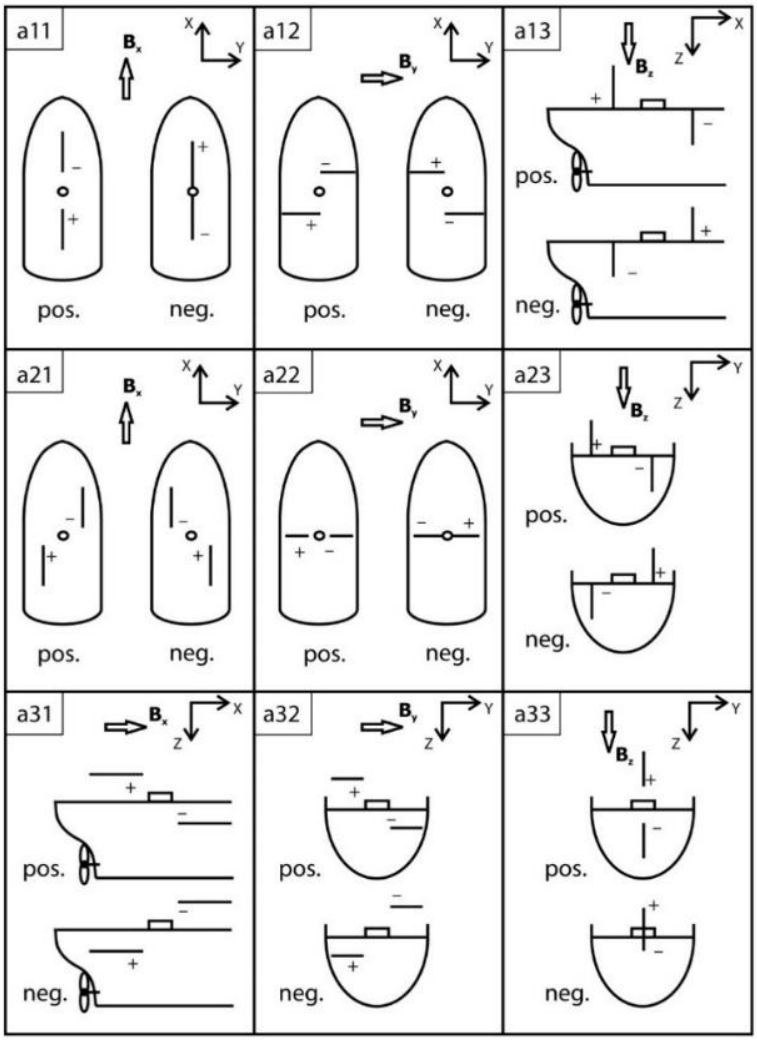

Figure A1-5. Bars of induction and their relation to the sign of the coefficients for the induced ship's field (König, 2006).

When there is no "figure eight" turn data on a cruise, we use the magnetic coefficients previously computed from the closest cruise of the same ship, hoping that the STCM sensor was not replaced or the vessel was not modified, and therefore the main coefficients of ship magnetization do not to show significant variations (Nogi and Kaminuma, 1999).

STCM data are relatively noisier at short wavelength than PPM data. The validity of the STCM data is usually tested by comparison with PPM data. However, the STCM surveys used in this study were not operating a PPM. STCM data after processing remain relative and cannot be directly to build a magnetic anomaly map. Their adjustment to the absolute PPM data is described in Part 1 of Supplementary material of Choe & Dyment (2019a) (see Chapter 2).

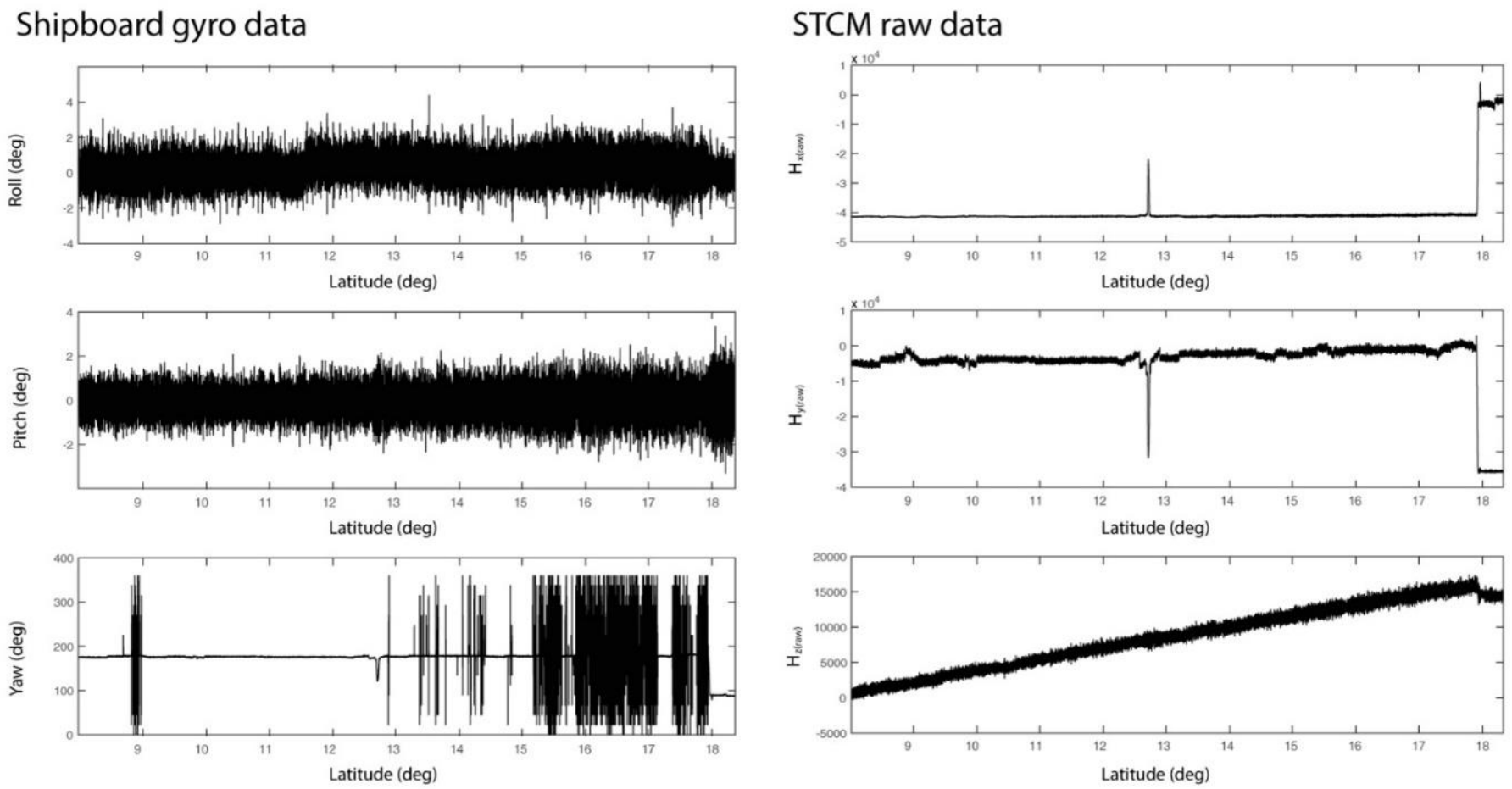

Figure A1-6. Raw STCM data of the Cruise MR06-05 Leg3. The dataset is composed of navigation, shipborne gyro and STCM data. The x-axis is latitude in degree.

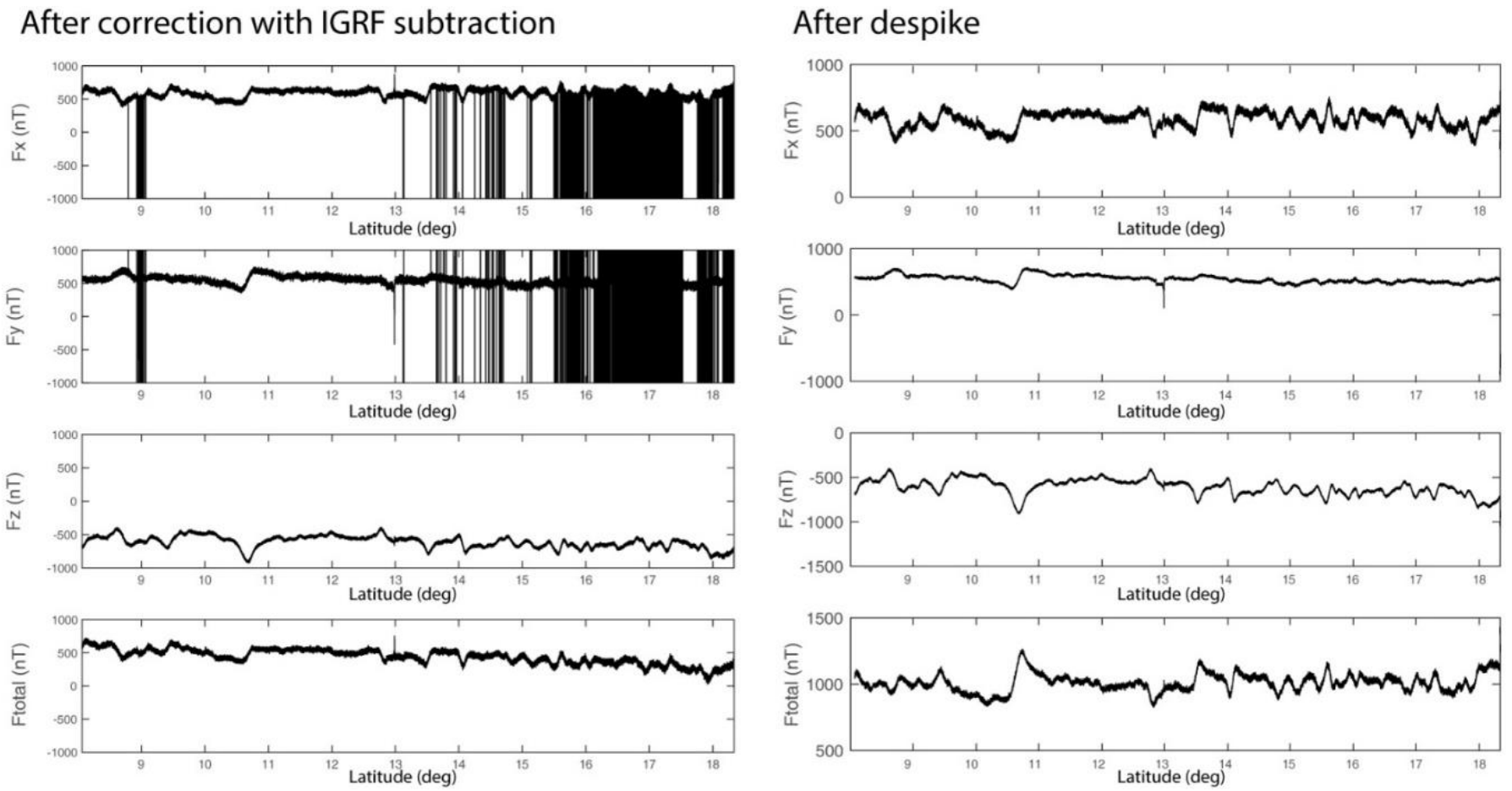

Figure A1-7. Corrected STCM data of Cruise MR06-05 Leg3 continued from the Figure A1-6. The dataset is composed of navigation, shipborne gyro and STCM data. The x-axis is latitude in degree.

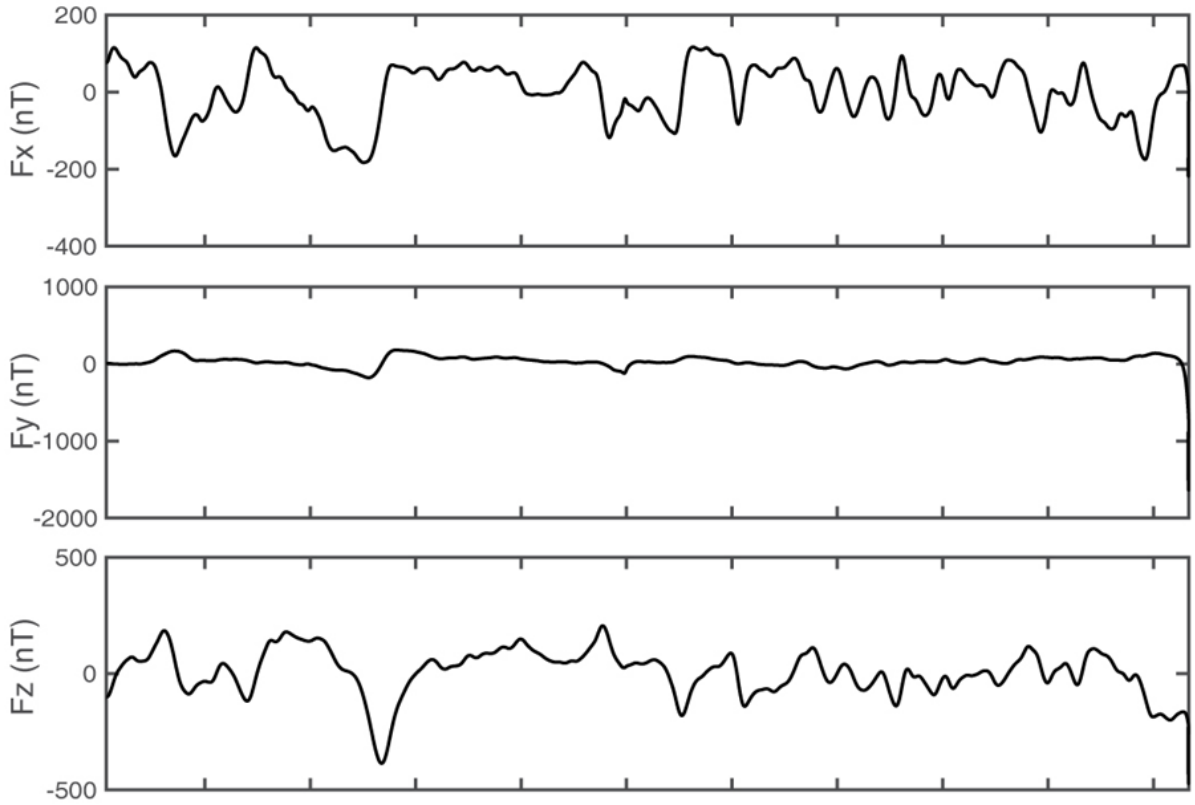

Figure A1-8. Bandpass filtered vector magnetic anomalies continued from the Fig. A1-7.

Appendix 2

Determination of the (magnetized) basement and uncertainties

A2.1 Introduction

Determining the magnetic basement is essential as variation in depth of the basement generates variation in the magnetic anomaly amplitudes. We therefore compute the depth of the oceanic basement before and after subduction by merging and correcting different grids. Basically, before subduction we subtract the sediment thickness grid from the bathymetry grid. The resulting grid seaward from the trench is cropped and merged with a slab geometry model (Figure B2-1). However, several grids have been proposed using different datasets and concepts, and we had to verify the validity and uncertainties of each grid.

A2.2 Misfit analysis

We use the high-resolution bathymetric grid from the Global Multi-Resolution Topography (GMRT; Ryan et al., 2009), two different World sediment thickness grids (Laske and Masters, 1997; Divins, 2003; see Figure A2-1) and two different global slab geometry models (Slab1.0, Hayes et al., 2011; Slab2; Hayes et al., 2018). We compare the misfit along the trench boundary between the slab geometry and the oceanic basement by subtracting each sediment thickness grid from the bathymetry grid(Figure A2-2). The misfit using the sediment thickness grid of Laske and Masters et al. (1997) and Slab1.0 (Hayes et al., 2018) show minimum errors (0-1km) in the Kuril Trench. However, in the Japan Trench, the misfit using the sediment thickness grid of Divins (2003) and Slab1.0 is lower than that using the sediment thickness grid of Laske and Masters et al. (1997). However, profiles across the southern Japan Trench (line 8 and 9 in Figure A2-2A) show misfits as large as 2-3 km between slab and oceanic basement for both grids. We finally use Divins (2003) sediment thickness grid since our study area is limited to the northern Japan Trench.

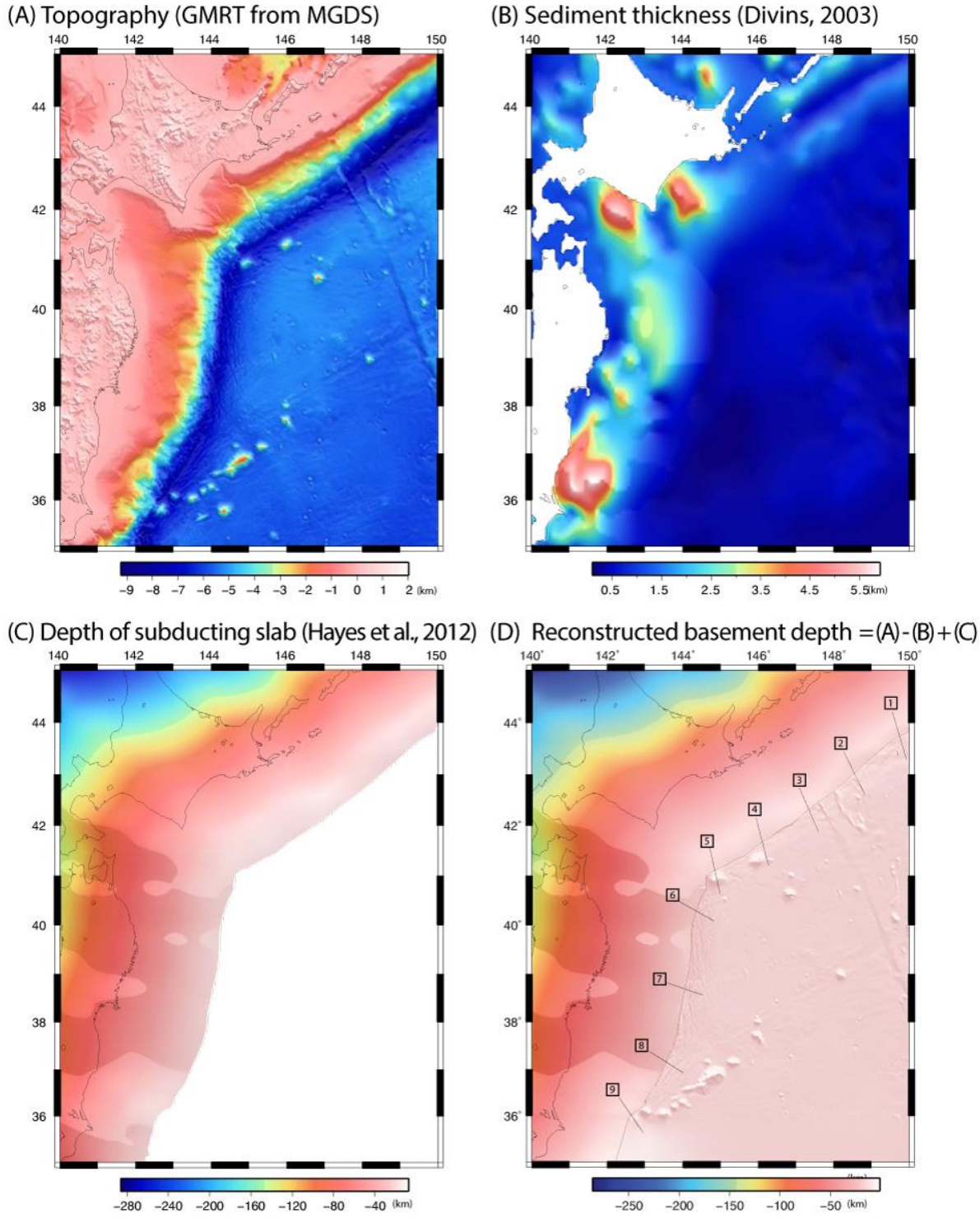

Figure A2-1. A, 2km interval topography grid from GMRT (Ryan et al., 2009). B, sediment thickness grid with the same interval (Divins, 2003). C, Slab 1.0 (Hayes et al., 2012). D, first reconstructed geometry of basement: sediment thickness grid is subtracted from topography grid and the result is merged with slab geometry after cropping unsubducted area along the plate boundary. Black solid lines indicate the profiles in Figure A2-2.

The trenches are the boundary between overriding and subducting plate and the deepest parts of the ocean floor. The subducting oceanic crust should display a regular, continuous downgoing geometry. However, we find that some misfits are due to erroneous locations of the trench as given by the global plate boundary file (Bird, 2003; Figure B2-2A). Since we interpolate known datasets to fill in gaps at the trench between the slab geometry grid and the oceanic basement depth grid, such erroneous location may generate additional errors. Any geometrical misfit between the two grids along the trench boundary is erased and re-interpolated using the Partial Differential Equation (PDE) surface method of D'Errico (2005) after we correct the position of the trenches. Profiles across the resulting grid is shown in Figure B2-2B. An analysis of the best choice between slab geometry grids Slab 1.0 and Slab 2 is given as an electronic supplement of Chapter 2.

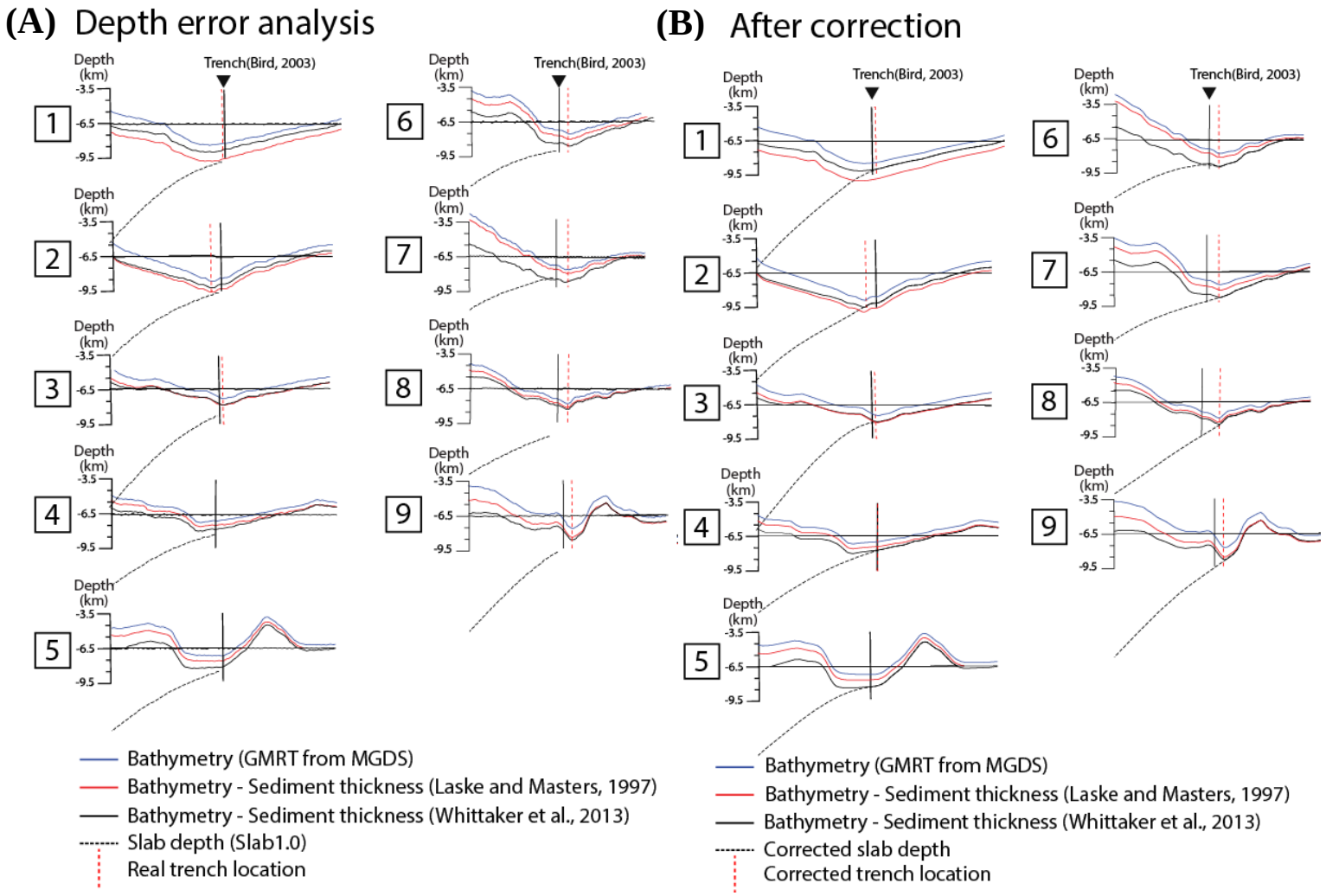

Figure A2-2. A, Analysis of the misfits between slab geometry and basement geometry. The depth error ranges between 0.5-3.0km. **B,** the differences in depth after the correction.

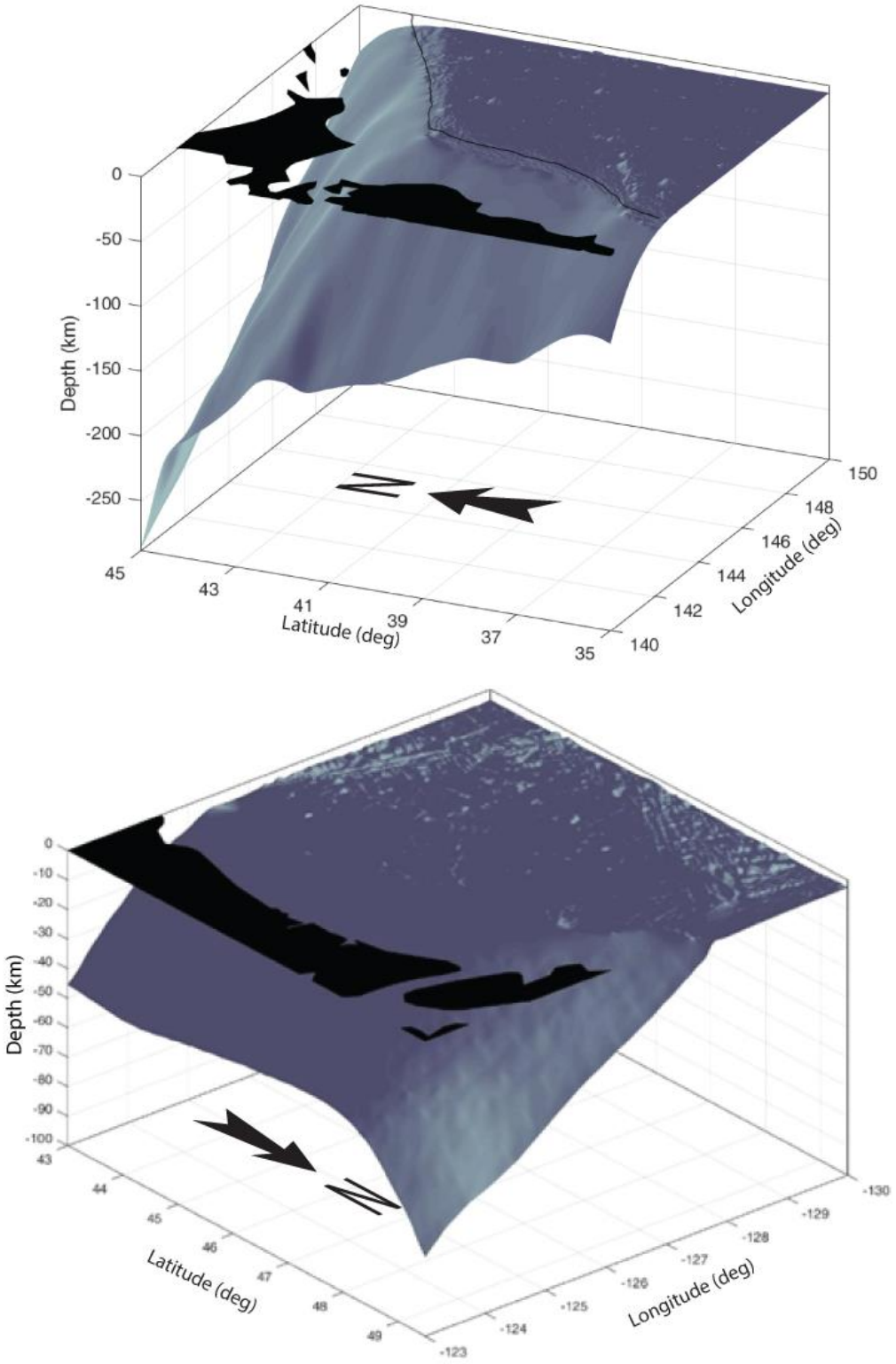

Figure A2-3. Reconstructed 3-D geometry of oceanic crust layer 2A in Japan subduction zone (up) and Cascadia subduction zone (down). Black area indicates the land and black solid line, the trench.

Bibliography

Amante, C., and Eakins, B.W., 2009, ETOPO1 1 Arc-Minute Global Relief Model: Procedures, Data Sources and Analysis: NOAA Technical Memorandum NESDIS NGDC-24, 19 p.

Bird, 2003, An updated digital model of plate boundaries: Geochemistry Geophysics Geosystems, v. 4, p. 1-52, doi:10.1029/2001GC000252.

Blakely, R.J., Brocher, T.M., and Wells, R.E., 2005, Subduction-zone magnetic anomalies and implications for hydrated forearc mantle: Geology, v. 33, p. 445–448, doi:10.1130/G21447.1.

Boston, B., Moore, G. F., Nakamura, Y., & Kodaira, S. (2014). Outer-rise normal fault development and influence on near-trench décollement propagation along the Japan Trench, off Tohoku. *Earth, Planets and Space*, *66*(1), 1–17, doi:10.1186/1880-5981-66-135

Canales, J.P., Carbotte, S.M., Nedimovic, M.R., and Carton, H., 2017, Dry Juan de Fuca slab revealed by quantification of water entering Cascadia subduction zone: Nature Geoscience, v. 10, p. 864–870, doi:10.1038/NGEO3050.

Cande, S.C., and Kent, D. V., 1995, Revised calibration of the geomagnetic polarity timescale for the late Cretaceous and Cenozoic: Journal of Geophysical Research, v. 100, p. 6093–6095, doi:10.1029/94JB03098.

Choe, H., Dyment, J., 2020a, Fading Magnetic Anomalies, Thermal Structure and Earthquakes in the Japan Trench: Geology, v. 48(3), p. 278–282, doi: https://doi.org/10.1130/G46842.1

Choe, H., Dyment, J., 2020b, Fading magnetic anomalies, lithospheric flexure and rejuvenated hydrothermalism off the Japan-Kuril subduction zone: Geophysical Research Letters (in revision)

Contreras-Reyes, E., Grevemeyer, I., Flueh, E.R., and Reichert, C., 2008, Upper lithospheric structure of the subduction zone offshore of southern Arauco peninsula, Chile, at ∼38°S: Journal of Geophysical Research: Solid Earth, v. 113, p. 1–19, doi:10.1029/2007JB005569.

D’Errico, J., 2005, Surface Fitting using gridfit, MATLAB Central File Exchange: https://www.mathworks.com/matlabcentral/fileexchange/8998-surface-fitting-using-gridfit (May 2006).

Delescluse, M., and Chamot-Rooke, N., 2008, Serpentinization pulse in the actively deforming Central Indian Basin: Earth and Planetary Science Letters, v. 276, p. 140–151, doi:10.1016/j.epsl.2008.09.017.

Dilek, Y., and Furnes, H., 2014, Ophiolites and Their Origins: Elements, v. 10, p. 93–100, doi:10.2113/gselements.10.2.93.

Divins, D.L., 2003, Total Sediment Thickness of the World's Oceans & Marginal Seas, NOAA National Geophysical Data Center, Boulder (available at https://www.ngdc.noaa.gov/mgg/sedthick/sedthick.html).

Dyment, J., and Arkani-Hamed, J., 1995, Spreading-rate-dependent magnetization of the oceanic lithosphere inferred from the anomalous skewness of marine magnetic anomalies: Geophysical Journal International, v. 121, p. 789–804, doi:10.1111/j.1365-246X.1995.tb06439.x.

Dyment, J., and Arkani-Hamed, J., 1998, Contribution of lithospheric remanent magnetization to satellite magnetic anomalies over the world’s oceans: Journal of Geophysical Research: Solid Earth, v. 103, p. 15423–15441, doi:10.1029/97JB03574.

Dyment, J., Arkani-Hamed, J., and Ghods, A., 1997, Contribution of serpentinized ultramafics to marine magnetic anomalies at slow and intermediate spreading centres: Insights from the shape of the anomalies: Geophysical Journal International, v. 129, p. 691–701, doi:10.1111/j.1365-246X.1997.tb04504.x.

Dyment, J., Choi, Y., Hamoudi, M., Lesur, V., and Thebault, E., 2015, Global equivalent magnetization of the oceanic lithosphere: Earth and Planetary Science Letters, v. 430, p. 54–65, doi:10.1016/j.epsl.2015.08.002.

Dziewonski, A. M., T.-A. Chou and J. H. Woodhouse, 1981, Determination of earthquake source parameters from waveform data for studies of global and regional seismicity, J.

Geophys. Res., v. 86, p. 2825-2852, doi:10.1029/JB086iB04p02825 and database (available at https://www.globalcmt.org/).

Finley, T., Morell, K., Leonard, L., Regalla, C., Johnston, S.T., and Zhang, W., 2019, Ongoing oroclinal bending in the Cascadia forearc and its relation to concave-outboard plate margin geometry: Geology, v. 47, p. 155–158, doi:10.1130/G45473.1.

Fujie, G., Kasahara, J., Hino, R., Sato, T., Shinohara, M., and Suyehiro, K., 2002, A significant relation between seismic activities and reflection intensities in the Japan Trench region: Geophysical Research Letters, v. 29, p. 4–7, doi:10.1029/2001GL013764.

Fujie, G., Kodaira, S., Sato, T., & Takahashi, T., 2016, Along-trench variations in the seismic structure of the incoming Pacific plate at the outer rise of the northern Japan Trench. Geophysical Research Letters, 43(2), p.666–673, https://doi.org/10.1002/2015GL067363

Fujie, G., Kodaira, S., Kaiho, Y., Yamamoto, Y., Takahashi, T., Miura, S., and Yamada, T., 2018, Controlling factor of incoming plate hydration at the north-western Pacific margin: Nature Communications, v. 9, doi:10.1038/s41467-018-06320-z.

Fulton, P.M., Brodsky, E.E., Kano, Y., Mori, J., Chester, F., Ishikawa, T., Harris, R.N., Lin, W., Eguchi, N., and Toczko, S., 2013, Low coseismic friction on the Tohoku-Oki fault determined from temperature measurements: Science, v. 342, p. 1214–1217, doi:10.1126/science.1243641.

Gee, J.S., and Kent, D.V., 2007, Source of Oceanic Magnetic Anomalies and the Geomagnetic Polarity Timescale, in Treatise on Geophysics, Elsevier, v. 5, p. 455–507, doi:10.1016/B978-044452748-6.00097-3.

Granot, R., and Dyment, J., 2019, The Influence of Post-accretion Sedimentation on Marine Magnetic Anomalies: Geophysical Research Letters, v. 46, p. 4645–4652, doi:10.1029/2019GL082265.

Grevemeyer, I., Ranero, C.R., and Ivandic, M., 2018, Structure of oceanic crust and serpentinization at subduction trenches: Geosphere, v. 14, p. 395–418, doi:10.1130/GES01537.1.

Harris, R.N., Spinelli, G.A., and Fisher, A.T., 2017, Hydrothermal circulation and the thermal structure of shallow subduction zones: Geosphere, v. 13, p.1425–1444, doi:10.1130/GES01498.1.

Harrison, C., 1987, Marine Magnetic Anomalies: The Origin Of The Stripes: Annual Review of Earth and Planetary Sciences, v. 15, p. 505–543, doi:10.1146/annurev.earth.15.1.505.

Hayes, G.P., Moore, G.L., Portner, D.E., Hearne, M., Flamme, H., Furtney, M., and Smoczyk, G.M., 2018, Slab2, a comprehensive subduction zone geometry model: Science, v. 362, p. 58–61, doi:10.1126/science.aat4723 and database (available at https://www.sciencebase.gov/catalog/item/5aa1b00ee4b0b1c392e86467).

Hutnak, M., & Fisher, A. T., 2007, Influence of sedimentation, local and regional hydrothermal circulation, and thermal rebound on measurements of seafloor heat flux. Journal of Geophysical Research, 112(B12), B12101, doi:10.1029/2007JB005022

Hayes, G.P., Wald, D.J., and Johnson, R.L., 2012, Slab1.0: A three-dimensional model of global subduction zone geometries: Journal of Geophysical Research: Solid Earth, v. 117, doi:10.1029/2011JB008524.

Hyndman, R.D., and Peacock, S.M., 2003, Serpentinization of the forearc mantle: Earth and Planetary Science Letters, v. 212, p. 417–432, doi:10.1016/S0012-821X(03)00263-2.

Institut français de recherche pour l'exploitation de la mer, 2014, Nautilus in IFREMER: http://donnees-campagnes.flotteoceanographique.fr/ (accessed January 2017).

Isezaki, N., 1986, A new shipboard three-component magnetometer: GEOPHYSICS, v. 51, p. 1992–1998, doi:10.1190/1.1442054.

Ito, A., Fujie, G., Tsuru, T., Kodaira, S., Nakanishi, A., and Kaneda, Y., 2004, Fault plane geometry in the source region of the 1994 Sanriku-oki earthquake: Earth and Planetary Science Letters, v. 223, p. 163–175, doi:10.1016/j.epsl.2004.04.007.

Japan Agency for Marine-Earth Science and Technology, 2016, Data and Sample Research System for Whole Cruise Information in JAMSTEC (DARWIN): http://www.godac.jamstec.go.jp/darwin/ (accessed January 2017).

Johnson, H.P., Hautala, S.L., and Bjorklund, T.A., 2012, The thermal environment of Cascadia Basin: Geochemistry, Geophysics, Geosystems, v. 13, doi:10.1029/2011GC003922.

Karson, J.A., 2002, Geologic Structure of the Uppermost Oceanic Crust Created at Fast- to Intermediate-Rate Spreading Centers: Annual Review of Earth and Planetary Sciences, v. 30, p. 347–384, doi:10.1146/annurev.earth.30.091201.141132.

Kawada, Y., Yamano, M., and Seama, N., 2014, Hydrothermal heat mining in an incoming oceanic plate due to aquifer thickening: Explaining the high heat flow anomaly observed around the Japan Trench: Geochemistry, Geophysics, Geosystems, v. 15, p. 1580–1599, doi:10.1002/2014GC005285.

Kelley, D.S. et al., 2001, An off-axis hydrothermal vent field near the Mid-Atlantic Ridge at 30° N: Nature, v. 412, p. 145–149, doi:10.1038/35084000.

Key, K., Constable, S., Matsuno, T., Evans, R. L., & Myer, D., 2012, Electromagnetic detection of plate hydration due to bending faults at the Middle America Trench. Earth and Planetary Science Letters, v. 351–352 (May 2019), p.45–53, doi:10.1016/j.epsl.2012.07.020

Kido, Y., and Fujiwara, T., 2004, Regional variation of magnetization of oceanic crust subducting beneath the Nankai Trough: Geochemistry, Geophysics, Geosystems, v. 5, p. 1–11, doi:10.1029/2003GC000649.

Kodaira, S., Nakamura, Y., Yamamoto, Y., Obana, K., Fujie, G., No, T., Kaiho, Y., Sato, T., and Miura, S., 2017, Depth-varying structural characters in the rupture zone of the 2011 Tohoku-oki earthquake: Geosphere, v. 13, p. 1408–1424, doi:10.1130/GES01489.1.

Koenig, M. (2006). Processing of shipborne magnetometer data and revision of the timing and geometry of the Mesozoic break-up of Gondwana. Phd Thesis, 139.

Laske, G. and Masters, G., 1997, A Global Digital Map of Sediment Thickness. EOS Transactions American Geophysical Union, 78, F483.

Lister, C. R. B., 1972, On the Thermal Balance of a Mid-Ocean Ridge. Geophysical Journal International, v. 26(5), p. 515–535, doi:10.1111/j.1365-246X.1972.tb05766.x

Macdonald, A.H., and Fyfe, W.S., 1985, Rate of serpentinization in seafloor environments: Tectonophysics, v. 116, p. 123–135, doi:10.1016/0040-1951(85)90225-2.

Malinverno, A., Hildebrandt, J., Tominaga, M., and Channell, J.E.T., 2012, M-sequence geomagnetic polarity time scale (MHTC12) that steadies global spreading rates and incorporates astrochronology constraints: Journal of Geophysical Research: Solid Earth, v. 117, p. 1–17, doi:10.1029/2012JB009260.

Marsh, B.D., and Leitz, R.E., 1979, RECONNAISSANCE GEOLOGY ISLAND ISLANDS ALEUTIAN:

Müller, R.D., Sdrolias, M., Gaina, C., and Roest, W.R., 2008, Age, spreading rates, and spreading asymmetry of the world's ocean crust: Geochemistry, Geophysics, Geosystems, v. 9, p. 1–19, doi:10.1029/2007GC001743.

Nakanishi, M., 2011, Bending-Related Topographic Structures of the Subducting Plate in the Northwestern Pacific Ocean. In Y. Ogawa, R. Anma, Y. Dilek (Eds.), Accretionary Prisms and Convergent Margin Tectonics in the Northwest Pacific Basin (v. 8, p. 1-38). Springer, doi:10.1007/978-90-481-8885-7

Nakanishi, M., Tamaki, K., and Kobayashi, K., 1989, Mesozoic magnetic anomaly lineations and seafloor spreading history of the northwestern Pacific: Journal of Geophysical Research: Solid Earth, v. 94, p. 15437–15462, doi:10.1029/JB094iB11p15437.

Nogi, Y., & Kaminuma, K. (1999, November 25). Measurements of vector magnetic anomalies on board the icebreaker Shirase and the magnetization of the ship. Annals of Geophysics. https://doi.org/10.4401/ag-3711

Obana, K., Fujie, G., Takahashi, T., Yamamoto, Y., Nakamura, Y., Kodaira, S., et al., 2012, Normal-faulting earthquakes beneath the outer slope of the Japan Trench after the 2011 Tohoku earthquake: Implications for the stress regime in the incoming Pacific plate. Geophysical Research Letters, v. 39(2), p. 1–7, doi: 10.1029/2011GL050399

Okubo, Y., and Matsunaga, T., 1994b, Curie point depth in northeast Japan and its correlation with regional thermal structure and seismicity: Journal of Geophysical Research: Solid Earth, v. 99, p. 22363–22371, doi:10.1029/94JB01336.

Okubo, Y., Makino, M., and Kasuga, S., 1991, Magnetic model of the subduction zone in the northeast Japan Arc: Tectonophysics, v. 192, p. 103–115, doi:10.1016/0040-1951(91)90249-R.

Ranero, C. R., J. P. Morgan, K. McIntosh, and C. Reichert, 2003, Bending-related faulting and mantle serpentinization at the Middle America trench, Nature, v. 425(6956), p. 367-373, doi:10.1038/nature01961.

Parker, R.L., and Huestis, S.P., 1974, The inversion of magnetic anomalies in the presence of topography: Journal of Geophysical Research, v. 79, p. 1587–1593, doi:10.1029/JB079i011p01587.

Ravilly, M., Dyment, J., Gente, P., and Thibaud, R., 1998, Axial magnetic anomaly amplitude along the Mid-Atlantic Ridge between 20°N and 40°N: Journal of Geophysical Research: Solid Earth, v. 103, p. 24201–24221, doi:10.1029/98JB01071.

Riddihough, R., 1984, Recent movements of the Juan de Fuca Plate System: Journal of Geophysical Research: Solid Earth, v. 89, p. 6980–6994, doi:10.1029/JB089iB08p06980.

Ryan, W.B.F. et al., 2009, Global Multi-Resolution Topography synthesis: Geochemistry, Geophysics, Geosystems, v. 10, doi:10.1029/2008GC002332 and database (available at https://www.gmrt.org/).

Sandwell, D.T., Müller, R.D., Smith, W.H.F., Garcia, E., and Francis, R., 2014, New global marine gravity model from CryoSat-2 and Jason-1 reveals buried tectonic structure: Science, v. 346, p. 65–67, doi:10.1126/science.1258213 and database (available at https://topex.ucsd.edu/grav_outreach/).

Seno, T., 2017, Subducted sediment thickness and M w 9 earthquakes: Journal of Geophysical Research: Solid Earth, v. 122, p. 470–491, doi:10.1002/2016JB013048.

Shillington, D.J., Becel, A., Nedimovic, M.R., Kuehn, H., Webb, S.C., Abers, G.A., Keranen, K.M., Li, J., Delescluse, M., and Mattei-Salicrup, G.A., 2015, Link between plate fabric, hydration and subduction zone seismicity in Alaska: Nature Geoscience, v. 8, p. 961–964, doi:10.1038/ngeo2586.

Spinelli, G. A., & Wang, K., 2008, Effects of fluid circulation in subducting crust on Nankai margin seismogenic zone temperatures. Geology, v. 36(11), p. 887–890, doi:10.1130/G25145A.1

Stein, C.A., 2003, Heat flow and flexure at subduction zones: Geophysical Research Letters, v. 30, p. SDE 4-1doi:10.1029/2003GL018478.

Stern, R.J., 2002, Subduction zones: Reviews of Geophysics, v. 40, p. 1031–1039, doi:10.1029/2001RG000108.

Thébault, E. et al., 2015, International Geomagnetic Reference Field: the 12th generation: Earth, Planets and Space, v. 67, p. 79, doi:10.1186/s40623-015-0228-9.

Tivey, M.A., Rona, P.A., and Schouten, H., 1993, Reduced crustal magnetization beneath the active sulfide mound, TAG hydrothermal field, Mid-Atlantic Ridge at 26°N: Earth and Planetary Science Letters, v. 115, p. 101–115, doi:10.1016/0012-821X(93)90216-V.

Tsuru, T., Park, J., Takahashi, N., Kodaira, S., Kido, Y., Kaneda, Y., and Kono, Y., 2000, Tectonic features of the Japan Trench convergent margin off Sanriku, northeastern Japan, revealed by multichannel seismic reflection data: Journal of Geophysical Research: Solid Earth, v. 105, p. 16403–16413, doi:10.1029/2000JB900132.

Tsuru, T., Park, J.-O., Miura, S., Kodaira, S., Kido, Y., and Hayashi, T., 2002, Along-arc structural variation of the plate boundary at the Japan Trench margin: Implication of interplate coupling: Journal of Geophysical Research: Solid Earth, v. 107, p. ESE 11-1-ESE 11-15, doi:10.1029/2001JB001664.

van Keken, P.E., Kita, S., and Nakajima, J., 2012, Thermal structure and intermediate-depth seismicity in the Tohoku-Hokkaido subduction zones: Solid Earth, v. 3, p. 355–364, doi:10.5194/se-3-355-2012.

Vine, F.J., and Matthews, D.H., 1963, Magnetic Anomalies Over Oceanic Ridges: Nature, v. 199, p. 947–949, doi:10.1038/199947a0.

Violay, M., Gibert, B., Mainprice, D., Evans, B., Dautria, J.-M., Azais, P., and Pezard, P., 2012, An experimental study of the brittle-ductile transition of basalt at oceanic crust

pressure and temperature conditions: Journal of Geophysical Research: Solid Earth, v. 117, p. 1–23, doi:10.1029/2011JB008884.

Wada, I., He, J., Hasegawa, A., and Nakajima, J., 2015, Mantle wedge flow pattern and thermal structure in Northeast Japan: Effects of oblique subduction and 3-D slab geometry: Earth and Planetary Science Letters, v. 426, p. 76–88, doi:10.1016/j.epsl.2015.06.021.

Wessel, P., 2010, Tools for analyzing intersecting tracks: The x2sys package: Computers & Geosciences, v. 36, p. 348–354, doi:10.1016/j.cageo.2009.05.009.

Yamano, M., Hamamoto, H., Kawada, Y., and Goto, S., 2014, Heat flow anomaly on the seaward side of the Japan Trench associated with deformation of the incoming Pacific plate: Earth and Planetary Science Letters, v. 407, p. 196–204, doi:10.1016/j.epsl.2014.09.039.

Yang, T., Dekkers, M.J., and Zhang, B., 2016, Seismic heating signatures in the Japan Trench subduction late-boundary fault zone: Evidence from a preliminary rock magnetic "geothermometer": Geophysical Journal International, v. 205, p. 332–344, doi:10.1093/gji/ggw013.

Zhou, W., Van der Voo, R., Peacor, D.R., Wang, D., and Zhang, Y., 2001, Low-temperature oxidation in MORB of titanomagnetite to titanomaghemite: A gradual process with implications for marine magnetic anomaly amplitudes: Journal of Geophysical Research: Solid Earth, v. 106, p. 6409–6421, doi:10.1029/2000JB900447.

UNIVERSITÉ DE PARIS

The Fate of Marine Magnetic Anomalies in Subduction Zone

par
Hanjin Choe

Abstract

The purpose of this study is to understand the causes of the decaying seafloor spreading magnetic anomalies on subducting oceanic crust. We investigate the magnetization of the oceanic crust both before and after subduction and extend our initial study area from the Japan-Kuril subduction zone to other subduction zones to try to generalize our observations. Before subduction, a 20% loss of magnetization between the outer-rise and the trench occurs in old seafloor, caused by rejuvenated hydrothermal circulations and alteration of magnetic minerals. Conversely, such a loss of magnetization is not observed for the young seafloor because the flexure remains very limited. After subduction, both exhibit a fast decay of magnetization due to thermal demagnetization of titanomagnetite (Tc:150-350°C) in the extrusive basalt, followed by a much slower one due to thermal demagnetization of magnetite (Tc: 580 °C) in the deeper crust. However, the fast decay is more rapidly achieved in the young seafloor due to differences in the thermal structure. Overall, the magnetic anomalies in subducting oceanic crust decay as an effect of flexure, normal faulting and hydrothermal alteration before subduction, and thermal demagnetization of the different magnetic minerals after subduction. The seawater injected in the oceanic crust before subduction is trapped by the sediment cover after entering subduction and may significantly heat up the slab through thermal blanketing, adding to the thermal gradient and possibly heat released by serpentinization of the mantle wedge. The speed of thermal demagnetization is modulated by the lithospheric thickness, hydration rate, and therefore the age of the seafloor.

Key-words: Subduction, magnetic anomaly, thermodynamics, thermal demagnetization,Curie temperature, hydrothermal circulation

Résumé

L'objet de cette étude est de comprendre les causes de la diminution des anomalies magnétiques océaniques dans la croûte océanique en subduction. Nous étudions l'aimantation de la croûte océanique avant et après l'entrée en subduction et étendons notre zone d'étude initiale des fosses du Japon et des Kouriles à d'autres zones de subduction afin de généraliser nos observations. Avant subduction, une perte de 20% de l'aimantation se produit entre la ride externe et la fosse pour un plancher océanique ancien, causée par le renouvellement de la circulation hydrothermale et l'altération des minéraux magnétiques. Une telle perte n'est pas observée pour un plancher océanique jeune car la flexure y est très faible. Après subduction, dans tous les cas sont observées une décroissance rapide de l'aimantation liée à la désaimantation thermique de la titanomagnétite (Tc 150-350°C) des basaltes extrusifs, suivie d'une décroissance plus lente liée à la désaimantation thermique de la magnétite (Tc 580°C) dans la croûte profonde. La première phase est plus rapidement achevée dans le plancher océanique jeune de par des différences de structure thermique. De manière générale, la disparition des anomalies magnétiques en subduction résulte de la flexure, de la fracturation et de la circulation hydrothermale avant subduction, et de la désaimantation thermique des différents minéraux magnétiques après subduction. L'eau de mer injectée dans la croûte avant subduction est piégée par la couverture sédimentaire après être entrée en subduction et pourrait significativement réchauffer le panneau plongeant par couverture thermique, s'ajoutant au gradient thermique initial et possiblement à la chaleur dégagée par la serpentinisation du coin mantellique. La vitesse de désaimantation thermique est modulée par l'épaisseur lithosphérique, le taux d'hydratation, et donc l'âge du plancher océanique.

Mots-clefs: Subduction, anomalie magnetique, thermodynamique, désaimantation thermique, Curie temperature, circulation hydrothermale